SLOWING ATOMS WITH A PERMANENT MAGNET ZEEMAN SLOWER & INVESTIGATING FIBRE PHASE NOISE ON AN OPTICAL CLOCK SYSTEM.

By

RICHARD BARRON

A thesis submitted to
the University of Birmingham
for the degree of
DOCTOR OF PHILOSOPHY

Cold Atoms Research Group
School of Physics and Astronomy
College of Engineering and Physical Sciences
University of Birmingham
March 2022

ABSTRACT

Optical atomic clock systems have recently broken out from being purely lab based devices to becoming portable and transportable systems. In order to facilitate optical atomic clock systems being used in non-lab based applications these systems must be made as robust, simple, and as affordably as possible. To that end investigations into non-powered versions of usually power hungry systems and off the shelf components for traditionally expensive ones are an attractive area of research. In this thesis investigations are made into a permanent magnet Zeeman slower to reduce power consumption, the effect of slits in Magneto Optical Trap (MOT) coils to improve physical robustness, and a Red Pitaya system for cancelling phase noise in fibres. The Zeeman slower designed, built, and characterised in this thesis is an iteration of previous work completed at the University of Birmingham being adapted for use in a system with reduced physical space on the system architecture. This presented a challenge on how to provide the magnetic field required for the Zeeman slower to work, without detrimentally affecting other parts of the clock system. The iqClock Zeeman slower design miniaturises previous work, and reduces the field in the MOT region, successfully forming a MOT of around seven million atoms. An investigation into the eddy currents that form in MOT coils was undertaken, proving the benefit of cutting a slit into the coil former to prevent inducted magnetic fields forming. The slit coils were tested against non-conductive and slit coils to determine the impact of the eddy currents. These coils were then tested to ensure they provided the 40 gauss/cm gradient necessary to form the MOT. They were then used to help form the MOT system that the Zeeman slower was tested on. Fibre phase stabilisation is a key part of clock networks, and allows the comparison signals from physically distance devices. As some of the subsystems for the iqClock testbed system are located in separate labs the issue of fibre phase stabilisation came into play the process of connecting finished clock systems was in progress. A system was designed and built to cancel the fibre phase noise present in fibres joining remote systems utilising "off the shelf" components.

DEDICATION

ACKNOWLEDGMENTS

There are many people without whom this thesis would not have been possible. Firstly thank you to my supervisors Dr Yeshpal Singh and Professor Kai Bongs, for all your advice over the course of this PhD. To the members of the strontium cold atoms group, Alok, Abhilash, Jonathan, Marcus, Manan, Sarah, Vijay and Yogi I would like to extend a heartfelt thank you, it has not been an easy few years with lab leaks and pandemics to contend with, but thank you for all your help and advice. I would also like to thank all my fellows in the wider colds atoms groups for their help and support. To mention a few in particular Jonny Bass for showing me the ropes as a new clocks PhD and his excellent insights into the experiments, Luuk Earl for his stirling PhD latex template, and Jonathan Winch for always being there to help with technical issues. To my housemates Dom, Jack, and Elli thank you for keeping me company and sane as we went through our respective courses, and your support during the write up. Finally I would like to thank my folks for putting up with me whilst I was writing up this thesis. That can't have been easy.

Table of Contents

List of Figures

Chapter One

Introduction

1.1 Timing in the modern era

The modern era of timing metrology (the science of measuring the passage of time) can be considered to have begun during the 13^{th} meeting of the International Committee of Weights and Measures between the 10^{th} and 16^{th} October 1967. During this meeting the second was defined as "The second is the duration of 9 192 631 770 periods of the radiation corresponding to the transition between the two hyper-fine levels of the ground state of the caesium 133 atom" [1]. This definition was considerably more accurate, as well as easier to calculate, than the Ephemeris time or Universal time standards (based on the Earths orbital period, and the mean solar day respectively [2]) that preceded the new atomic definition. The caesium definition has an uncertainty of around 10^{-10}, and has endured since its inception in 1967 even as current generations of clocks begin to push into the 10^{-18} territory [3]. There is now debate over when the next redefinition of time will take place, and if current technology levels are developed enough to facilitate this transition [4].

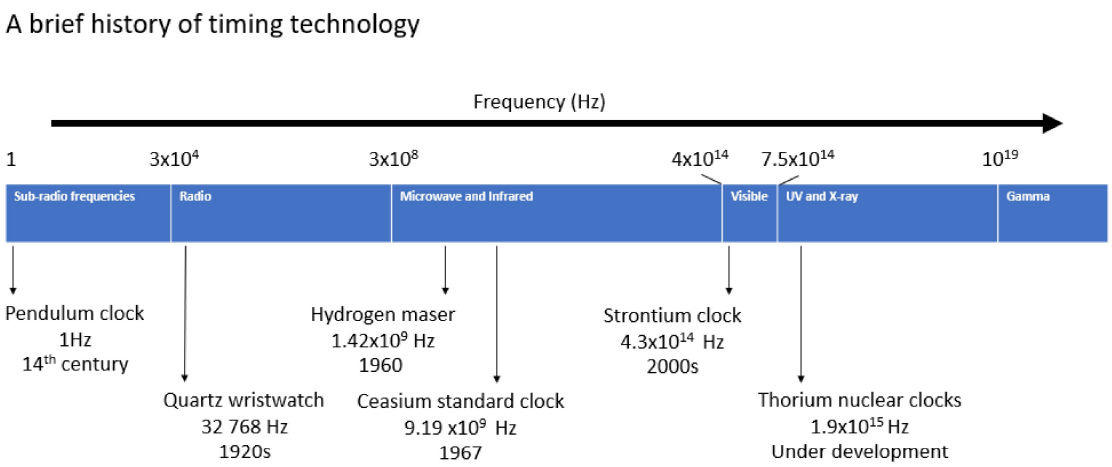

Figure 1.1 As each new generation of clocks was developed advancements were made in the frequencies that they oscillated at. As can be seen in the latter half of the 20th century till the modern day huge advances have been made in the frequencies that can be reached, coinciding with the development of stable laser technology among other things.

1.1.1 A brief timeline of timekeeping

At the heart of all timekeeping devices is some system that has a steady frequency, and from counting the oscillations of that system units of time can be derived. Early mechanical clocks used pendulums or wound springs to operate and, with daily upkeep, were accurate to a few tens of seconds per day. With modern machining methods these devices can be made to a much higher standard, only drifting by around a second every hundred days [5]. Mechanical timepieces were developed sometime in the middle ages [6], with multiple cultures working to develop accurate time pieces for regulating their days, and for naval navigation. The development of clocks to aid with navigation was often sponsored at the highest level, with governments offering large bounties to those who could develop accurate devices for use at sea [7]. A basic overview of timing through history can be seen in figure 1.1, with each new technology splitting time into smaller and smaller increments.

As technology progressed to the early 1920s crystal oscillators came onto the scene, these oscillators are now at the heart of most modern timing devices, being found in

nearly all digital systems that have internal clocks, such as wrist watches, computers, phones, and radios. The crystal oscillator operates through the deformation and relaxation of the crystal under the application of an external voltage.

Despite the maturity of the technology, crystal oscillators are limited by their crystalline nature. They are vulnerable to external factors such as changing temperature; the crystal will experience thermal expansion which affects its relaxation rate under the applied voltage [8]. The crystalline oscillator is also very difficult to accurately reproduce, as defects in the crystalline structure will change it's response to external stimuli, including the voltage used to drive the relaxation. These vulnerabilities in crystal oscillators are not large enough to affect most personal applications, such as wrist watches, but for applications that require higher levels of accuracy they render them unsuitable. An everyday quartz wrist watch will be accurate to a few tens of seconds a month [9], with higher precision devices needing to be sealed away from environmental factors in order to reach their ultimate accuracies and stabilities [10].

The common theme with all of the above clock technologies is the physical nature of the oscillator, the frequency of the device is linked to a mechanical change in a single physical system, the swinging of a pendulum or the physical deformation of a crystal. This leaves them vulnerable to environmental changes such as temperature or pressure, and also to physical wear and tear on the mechanisms that make them tick. For example material expansion in a pendulum clock due to temperature increase would cause each oscillation to take longer as the path length of the pendulum increases, and wear and tear on the gears in a clockwork device can cause skips and jumps between cogs.

First having been developed by Essen in 1955 clocks utilising atomic transitions quickly superseded traditional oscillator types in terms of accuracy [11]. Instead of using a mechanical oscillator, atomic clocks instead lock a resonator to the frequency of a specific atomic transition. Using an atomic system as the basis for a time piece gives several advantages over manufactured oscillators. As each atom of a particular

isotope is identical, unlike in a purely mechanical system where it is a near impossibility to exactly replicate a quartz crystal or other pendulum system. This means that any clock based on the same atomic transition should give the same frequency of oscillation, no matter where it is or how it has been constructed. Additionally atoms are also not vulnerable to the same wear and tear that mechanical components are subjected to, meaning that the same frequency will be obtained from a sample of atoms no matter when or where they are tested. Obviously the system surrounding the atoms will require maintenance to properly function over long periods of time, but the fundamental transition frequency of the atoms will not change over time.

Atomic clocks now come in myriad shapes and sizes, from the large fountain clocks currently defining time to smaller hydrogen masers and rubidium systems used on GPS satellites [12]. As a relatively mature technology atomic clocks have been brought down to small sizes [13] but are reaching the limit of the stability that they can reach, as they are limited by the transitions used.

The architecture of an atomic clock can vary significantly between designs. In the "fountain" clock design the atoms are first corralled into a sphere through a series of counter-propagating lasers. This process both confines and cools the atoms. Once in this sphere the atoms are pushed upwards through a microwave chamber through use of a pair of "launch" lasers, as the rest of the lasers are switched off [14]. As the atoms pass through the microwave chamber they are moved to a higher excitation state. At the end of the journey the atoms are interrogated by a probe laser to determine how many of the atoms moved to the higher excitation state. On the next pulse of atoms the microwave frequency is tuned slightly to try and maximise the excited atom population, by maximising the excited population a transition can be homed in on and locked to as the clock frequency. A common alternate method to the fountain design is using a vapour cell to hold the atoms in place [15]. As clocks using vapour cells are much smaller than fountain designs they are often used in applications where size, weight, and power are at a premium such as on satellites

[12].

Masers differ from atomic clocks as they do not use laser stimulated emission to drive the transition. Instead the maser (Molecular Amplification by Simulated Emission of Radiation) works through the confinement of an atomic gas (often hydrogen) within a microwave cavity; by applying tuned microwaves to the gas a feedback loop can be achieved to create an emission locked to an electron transition in the gas. In comparison to atomic clocks masers have very good short term stability, but a lower accuracy. Over short time scales the signal provided by a hydrogen maser will drift less than the signal from an atomic clock. This means that atomic clocks and hydrogen masers can be used in parallel, with each device shoring up the weaknesses of the other. The masers are often employed as "fly-wheels" to keep the frequency of the atomic clock from drifting during the dead time of an experimental cycle, and then the higher accuracy of the atomic clock is used to provide the actual value from the experiment. The frequency of the hydrogen maser lies at $1.42GHz$ with rubidium and caesium lying at $6.8GHz$ and $9.2GHz$ respectively [16].

For most everyday modern applications there is no need to go beyond a well made mechanical or crystal oscillator system, with more complex applications such as GPS requiring atomic systems. However by going beyond the microwave frequencies into the optical regime clocks transform from being merely devices for measuring time, and can be used for far more esoteric uses such as probing the stability of fundamental constants [17] and for mapping gravitational fields [18]–[23], amongst myriad other uses.

1.1.2 Optical atomic clocks

Optical atomic clocks are the next step in timing metrology. From a theoretical perspective they are remarkably similar to their microwave based predecessors. An

atomic transition is excited in order to create an oscillating system and a time signal is extracted from that. The key difference being the use of using atomic transitions in the optical frequency range instead of transitions with microwave frequency. Having a higher frequency results in a more stable clock, thus using an optical transition over a radio or microwave frequency increases the potential stability of a clock many times over. Designs for optical lattice clocks were proposed in the early 2000s, these designs removed the atomic fountain from the system and instead replaced it with a cloud of super cooled atoms in confined in a lattice trap [24]. Images of the atoms in an optical atomic clock system under construction are seen in figure 1.2. However in order to realise an optical lattice device several technological hurdles needed to be overcome.

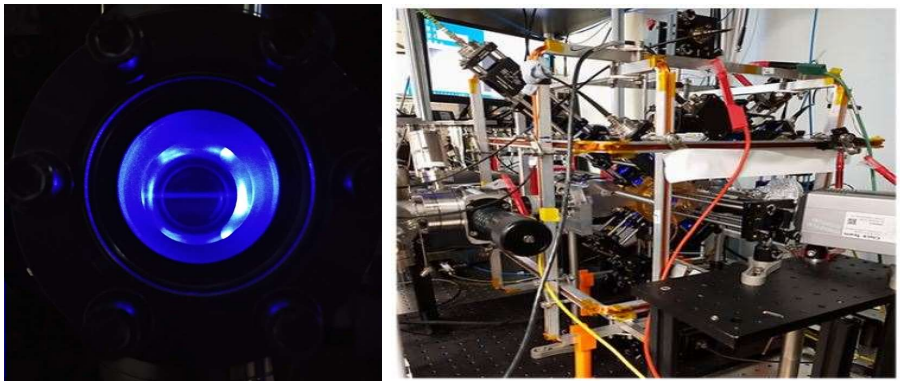

Figure 1.2 Photographs of an optical clock system. The first photograph shows blue fluorescence from a beam of strontium atoms taken on the iqClock system by the author. The second picture is of the atomic systems, reproduced from [25], for the iqClock project at the University of Birmingham. The image of the fluorescence was taken on the iqClock system at an earlier stage of development.

Key technologies for optical lattice systems

The shift from microwave to optical transitions complicated the system structure of atomic clocks. Firstly to explore these higher frequency transitions lasers must be available in the correct frequency range. For atoms such as strontium which have key cooling transitions the blue optical region, they could only be used in atomic

clocks once stable blue lasers had been developed around the turn of the millennium in order to properly control the atoms. The next hurdle to overcome is the high frequency of the transition itself. Although the use of optical transitions comes with many advantages over microwave transitions as outlined above, they make the measurement of the frequencies more complex. Electronic counters are not quick enough to measure such oscillations in the optical regime, and without a way of actually extracting a usable signal the clock is limited in its applications. Thus, as it is with many technologies, optical atomic clocks could only begin to be realised once an ecosystem of "building block" technologies had developed in order to construct them.

The ability to create an optical atomic clock is limited by many supporting technologies, some of which are briefly described below.

In order to take advantage of any optical transition the atoms must be well controlled and contained, before any measurements can be taken. This control requires several frequencies of highly stable, narrow linewidth, lasers with which to drive cooling transitions, provide trapping forces, and finally probe the clock transitions. The development of such laser systems was achieved relatively recently, and without which the process of making an optical atomic clock would be quite impossible [26]

Ultra high vacuum (UHV) systems are a necessary part of trapping the atoms- the atomic package in figure 3.3 is all under UHV conditions. In an UHV system the aim is to remove all background atoms other that the ones to be studied. This is especially important when trapping atoms in a system such as a Magneto Optical Trap (MOT) or a lattice, as the contaminant atoms will not be effected by the same laser cooling scheme and their high velocity can knock confined atoms out of the trap. These collisions reduce the number of trapped atoms and reduce the signal to noise ratio when taking transition measurements [27]. The fewer background atoms have left in the system when the clock species is introduced the less noisy the measurements will be.

The issue of measuring the optical frequency, when traditional electronic counters are unable to process such frequencies is solved by the use of a frequency comb[28]. The frequency comb works by providing an array of equally spaced microwave frequencies in a "comb". This can be thought of as a ruler for optical frequencies. By measuring the beat notes between comb teeth and the unknown frequency the unknown signals frequency can be determined. Taking the analogy of a grandfather clock, if the swinging of the pendulum is the atomic frequency, the frequency comb is the series of cogs that take that swinging oscillation and supply it to the clock face. A more in depth look at frequency combs can be seen later in section 3.6.1. Frequency combs in turn require a host of their own supporting techs, most notably mode locked pulse lasers. The size of frequency combs is currently one of the limiting factors in the development of truly portable optical atomic clocks, as modern examples have a large form factor and energy requirements, but steps are being made to reduce the size of these systems [29]–[32].

With all of these technologies each playing a key part in the smooth operation of the clock, there has had to be a whole ecosystem of related systems developed to allow the development of optical atomic clocks. By integrating the research and development of these systems with multiple industrial partners each handling a specific aspect of the clock, the pace of development can be increased. This collaborative system of working also ensures that the end pieces of kit can make the transition from lab to "real world" applications with less complications, as the real world had a hand in their development, and that the benefits of this technology can be utilised sooner.

Alternative technologies

One of the challenges facing optical atomic clocks is that many of the applications that they would be useful in are in very challenging environments, high vibration platforms such as aircraft or spacecraft and high pressure applications such as borehole telemetry [33], are both very difficult to control super cold gaseous atomic clouds in. To this end vacancies in crystalline structures such as diamond present attractive alternatives [34]. The benefits of using nitrogen vacancy defects in diamond include higher robustness to both pressure and temperature fluctuations in the environment. Unlike the crystal oscillators mentioned earlier the nitrogen vacancy cell systems do not have the same drawbacks as the oscillator isn't the crystal itself, but the atoms contained within defects in the crystal. This means that a deformation in the crystal due to a temperature change doesn't actually effect the atoms contained within. Nitrogen vacancy devices are not yet approaching the high stability levels seen in optical atomic clocks, as various technical challenges remain to be overcome, but present an potential alternative to traditional optical devices.

Although far from maturity there are projects currently looking into even higher frequency transitions in the nucleus of atoms that present the next frequency step after mastery of the optical regime [35]. Most of these plans are using isotopes of thorium as the nucleus in question, and plan to excite the transition through very high frequency ultraviolet radiation. This technology will require quite some time to reach maturity as it needs to develop stable UV lasers, and find ways to illuminate the nucleus directly and avoid any shielding effects from orbiting electrons. However if it can be realised then nuclear clocks show some promising theoretical advantages; much like the benefit of using an optical transition over a microwave transition the higher frequency of the nuclear transition increases the clock stability; added to this the nucleus is a solid object, and therefore much less influenced by external magnetic and electrical fields that the orbiting electron cloud is; finally nuclear clocks may be able to utilise solid blocks of matter with gamma radiation exciting the nuclei.

1.1.3 Applications of highly precise timing

The drive to gain ever more accurate instruments to measure the passage of time is down to the shear number of applications that rely on timing in many different sectors of the modern world. From an everyday perspective the applications of such accurate clocks are somewhat hidden, a clock with a stability of 10^{-16} is a somewhat excessive and expensive option for common household uses. However many technologies that are used everyday, such as GPS navigation, rely on atomic clocks in order to function [36]. Navigation is not the only function of the GPS either, as many devices use these satellites as a reference to keep their own internal clock accurate relative to each other [37]. Other applications of accurate timing in industry include the time stamping of financial transactions, to aid auditing and prevent fraud. Such transactions require that all the devices stamping them are correctly calibrated to the same master device which in turn needs to have a high stability (in the case of NASDAQ this is the NIST atomic clock in Boulder Colorado) [38], [39]. Broadcasting and communications networks also require the use of high precision timing. The deployment of optical atomic clocks is key to developing technologies in 5G networks and satellite internet plans as synchronisation of all aspects of the communication network is of major importance to keep different sectors of the system communicating with each other [40].

For similar reasons to communications networks the production and allocation of electricity in power grids also require accurate and stable time keeping systems. The use of high accuracy clocks can be used to detect faults and the overall stability of the system. The synchronisation of all aspects of the grid together requires multiple smaller clocks locked to a central master system [36]. For large power and communication networks that feature smaller clocks locked to a master clock to keep the distribution of time even throughout the system, a potential failure of the master clock could cause havoc as the smaller clocks will quickly de-sync with each other. To shore up this potential issue having back up transportable holdover devices that

can be quickly deployed and setup to provide a reference to the locked clocks is an important asset to have.

Optical atomic clocks are sensitive to all manner of electromagnetic and gravitational fields. Whilst this can be an issue when trying to isolate a pure clock signal with no perturbations, this sensitivity can be useful in certain applications. For instance the sensitivity of optical atomic clocks to changes in the gravitational field means measurement of the local gravity field is possible. Measurement of geodesy using optical atomic clocks could provide data about changing densities under the earths surface, which could be used to determine the water saturation level of the ground, potential sites for oil wells, or even the build up of magma that could precede a volcanic eruption [20], [23]. These are some of the major areas that accurate timing devices aid the smooth operation of modern society. But some of the most exciting applications are related to the investigation of fundamental sciences. Areas that can be investigated by highly accurate timing devices include measurement of the gravitational relativity, investigations into dark matter and energy, and the quantum sensing of fields [18], [41].

Distribution of time signals

In discussions of systems that are designed to be moved around there can be some confusion about what exactly is meant with terms such as transportable and portable. In this thesis the following definitions will be used: a static system is one that is built into a laboratory and cannot be moved to a new location without extreme effort; a transportable system is one that can be disassembled into subsystems relatively easily for transport via vehicle, and can be easily set up on the other end with tools; finally a portable system is one that can be easily moved from point A to point B with no requirement for tools during this process. An example of a static system might be a clock investigating fundamental constants in a lab, a transportable system might be a clock designed as a calibration machine for other systems, a portable

system might be designed to fit on a drone or to be used in a moving van.

Moving the time signal is a key part of any system that involves atomic clocks. A time signal is of limited use if it cannot be disseminated between devices. Within a laboratory setup or integrated system this can be achieved through the use of optical fibres. Between cities and longer distances the use of fibre optics becomes more difficult and necessitates the use of signal booster stations [18], [37], [42] to keep the signal strength up. These links are key to keeping smaller devices stable over long periods of time. By checking them against a more stable system, any drift in the clocks can be accounted for and corrected without much issue.
Transportable systems can be used as holdover devices should a static station breakdown, or a satellite go down meaning that the ground devices link to it no longer have their master connection. The transportable system in this application could be quickly moved to where it is needed and set up to cover the absence of the dedicated system whilst repair or replacements are being completed. Portable clocks can be placed upon drones or in satellites, there they can act to calibrate other subsystems or to aid in navigation. Especially in places where GNSS is denied (such as underwater navigation) an accurate on board clock is paramount to successful exploration. The sub-sea vehicles need to remain in synchronisation with each other and the base vessel on the surface in order to determine where they are relative to each other[43]–[45].

1.2 iqClock

The iqClock project is an international European consortium of academic institutions and industry partners working together to help develop the next generation of optical atomic clocks. The collaboration of these groups aims to bring optical atomic clocks from the laboratory to real world applications in compact and transportable

form[46]. The experimental work in this thesis took place on the University of Birmingham testbed system [25]. This clock is being built by University of Birmingham with the aim of comparing it to the clocks with systems developed by industry partners. Thus the University of Birmingham system is not in itself going to be a portable system, but instead be a reference to other systems. This makes it an ideal place to test various improvements to the building of clocks and the impact of these improvements on the construction, running, and performance of a clock. Examples of such developments include the application of an ultrablack coating to the inside of the MOT chamber to reduce background light [47], and the use of a miniaturised version of the Zeeman slower based on previous work in the LRI (Long Range Interaction) project also being run at the University of Birmingham.

1.3 Thesis layout

This thesis will be mostly concerned with the production and capturing of the cold atoms, with some later focus on linking clocks and optical fibres. Chapter 2 will investigate the stability and uncertainty of clock, and will investigate the errors that are present in such a system. Chapter 3 will give a rundown of what makes a good atomic candidate for an optical atomic clock and then the physical system that are built to get from an atomic sample to a time signal. Chapter 4 will look in detail at Zeeman slowers and the characterisation of the iqClock Zeeman slower and investigations into the reduction of stray magnetic fields over the MOT region. Chapter 5 is an overview of the MOT coils used for the iqClock testbed system and an investigation into the eddy currents that can form in them. Chapter 6 looks at communication between clocks for the purposes of creating clock networks and the reduction of phase noise in fibre optics that link clocks over large distances. Chapter 7 gives a brief mention to some of the other projects worked on over the course of the PhD and the outlook for the iqClock testbed system.

Chapter Two

Stability, uncertainty, and sources of errors

2.1 What is a Clock?

Simply put a clock is a device that converts the oscillations of some regular system into a usable format for telling time. For instance in a grandfather clock the regular swinging of the pendulum is converted to a readable time on the clocks face through a system of cogwheels and gears, or the orbits of the earth around the sun casting shadows on a sundial. In an atomic clock the oscillating system is an atomic transition driven by a laser, with the cogwheels being the systems used to control the laser and extract the signal from the atoms. All clocks share a series of traits; namely stability, accuracy, and uncertainty; that determine what applications they could be used for. It is the pursuit of more refined values of these traits that drives the move from one technological system to the next.

2.1.1 Qualities of a clock

In order for a clock to be useful then certain qualities of it must be well understood. For certain applications perhaps the ultimate accuracy is not so critical compared to the long term stability, or that the uncertainty in the measurement is within

allowable limits.

- Accuracy: The accuracy of a clock determines how close to the true unperturbed value of the clock transition of our target atom that a system can reach. An example of a factor affecting accuracy would be stray magnetic and electrical fields shifting atomic energy levels away from their rest state.

- Stability: The stability of a clock system is the measure of how similar each measurement is to other measurements on the same system. In a system with low stability the value of the second will drift away from the expected value over time.

- Uncertainty: The higher the uncertainty of a system the larger the range of values the measurement lies in. The uncertainty is a measure of how well understood the processes are that will affect the reading of the transition, either through direct shifting of energy levels, relativistic effects changing the measured result, or errors in the system leading to shifts in the measured result. Reduction of uncertainty requires careful design and characterisation of the system to identify factors that might shift the transition frequency or cause errors in the measurement of said frequency.

- Allan Variance: Allan variance is the measure of frequency stability of a timing system [48]. The Allan variance measures how the noise in the frequency signal of the clock varies over time. For a white noise variance will average down over time, the faster this is achieved the better the stability of the clock is.

2.1.2 Clock Stability

As mentioned above the stability of a clock is its ability to continue giving the same measurement over time. This value might not be the closest possible to the true value of the atomic transition being used, but it will remain constant over many

clock cycles. High short term stability is one of the reasons that hydrogen masers are still employed alongside other atomic clock designs that may have higher accuracy.

The stability of a clock comes from two sources, the inherent properties of the oscillator; and the system built around the oscillator. For instance in the hydrogen maser the short term stability is good compared to a caesium atomic clock thanks to the hydrogen transitions high quality factor, but its long term stability suffers as the resonance frequency of the cavity will drift due to physical changes caused by environmental factors such as vibrations or temperature changes .

The fundamental instability of an optical atomic clock, disregarding shifts caused by the system, can be seen in equation 2.1

$$\sigma_y(\tau) \approx \frac{\Delta\nu}{\nu_0\sqrt{N}}\sqrt{\frac{T_c}{\tau}} \tag{2.1}$$

$\sigma_y(\tau)$ is the instability, with Δv being the line width of the clock transition, v_0 is the oscillator frequency, N is the number of atoms probed in a single measurement taking time T_c, with τ being the averaging period. This equation immediately reveals why the frequency of the oscillator is so key in improving the stability of a clock system. By increasing the value of v_0 from a microwave to an optical frequency the instability of the system is decreased. It also shows that any potential clock transition requires a narrow linewidth and a shorter cycle time as reduction of the Δv and T_c values helps to further reduce the instability. The final major factor important in the stability of the clock system is the number of particles interrogated at once, N. The factor $\sqrt{N}$ is the quantum projection noise, the greater the value of N the greater the signal to noise ratio in the measurements [49]. Equation 2.1 assumes that the only noise process is white noise. As white noise is random over many measurements this can be averaged down to zero, but other noise sources do not behave in this way and must be accounted for. To take into account for other unavoidable noise sources such as the noise of the probe laser ,γ, the RMS fluctuation in the atom number,σ_N, or noise caused by detecting the photons emitted from the atoms, $n_p h$ (the photon

shot noise); additional terms are added to 2.1 to receive:

$$\sigma_y(\tau) = \frac{1}{\pi Q}\left(\sqrt{\frac{1}{N} + \frac{1}{N n_p h}\frac{2\sigma_N^2}{N^2} + \gamma}\right)\sqrt{\frac{T_c}{\tau}} \tag{2.2}$$

[50]

As can be seen from 2.2 each additional noise source adds a new term to the equation. The first term is the quantum projection noise, the second the photon shot noise, the third the noise caused by atom number fluctuation, and the fourth the noise in the probe laser. The first three terms all depend on the number of atoms probed, and the larger the value on N the smaller the instability. As scaling the number of atoms indefinitely to increase stability is unfeasible, other methods to reduce these terms can be taken. Although the quantum noise limit is a fundamental part of any high sensitivity system it can be undercut through methods outlined in [51] and [52]. In strontium the photon shot noise can be reduced through driving the $^1S_0 - ^1P_1$ state repeatedly whilst the atom is in the excited $^3P_0$ clock state. By driving this transition multiple times multiple photons are received per atom, reduces the value of this term, often below the quantum projection noise floor. The fluctuation in the atom number is best reduced by measuring the populations of the ground and excited clock states and determining how this changes over different measurement cycles. This value can then be normalised against the atom number fluctuation to provide a base with which to calculate the noise emanating from this source [53]. Reduction in the laser source is the only one that does not stem from the atoms themselves, and thus cannot be solved from within the science chamber. Much of this noise stems from the fact that the system is not constantly interrogating the atoms, and the laser must maintain its frequency during the preparation phases of the experiment. Using dual system where atoms are always available to be interrogated as in the NIST Yb system [3] will help to reduce this noise. Alternatively a non destructive measurement of the atoms could be used as in [54]–[56].

2.1.3 Allan variance

Allan variances were developed during the 1960's to help characterise metrology systems [48].

The two sample Allan variance (AVAR) used for clocks can be written as:

$$\sigma_y^2(\tau) = \frac{1}{2}\langle(\Delta y)^2\rangle = \frac{1}{2\tau^2}\langle(\Delta^2 x)^2\rangle \tag{2.3}$$

Where τ is the averaging time, and Δy and Δx are the variances in the frequency and time domains respectively [57]. AVAR is used to characterise the frequency drift in clocks and frequency standards. The Allan deviation (ADEV) is the square root of the AVAR. AVAR has a limitation in the time domain that at certain bandwidths it becomes difficult to determine what is flicker noise and what is white noise. Thus the Modified Allan Variance (MVAR) was developed, by post measurement variance of the bandwidth the flicker noise can be seperated from the white noise. MVAR is used to determine the performance of time distribution systems [57]. The final version of AVAR is the Time Variance (TVAR). TVAR is used to determine the synchronisation errors in telecommunication networks [58].

2.2 Errors from fundamental shifts

The aim for optical atomic clocks is to provide a new era of highly accurate, stable time keeping devices. To this end the sources of errors in such devices must be well understood, characterised, and minimised. For a static lab based system these sources can be more easily identified and controlled for than a portable system out in the field. For a portable system one of the major challenges is to create a robust system that is relatively insensitive to changes in the environment without adding too much to the SWAP profile (Size Weight and Power).

Fundamental shifts are those that directly effect the observed transition within the atom. Either directly shifting energy levels as in the case of electromagnetic or

gravitational fields (EMG fields) that pass through the MOT region, or from effects that change the observed transition in the lab reference frame, such as Doppler shifts.

2.2.1 Zeeman shifts

As exploited by the Zeeman slower, external magnetic fields cause shifts in the energy levels of the atom. Whilst useful in the cooling and trapping stages of the experiment, these shifts are unwanted when trying to determine the true unperturbed clock transition of the atom.

Both first and second order Zeeman shifts must be accounted for when designing a clock to reach the furthest limits of accuracy. The Zeeman effect describes the influence of an external magnetic field on the atomic energy levels in an atom. The first order frequency shift caused by magnetic fields on the internal structure of the atom is given by,

$$\Delta\nu_{first} = \delta g_J m_j \mu_B B/h \tag{2.4}$$

Where $\mu_B = e\hbar/2m_e$ is the Bohr magneton, and m_j is the magnetic quantum number. The number of spectral lines formed is dependant on the orbital angular momentum quantum number l, as $m_j = [-l, ...0... + l]$. The value δg_J is the difference in the lande g factor between the ground and excited states of the transition being looked at. By choosing clock transitions with $m'_j = m_j = 0$ the first order Zeeman shifts can be suppressed [59].

However the second order Zeeman shift arising from the interactions between the triplet states in the atom under the effect of an external magnetic field cannot be so easily suppressed. For an atom with triplet states, such as strontium or ytterbium, separated in energy by $\Delta E_{trip}h$, the second order Zeeman shift is given by [60], [61]:

$$\Delta\nu_{second} = \frac{2\mu_B^2}{3\Delta E_{trip}h^2} \tag{2.5}$$

For most applications the second order shifts are so small as to be negligible, but

when probing the potential variance of fundamental constants or investigating dark matter then it is necessary to take them into account.

Suppression of magnetic fields can be either active or passive. An example of active suppression might be compensation coils built around the system with sensors to adjust the current through them to provide a counteracting magnetic field depending on the amount of external magnetic field at any one time. For passive methods magnetic shields provide an alternative to powered active methods by reducing the magnetic field through an area through concentric layers of highly magnetically conducive material such as μ metal [62], [63]. On the science chamber MOT coils are used in the initial stages of trapping in the red and blue MOT stages, these coils can then be turned off once the atoms have been confined within the final, purely optical, stage of trapping. A further passive reduction in magnetic fields can also be achieved by building the science chamber away from sources of magnetic fields. Sources of potentially disruptive magnetic fields may be electronic devices or from elements of the system such as a Zeeman slower. Building the system so as to maximise the distance between the sources of fields and the science chamber can go a long way to reducing the need for shielding, as was found during the construction of the iqClock testbed system explored in more depth in Chapter 4.

2.2.2 Stark shifts

In much the same way that magnetic fields induce Zeeman shifts in the atoms, electrical fields also cause shifts in atomic energy levels. Stark effects can arise from a variety of sources, including build up of static charge on system components and shifts from the laser fields.

For stark effects originating in the broader electronics of the system the best method to reduce these effects is to keep superfluous electronics off during the measurement phase and to mount such systems as far away from the science chamber as possible.

Stark shifts from laser fields .

The stark shift caused in a transition from an electric field comprised of components E_i and E_j is given by:

$$\Delta\nu_{stark} = -\frac{\frac{1}{2}E_i E_j \alpha_{ij}}{h} \tag{2.6}$$

With α_{ij} being the polarisability coefficient of the atom currently being investigated. This polarisability constant is the key aspect that controls how an atom responds to an electric field, and can be split into three tensors; α^S the scalar factor, α^V the vector contribution, with α^T being the tensor[53].

Under normal circumstances the scalar contribution is largest with,

$$\Delta\nu_{scalar} = \frac{-\alpha^S E_o^2}{4h} \tag{2.7}$$

and can easily produce frequency shifts on the order of a MHz in a clock transition. As an optical lattice is an integral part of the clock system, holding the atoms in place whilst they are being probed, it would seem that this stark shift would be inevitable. However if the lattice wavelength is tuned close to the so called "magic wavelength" the α^S contribution can be neutralised. At the magic wavelength the stark shift on the transition shifts both the ground and excited states by the same value and in the same direction, this results in a net zero change in the transition value. By using a magic wavelength for the optical lattice the stark shift on the transition effects both the ground and excited state by the same amount in the same direction, leading to a net change of zero in the energy between the energy levels [64], [65].

The vector contribution of the polarisability constant is tied to the polarisation of the laser field that the atoms are present in.

$$\Delta\nu_{vector} = -\alpha^V \frac{m_f}{2F}\xi\frac{E^2}{2h} \tag{2.8}$$

ξ is the measure of the ellipcicity of the field, with a value of ± 1 for circular light and 0 for linear. For a 1D lattice this ellipcicity can be relatively easily controlled but when scaled up to a 2 or 3 dimensional lattice then interactions between the electric field vectors can lead to variations in the polarisation across the lattice [53]. Thus the contribution from the vector atom polarisability has to be well understood and factored into the signal processing as it cannot be entirely removed [65], [66].

The final contribution from the polarisability, α^T, contributed to the stark shift through the angle, θ', formed between the quantisation axis of the atoms and the polarisation axis of the light field.

$$\Delta\nu_{tensor} = -\alpha^T \frac{3m_f^2 - F(F+1)}{F(2F-1)} \frac{3cos^2\theta' - 1}{2} \frac{E^2}{2h} \tag{2.9}$$

Usually the effect of this tensor contribution is small [54], [67], but can be reduced further through careful set up of the system.

The introduction of laser field stark shifts does not only arise from the lattice field. Any light atom interactions can cause shifts on the atomic transitions. For instance interactions with the probe laser can also cause stark shifts and broadening of the clock transition. The intensity of this laser is the key factor in the amount of stark shift that is produced, the higher the intensity the larger the shift. Currently the uncertainty of this effect between the 10^{-17} and 10^{-18} level [60]. An increase in laser coherence time [68], [69] and techniques to reduce clock transition sensitivity [70], [71], are the next steps to reduce the effects of these stark shifts. Finally any light reflected off surfaces in the system can cause shifts in the atomic transition [47], and the light can cause noise in the measurement stage.

DC Stark shifts .

If static electrical fields are allowed to build up in the chamber then they can also cause Stark shifts. Which will have similar perturbations on the atomic transitions as stark shifts induced by black body or laser radiation. It is relatively simple to

ground metallic components such as vacuum chambers and connectors, but the build up of static that can occur on non metallic optical windows or other components is much more difficult to disperse. Static charges on non-grounded components can linger in the system for days. The effect of such build ups is usually minor at around the 10^{-17}, but in poorly grounded systems can reach 10^{-13} [72].

Stark shifts from black body radiation .

Black body shifts are caused by the thermal black body radiation emitted by objects that have thermal energy [73]. As there will always be some thermal energy present in the clock architecture there is no complete way to remove BBR from the system. This thermal radiation causes AC Stark shifts in the atom. The frequency shifts arising from the BBR can be written as:

$$\Delta\nu_{BBR} = \frac{-\Delta\alpha_s\langle E^2(T)\rangle}{2}[1+\eta(T^2)]/h \tag{2.10}$$

Where T is the radiative temperature from the system currently affecting the atoms, η is the dynamic correction factor, and $\Delta\alpha_s$ is the static polarizability. The term $\langle E^2(T)\rangle$ is given by

$$\langle E^2(T)\rangle = \epsilon_0^{-1}\int_0^\infty \rho(\nu)d\nu \tag{2.11}$$

Where $\rho(\nu)$ is the spectral density given by the Plank formula,

$$\rho(\nu) = \frac{8\pi\nu^2}{c^3}\frac{h\nu}{e^{\frac{h\nu}{k_BT}}-1} \tag{2.12}$$

Each of these factors must be well understood to estimate the effect that the temperature is having on the atoms. A large component of the uncertainty in this shift is due to the fact that it is very difficult to accurately estimate the temperature T at the point where the MOT is forming [53].

2.2.3 Doppler shifts

Doppler effects arise from the movement of the atom causing a change in the observed atomic transition frequency to the transition frequency in the atom's reference frame. Reduction of Doppler effects is one of the key reasons for slowing, cooling, and trapping the atoms. Having the atoms at rest means there will be no difference in the emitted radiation between the atoms or observers reference frame. The equation for the Doppler shift in the frequency is as follows;

$$\delta\nu = \mathbf{k}.\mathbf{v} - \frac{1}{2}\nu_o\frac{\mathbf{v}^2}{c^2} \mp \frac{\hbar\mathbf{k}^2}{2m} \tag{2.13}$$

Where $\mathbf{k}$ is the wave-vector of the emitted photon, ν_o is the atomic transition frequency in the atomic reference frame, and $\mathbf{v}$ is the atomic velocity vector.

Each term of equation 2.13 is formed of the Doppler shifts to be considered when dealing with the atoms. The first term is the Doppler shift from the atoms movement. This term is based on the thermal distribution of velocities of the sample, and causes a Gaussian broadening of the measured transition. It is this term that is most reduced by the cooling and trapping of the atoms into an optical lattice. The second term is the second order Doppler shifts. These second order shifts are asymmetric in nature and are much harder to remove even with trapping and cooling of the atoms, often requiring sub-Doppler cooling regimes to reduce the effects [74]. The final term are the recoil effects from the emission of the photon. For obvious reasons this cannot be reduced or removed, and thus must be taken into account for in the final measurements [75].

The first optical systems were based on Ca and Mg, and were very similar to the Cs clocks previously built, with the atoms interrogated within a vapour cell or as they were released from a MOT [14]. Neither of these techniques were very effective at suppressing the Doppler shifts, as the atoms were free to move during the clock interrogation phase. Trapping the atoms within the MOT during the interrogation phase is not ideal as the Zeeman effect induced in the atoms from the magnetic fields

comprising the MOT will perturb the clock transition. Optical lattices are instead used to confine the atoms without the need for magnetic fields, and using the magic wavelength mentioned earlier, do not affect the transition frequency through the stark effect either. The trapping potential of an optical lattice is small compared to the MOT, and so the atoms must be cooled as much as possible before the lattice phase in order to keep as many atoms trapped as possible [76].

Although there are mechanisms through which Doppler effects can be reintroduced to the system, such as through tunnelling between lattice sites [56] and interference between the optical lattice and the clock laser [77]; these effects can be suppressed relatively simply through keeping lattice sites non degenerate, and through active and passive control of the lasers used.

2.2.4 Dipole interactions/ cold collision shift

These are perturbations induced into the atomic transitions by collisions between the atoms in the sample itself. One of the benefits of neutral atomic clocks is that the high number of atoms in the sample means that the signal to noise ratio is very high, but this same large number of sample atoms is also the cause of uncertainties in the value of the atomic transition. This leads to a trade off between the higher stability afforded by higher atom numbers, and the greater accuracy achieved when the atoms are not interacting with multiple neighbours. The fundamental process for the origin of these shifts is the same as that which gives rise to Van der Waals forces, the deformation of atoms orbitals in response to the repelling presence of another atoms electron cloud. This deformation gives rise to short lived dipoles where the negative charge on the atom is concentrated on one side of the nucleus. To reduce the chances of a collision and thus the shift in energy levels efforts are made to separate the atoms as much as possible. In an ideal world each lattice site would contain only one atom at the time of measurement. Whilst this helps to remove the effects of close contact between atoms there is still the question of long range dipole effects,

and whether these also need to be accounted for, it is this question that the Long Range Interaction (LRI) project at Birmingham is seeking to understand [78]. The cancellation of these cold collision shifts is one of the key areas of research for groups looking to set new records with the accuracy of their clocks [79], [80].

2.2.5 Gravity shifts

The local gravity of a region is the specific gravitational field at a precise location, and has an effect on the measurements taken by an atomic clock. The gravitational field between two points on the earths surface will vary depending on a variety of factors. An example of a factor that would affect the local gravity is dense, heavy material in the Earths crust in that location. An area with an abundance of dense material would have a higher gravitational field than an area with a less dense crust composition, even if the locations were otherwise identical. The effect the local gravity will have on the measurements provided by a clock is predicted by the general theory of relativity [81], [82], whereby the measurement of the passage of time in a region with a stronger gravitational field will be slower than the measurement performed in a region with a lower gravitational field. The shift in the frequency due to this effect is as follows;

$$\frac{\nu^{'} - \nu_o}{\nu_o} = \frac{g\Delta h}{c^2} \tag{2.14}$$

For a change in height of $\Delta h = 10cm$ the resultant shift is around 10^{-17}. As this is a very minor shift only the most accurate clocks can detect it. This leads to the ability to use clocks to measure geodesy [20] through the determination of the difference in gravitational field as measured in separate locations; and to investigate the relativistic shifts caused by gravity itself [83]. However the gravitational shift is not under measurement when attempting to make a clock network for applications such as searching for the effects of dark matter or the gradual change of fundamental constants [84], and must thus be factored in as an error to the measurement. Unlike magnetic fields, there is no way to "shield" against gravitational fields. Thus the

best way to factor in the gravitational effect is to understand the gravity field in that region. This shift is temporally static for any physical position of the clock, and will only change as the clock itself is moved into areas with a differing gravitational field. As long as the clock is static in location, so too will be the gravitational shift. Thus if the gravitational field can be accurately understood at a location the effect it has on the clock measurement can be calculated and accounted for.

2.3 Errors from the system

These are processes that do not affect the atom itself, but through their influence will cause instability in the laser systems or other parts of the architecture.

Material creep and thermal expansion

There are two major sources of warping that may occur in a given system. Firstly material creep will occur in components that are under high levels of stress. This may cause delicate components to bend and deform. The solution to this is to take care in the design of the system to prevent stress points in the architecture of the system. The other major source of physical deformation is thermal expansion; a material subject to varying temperatures will expand and contract as the temperature rises and falls. This can be exacerbated as materials with different thermal coefficients will expand and contract different amounts over a temperature range causing unequal expansion/contraction. Materials under high temperatures will also warp under lower levels of stress than they would at lower temperatures. Laser cavities are at high risk of thermal expansion, as any movement will change the optical path length and therefore the laser frequency.

Other than reducing the mechanical stress on components and controlling the temperature in the environment, these effects can be reduced deliberately building with materials chosen for their thermal coefficient for example using spacers in a cavity

which have a very low expansion when exposed to rising temperatures. The geometry of such components can also make a large difference in the amount of expansion that it undergoes in response to temperature fluctuations.

Vibration

External vibrations can come from a variety of sources. From construction work on the floor below, the lab door shutting too violently, or the whirring of a computer cooling fan. Each of these sources can introduce vibrations into the system that can alter path lengths, disturb laser systems, and introduce noise into optical fibres. For each vibrational source they must first be characterised, minimised, and compensated for. For example in the iqClock lab at Birmingham a Wilcoxon 731A Seismic accelerometer was used to find the quietest area, and areas to avoid building high sensitivity experiments. For instance, if the lab door closes with force then building a high sensitivity experiment next to the wall the door is in may not be the ideal space for it. Reduction of vibrations can be tackled in multiple ways depending on the source of the vibration. For instance the footsteps of people walking across the lab floor can be reduced by the introduction of damping table legs, and the impact of a heavy door closing can be reduced by adjusting the closing mechanism. Each mitigation method may not completely remove all vibration from a source, but all reductions in vibration are to be desired.

2.3.1 Errors in the iqClock system

The iqClock system uses many of the techniques outlined above to reduce the effects of errors in the system. To suppress and understand the vibrational contributions in the iqClock lab at Birmingham a Wilcoxon 731A Seismic accelerometer was used to find the quietest area, and areas to avoid building high sensitivity experiments. Additionally the optical tables were outfitted with shock absorbers, and the door to the lab was modified to prevent it slamming. As the temperature of the lab was set

to a constant level the thermal expansion effects that would affect the system were from individual components heating up whilst running. These were mounted away from the atomic package to prevent conduction into the system.

To suppress and control fundamental errors the first step was to mount magnetic compensation coils around the volume where the atoms are to be interrogated. This will suppress any stray magnetic fields from electronic equipment or other sources from entering this region and perturbing the transition. Static stark shifts are prevented by grounding the system and shifts from reflected light are prevented by an ultra-black coating on the inside of the chamber. As the system is not planned to be a test of ultimate accuracy and is to be static in the lab, the gravitational field and therefore gravitational shift will be constant and does not pose an issue in this iteration of the project, but will have to be considered should later iterations want to delve into testing the variation of fundamental constants.

Chapter Three

Overview of an optical clock system

3.1 iqClock

The iqClock project is an international European consortium of academic institutions and industry partners working together to help develop the next generation of optical atomic clocks. The collaboration of these groups aims to bring optical atomic clocks from the laboratory to real world applications in compact and transportable form, and to investigate the potential of supper-radiant clocks [46].

The experimental work in this thesis took place on the University of Birmingham (UoB) testbed system. This testbed clock is being built by UoB with the aim of comparing it to a clock with components developed by industry partners, also to be constructed at UoB. Whilst the UoB system is not in itself going to be a portable system, but instead be a reference to other systems. This makes it an ideal place to test various improvements to the building of clocks and the impact of these improvements on the building and running of a clock. Such developments include the application of an ultrablack coating to the inside of the MOT chamber to reduce background light and the use of a miniaturised version of a Zeeman slower used in the LRI project also being run at the university of Birmingham.

3.2 Choice of atom

In order to make an optical atomic clock there are two things that are absolutely vital: a source of atoms, and sources of laser light. The first choice that should be made then is which atomic species to be used, and from that, which lasers must then use to manipulate the atoms and take measurements using them. This section will look into what makes a good candidate for an atomic clock, how strontium fits those criteria, and what other atoms could fill that position.

The first choice to be made, before the species of atom is chosen, is whether to use ions or neutral atoms. The benefit of using an ionic candidate over a neutral one is that ions are more easily manipulated and trapped through magnetic and electric fields due to their innate charge, and can thus be easily isolated to be interrogated as a single particle. This leads to a very accurate signal with greatly reduced inter-sample interactions. Conversely neutral atoms are more difficult to manipulate, and it is difficult to load a single atom only into each trap site, but the increased number of atoms interrogated at once improves the signal to noise ratio of the clock [53], [85].

3.2.1 Attributes of a good atomic candidate

A good candidate for the atom species to be used as an oscillator in an atomic clock should have the following attributes.

- A high Q factor (quality factor).

  A Q factor is a measure of how good an oscillator is at remaining stable.. With a high Q factor oscillations will remain constant for a long time. Thus a high Q factor is an important consideration for a clock as it governs how stable the clock will be and the drift it will suffer. The Q factor is the frequency of the atomic transition over the transition linewidth, $Q = \frac{\nu_o}{\delta\nu v}$; where ν_0 is the output frequency and $\delta\nu$ is the frequency line width. Thus it can be seen that

an ideal clock transition has both a high frequency and narrow linewidth. The linewidth used in the calculation of the Q factor is normally the "natural" one for the transition, but as there are elements that may perturb this such as time dilation Doppler shifts or magnetic fields, the observed linewidth can be used. Thus the Q factor for an atom can be improved via control of these elements and the stability of the clock can be increased [86].

- Clock transition which is relatively insensitive to external fields.

  Having an insensitive clock transition means that the clock is naturally resistant to external factors that could perturb the value of the transition. The more resistant a transition is to external magnetic and electrical fields among other affects, the easier it is to get to an accurate value for the clock transition.

- An internal structure that allows easy cooling and trapping.

  With easy to access transition frequencies, ground state magnetic moments. The easy availability of key transitions is a major factor in the choice of which atoms to use, an atom might have a perfect clock transition, but if the atom can't be manipulated and trapped then this single perfect transition is functionally useless. This final point is determined by the technology available at the time the clock is being developed, and is why the progression to optical transition frequencies was only possible with the advent of laser and measurement technologies that could interact and extract information from such high frequency transitions.

Ideally an atom would have all three of the above points to be a good candidate for atomic clocks. Alkali elements such as Cs and Rb are often used in modern commercial clocks, along with the hydrogen maser, which uses a slightly different process to reach its frequency standard.

3.2.2 Alkaline earth metals

Alkaline earth metals are the natural choices to supersede alkali elements as they possess higher frequency transitions that remain relatively insensitive to external fields. Access to their internal structure was limited until blue high stability lasers were available around the turn of the millennium [26], and methods were developed to measure these transitions, as traditional electronic systems used in microwave regime clocks are too slow to react to the optical frequencies. The technologies required to achieve the measurement of the optical transitions, frequency combs, will be investigated in more detail in chapter 3.

Alkaline earth metals are good candidates for optical atomic clocks for the following reasons; insensitive narrow linewidth clock transition, high Q factor, magic wavelength for trapping, and an easily accessible efficient cooling transition.

Electronic structure of strontium

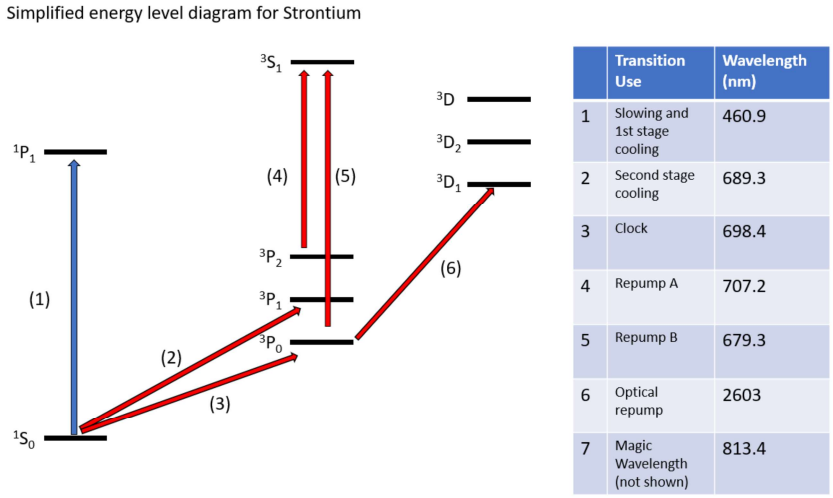

	Transition Use	Wavelength (nm)
1	Slowing and 1st stage cooling	460.9
2	Second stage cooling	689.3
3	Clock	698.4
4	Repump A	707.2
5	Repump B	679.3
6	Optical repump	2603
7	Magic Wavelength (not shown)	813.4

Figure 3.1 Simplified schematic of the energy diagram for strontium. The line widths for the the first and second stage cooling transitions are 32MHz and 7.5 kHz respectively. The clock transition in comparison has a linewidth of only 1 mHz. This allows for much better accuracy on the timing measurement over using either of the other two transitions.

Figure 3.1 shows an energy level diagram for Sr, this diagram with a few adjustments to the energy of the transitions can be applied to other Alkaline earth metals such as Yb and Hg. The $^1S_0 - {}^1P_1$ transition (labelled (1) on the diagram) is ideal for laser cooling and trapping for numerous reasons. It has a short lifetime, allowing fast absorption/ emission cycles, has very few branching decays, and those electrons that do weakly decay from $^1P_1$ to the ^3P triplet can be accessed through re-pump lasers to return them to the main cooling cycle. This decay is weak enough that experiments can be run without re-pump lasers for this transition, but including them increases the lifetime of the trapping stage of the experiment. For Sr the first stage cooling is performed on the $^1S_0 - {}^1P_1$ which lies at a wavelength of 460.9 nm. The fact that this transition is in the blue range of the optical spectrum also held back development of systems using Sr until the blue laser technology was sufficiently powerful and stable enough to drive the transition effectively. This transition cannot be relied upon solely to cool the atoms to a lattice trap-able temperature however, as the relatively large linewidth of 32 MHz leaves it with a high Doppler cooling limit. Thus a second stage cooling ((2) on the diagram) is used to reach lower μk temperatures suitable for loading into a lattice. Additionally this first stage cooling transition is not completely closed. This means that electrons can fall from the $^1P_1$ to the $^3P_2$ or $^3P_0$ instead of the $^1S_0$. If the atom has an electron in the $^3P_2$ or $^3P_0$ then it does not participate in the cooling cycle, thus repump lasers at $707nm$ and $679nm$ are needed to return the atom to the main cooling cycle, these lasers are labeled (4) and (5) in figure 3.1. The clock transition for these elements is naturally very narrow, which improves the Q factor, and thus the stability of the clock. Not shown on the diagram is the magic wavelength. The existence of a magic wavelength in strontium allows it to be used in optical lattice setups without the need for complex post processing to calculate the stark shift from the laser fields. Taking all these factors together strontium is an attractive prospect for optical atomic clock systems. Strontiums easy to manipulate cooling cycle and its narrow linewidth, along with

the relative ease of handling and natural abundance vs ytterbium or mercury, are reasons it has been chosen for use in the iqClock system.

3.2.3 Other atomic candidates

It is not just strontium that can be used in cold neutral atom clocks, many other elements can be used, if their electronic structure allows. Along with strontium, ytterbium and mercury [87], [88] are the most commonly used alkaline earth metal candidates for neutral atom clocks; but other candidates such as calcium [89], magnesium [90] and beryllium [91] also show some signs of being potential avenues for investigation.

Each of these candidates have their own challenges and quirks in electronic structure, and before taking into account different isotopes of the same element which will also change the electronic structure within atoms of the same element. Certain spins only exist in any great abundance in certain elements, for example the nuclear spin $\frac{1}{2}$ Yb^{171} is a considerably simpler system to work on than the nuclear spin $\frac{9}{2}$ Sr^{87} [68]. Ytterbium has also shown promise in intruiging systems that use two clock transitions within the same atom [92]. The choice of atom informs the sort of system that is going to be built. For an investigation into the fine structure constant α, the dual clock transition in neutral yterrbium may be better suited, but the maturity of strontium technology makes it an attractive proposition for building benchmark systems, as is the case for the iqClock testbed.

3.2.4 Isotopes, Fermions, and Bosons

Once an element has been chosen there is one more decision to be made, which isotope to use? Both fermionic (particles with non integer spin of $\frac{1}{2}$, $\frac{3}{2}$...), and bosonic (integer spin) isotopes of an element will exist, each changing the internal electrical structure of the atom. The first thing to factor in is the relative natural abundance of the isotopes of an element. For example in strontium there are four naturally occurring

stable isotopes with the following abundances; Sr^{88} is the most abundant with a occurrence of $\sim$ 83%, followed by Sr^{86} at $\sim$ 10%, then Sr^{87} at $\sim$ 7%, and finally Sr^{84} at $\sim$ 0.5%. This would suggest that for ease of use that Sr^{88} is the ideal isotope to use as it has the highest abundance. For for a sample of natural strontium most of the sample would be lost if the system were to use an isotope other than Sr^{88}, and samples artificially enriched with a different isotope are expensive compared to natural strontium.

However, the fermionic nature of Sr^{87} makes it an attractive prospect. Fermionic species are easier to excite without the use of external fields, and suffer smaller systematic shifts than bosonic isotopes [59]. When constrained in an optical lattice fermions experience much lower degrees of cold collision shift due to Pauli blocking of the s-wave collisions [65], [93].

The downside of using such a fermionic system is that it is more sensitive to first order Zeeman effects, although these can be averaged over two transitions with opposite dependence's [94]. Additionally the hyperfine splitting present in fermions can make the slowing and trapping laser architecture more complex. Taking the example of Sr^{88} and Sr^{87}, the cooling cycles in Sr^{87} are complicated by this splitting. The nuclear spin on Sr^{87} is $I = 9/2$, and the angular momentum J value for the $^3P_2$ is 2, so taking $F = J+I...J-I$ in integer steps, the splitting of the $^3P_2$ state is $F = 13/2$, 11/2, 9/2, 7/2 and 5/2.

The atoms in the cooling cycle that may decay to the $^3P_2$ state from the $^1P_1$ can now fall down into any of these five states. This means that the $707nm$ laser that would usually prevent this dark state from forming has to be modulated using an Electro Optical Modulator (EOM) or similar technique to scan over the range of frequencies necessary to stimulate all of the $^3P_2$ dark states. This range encompasses a few GHz. For Sr^{88} there is no nuclear spin so this splitting of the $^3P_2$ state does not occur, meaning that the EOM scanning is not necessary. The difference in the cooling cycle on the $^3P_2$ transition between Sr^{88} and Sr^{87} is described in figure 3.2.

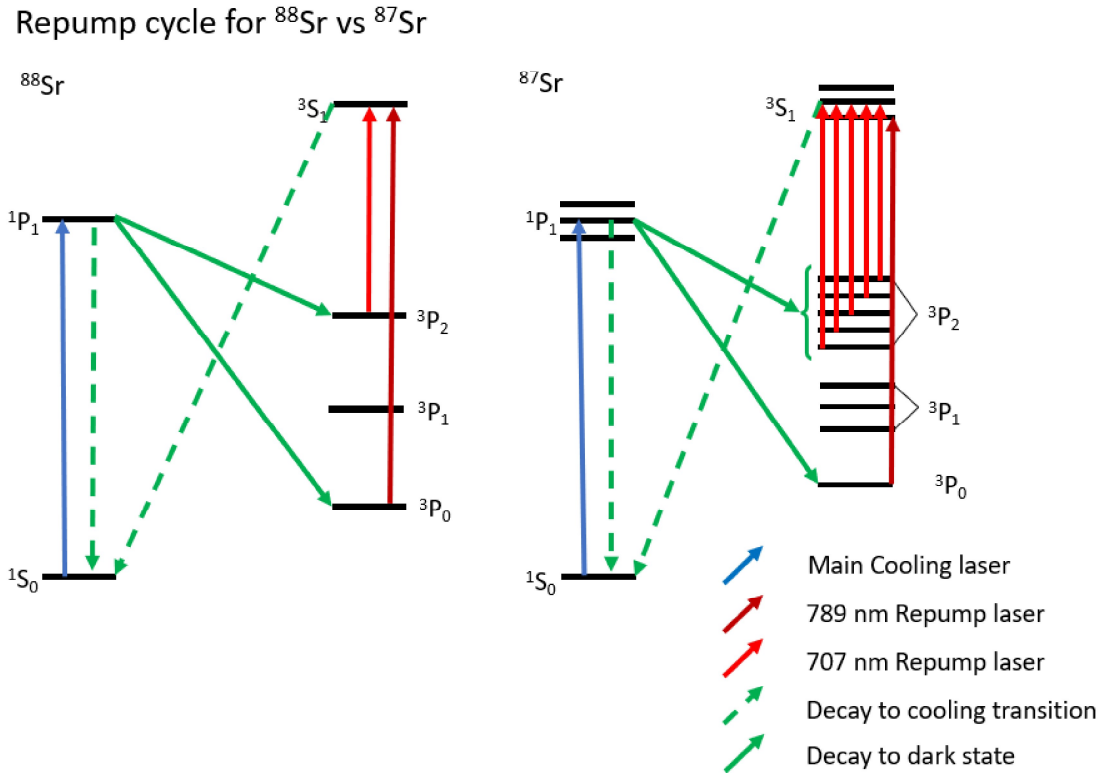

Figure 3.2 Diagram showing the difference in splitting between Sr^{88} and Sr^{87}. The key difference is the splitting on the $^3P_2$ in Sr^{87}, meaning that the frequency of the $707nm$ re-pump must be scanned over a range to promote any electrons in this dark state back into the cooling cycle. Not shown on the diagram for clarity are the $^1D_2$ states that the electrons pass through to the $^3P_2$ and $^3P_0$ dark states.

Thus it can be seen that although the bosonic isotope Sr^{87} is much more readily available, the fermionic nature of Sr^{87} gives it a natural advantage in lower systematic shifts. However both bosonic and fermionic isotopes hold promise of interesting results and highly stable systems should the problems presented by their nuclear spins be sufficiently overcome [93], [95].

3.3 Sections of an optical atomic clock system

With the choice of atomic species made, and an understanding of where and what errors can creep into our clock; design of the rest of the system can commence. The function of a clock into three broad areas.

- Production of the atomic beam
- Trapping and cooling of atoms
- Interrogation of atoms and the extraction of a usable signal

These areas can be seen in figure 3.3. The atomic package is the where the items in the list above take place, but only with the input and control of the other system blocks. The atomic package itself is under UHV to prevent contamination from outside atoms, so access for the lasers is through optical windows in the system. The placement of these windows and the light that they allow through must be carefully considered in the design stage of a clock system to allow laser interactions to occur where they are needed.

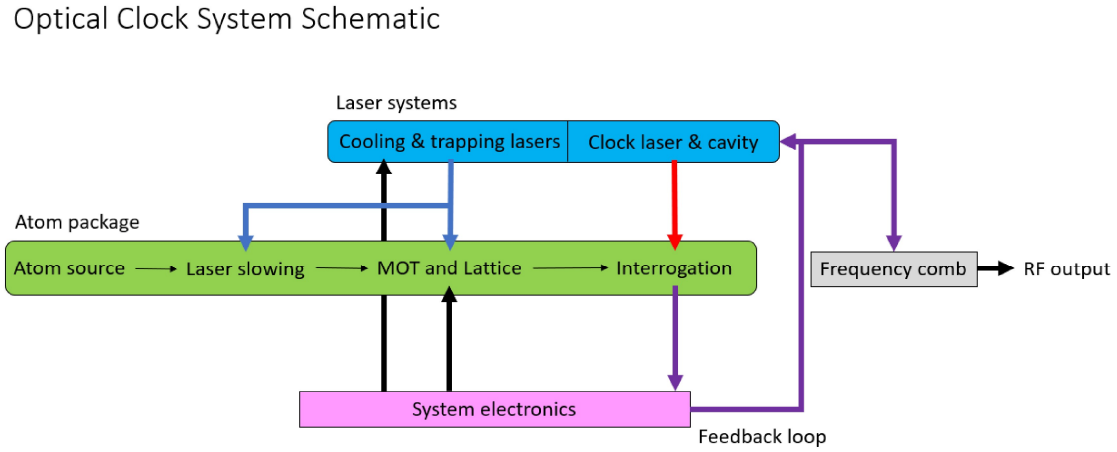

Figure 3.3 A stylised schematic of an optical clock system. Showing the key structures necessary to build an optical clock system. The atomic package (in green) is where the production, slowing, trapping, cooling, and interrogation of the atoms takes place. The lasers necessary for this are transferred to the atomic package via fibre optics or free space optical links. The electronic systems and frequency comb keep the lasers on resonance and extract a usable signal from the optical frequency.

3.4 Production and slowing of an atomic beam

In order to probe the transitions of atoms for use in time keeping devices a sample of atoms must be contained in such a way as to reduce thermal effects and minimise the effects of perturbations. The process of production and containment starts with a sample of the atomic material in question and ends with an ultra-cold cloud of individual atoms trapped in an optical lattice. In brief this process goes as follows; an atomic beam source produces a beam of hot atoms, these are then slowed to a trappable velocity and contained in a magneto optical trap, this trap then collects and cools the cloud to ultra low temperatures suitable for loading into an optical lattice. Within this lattice the atoms have very little thermal energy and are insulated from other atoms and external fields, ideal for interrogation. It is once the atoms are in the lattice that the probing of the clock transition and measurements can take place.

3.4.1 Production of the atomic beam

In order to capture atoms for study, you first need to produce a sample of the atoms in question. For some clock systems a vapour cell of atoms can be used to contain a permanent cloud of atoms that can be probed at any time. This method is often used in masers or compact atomic clocks [82], [96]. However for high accuracy systems the atoms require cooling, and containment in a vapour cell leaves too many hot atoms within the system that can knock cold trapped atoms out of a lattice. Thus for cold atoms systems the atoms must be produced separately for each trap that is to be formed.

The most common method for the production of neutral atoms in cold atoms experiments is the use of an atomic oven. In this oven a sample of the atomic material is heated up to a point where it vaporises. As vapour inhabits more space than the solid material this cloud of hot gas attempts to expand, a small opening in the oven is the only escape route for this expanding gas, resulting in a beam of hot atoms exiting

the oven. In order to prevent a spray of atoms, and to collimate the beam, methods such as rifling and capillary networks are used to keep the beam size constant [97]. Dispensers are very similar to ovens in that they too heat a sample to a vapour, which then exits through a small opening. The primary difference between the two methods primarily being one of scale. With dispensers being smaller, cheaper, and requiring less power than a full fledged atomic oven, but conversely not giving such good beam collimation or atomic number [98].

Production of a strontium beam

One of the issues with using strontium in an optical atomic clock system is that it has a relatively low vapour pressure. This low vapour pressure requires that the oven operates at a high temperature to get a useful flux of atoms. As high temperatures are not ideal for a system that is sensitive to thermal effects, steps must be made to compensate for this. Often this issue is solved through the use of UHV vacuum to prevent the convection of heat through the system, but this means that the process of removing and replacing an exhausted oven requires breaking vacuum and re-baking the system. Other methods for isolating the oven include the installation of a glass or ceramic thermal break between the oven and the vacuum chamber [99]. These methods are a good way of reducing the conducted heat from the oven effecting the rest of the system, but the radiated energy from the oven is in a direct line with the trap being formed. Unlike ions, a thermal beam of neutral atoms cannot easily be persuaded to turn a corner, so other methods must be used to reduce this source of back body radiation. The first and simplest is to have an aperture that cuts off the atomic beam from the MOT region, thus also cutting off the direct line for the thermal energy. The aperture itself will however heat up and become its own source of BBR. Another method is to first trap the atoms in a 2D MOT, and use this MOT as the new source of the atoms. The benefit of this method is that the 2D MOT can be loaded from a transverse direction, essentially meaning that the

atomic path from oven to interrogation chamber has a 90° angle. This removes the oven from direct line of sight of the interrogation chamber, reducing the BBR [100]. Other methods for producing atoms from solid samples are also being researched in regards to strontium to avoid the issues caused by the high temperature of the ovens and dispensers required to form the atomic beam. Techniques where atoms are released from a surface via resonant laser light are an interesting area of research at the moment [101], [102]. Such a system would potentially allow atoms to be loaded directly from a source mounted within the MOT chamber itself, reducing the size of the system; and reducing the amount of thermal energy present in both the system and the atoms by removing the heating elements used in an oven or dispenser.

For the iqClock system a standard atomic oven is being used, as the previous efforts in the group to investigate the laser assisted atom production had not yet produced results when the system was being designed. Thus the atomic beam being produced is moving at hundreds of meters per second when emitted from the oven, and will require considerable slowing to the tens of meters per second required for trapping.

3.4.2 Slowing the atomic beam

Laser cooling of atoms is one of the most powerful tools currently available to atomic physicists [103], [104]. With this method atomic temperature can be reduced to a fraction above absolute zero, allowing them to be trapped and studied in unprecedented detail. The first step of reaching these ultra low temperatures is slowing the atomic beam. Out of the oven atomic beams are moving at hundreds of meters per second; an oven temperature of 450 degrees needed to produce strontium atoms leads to the average atomic speed in the beam being around 450 m/s [105]. The momentum of the atoms in this beam is far too much for the magneto optical traps and lattices used in the physics chamber to contain, thus before reaching this section

of the system the atoms must have their velocity reduced to around 60 m/s.

Laser slowing

Laser slowing is the process by which the hot atomic beam out of the oven can be slowed down by counter propagation with a suitably detuned laser beam [103], [104]. Laser slowing is one of the key building blocks for any cold atoms experiment as the velocity of the atoms out of the oven is too great for the forces present in the trapping region, and only a very low percentage of atoms will be confined. Thus the process of laser cooling greatly increases the number of trapped atoms by reducing the atoms velocity, allowing them to be trapped for further cooling. In strontium the transition used is between the $^1S_0$ and the $^1P_1$ with a wavelength of 461nm.
The momentum exchange between the counter propagating slowing laser and the atoms they are interacting gives a radiative optical force;

$$\boldsymbol{F} = d\boldsymbol{p}/dt = \hbar \boldsymbol{k} \gamma_p \tag{3.1}$$

[106]
In this process the atoms absorb counter-propagating photons, this results in loss of momentum $\hbar k$ in the direction of photon propagation, and the promotion of an electron from the $^1S_0$ to the $^1P_1$. As the atoms can only absorb photons whilst they are in the ground energy state the force is dependant on γ_p, the excitation rate of the atomic transition, the faster the atom excites and de-excites the more photons it can interact with in a set time period, meaning a larger total force. As the atom de-excites it remits the photon in a random direction, gaining a momentum kick of $\hbar k$ in the direction opposite to photon emission. It can be seen that over many cycles of absorption and emission that the atoms will slow in the direction of propagation due to the directed absorption, but the random direction emissions will add no net momentum to the atom.
One of the main difficulties with slowing an atomic beam is one of detuning. In order

for the photons to interact with the atom the atom must "perceive" the photon of having the correct wavelength in its reference frame. As the atoms are moving opposite to the photons there is a considerable Doppler effect to contend with. Thus the detuning of the laser, $\delta = \omega_{laser} - \omega_{atom}$, must be changed to account for the Doppler effect caused by the velocity of the atoms, $\omega_D = -\boldsymbol{k}.\boldsymbol{v}$. This gives us a more in depth look at the atomic excitation rate;

$$\gamma_p = \frac{\Gamma}{2}\frac{S}{1 + S + (2(\delta + \omega_D/\Gamma))^2} \tag{3.2}$$

If this is plugged into equation 3.1:

$$F_{Rad} = \frac{\hbar k \Gamma}{2}\frac{S(z)}{1 + S(z) + 4(\delta_0 + kv)^2/\Gamma^2} \tag{3.3}$$

[107]

Γ is the transition line width, and $S(z)$ is the local saturation parameter given by $S(z) = I(z)/I_s = I(z)/(\pi hc\Gamma/3\lambda^3)$, where $I(z)$ is the local light intensity and I_s is the saturation intensity. It can be seen that the maximum radiative optical force is when $\delta = \omega_D$. From 3.1 the maximum deceleration of an atom of mass M can be calculated as:

$$a_{max}(z) = \frac{\hbar k \Gamma}{2M}\frac{S(z)}{1 + S(z)} \tag{3.4}$$

The force however is not constant throughout the slowing region. As the atoms slow, the amount of Doppler shift they produce is reduced, meaning that $\delta - \omega_D \neq 0$. This reduction in Doppler shift leads to the atoms moving out of resonance with the slowing laser. The slowing cycle ceases when the atoms can no longer interact with the laser when the Doppler shift has been reduced by a significant fraction of the transition line width Γ. In order to keep the atoms in the cooling cycle for longer it is therefore necessary to compensate for the reduction in Doppler shift as the atoms slow. This can be done directly by chirping the laser over the range of frequencies necessary to interact with all speeds of atom present in the beam. However this is

difficult to accurately control, and means that only certain atoms are being excited by the laser at any one moment in time. In order to keep all atoms on resonance with the laser at once it is possible to introduce different amounts of Doppler compensation by manipulating the atomic energy levels by different amounts throughout the slowing region [108]. This can be achieved through the use of a device called a Zeeman slower, which will be investigated in more depth in the following section.

An additional complication can come from the electronic structure of the atomic species being used. Atoms promoted to an excited energy state will often have multiple routes for the electron to de-excite, passing through many energy states before returning to the ground state. If the electron falls into a long lived state between the excited and ground states then it will no longer be able to interact with the slowing laser, this is known as an optical dark state. As any electron in the ground state will be promoted via the slowing laser, even if the chance of it then falling to the dark state is very low on any one cycle, the chance of it ending up in the dark state increases with the number of cooling cycles the atom goes through. Repump lasers are required to promote electrons out of dark states up to another excited state from which they will then decay back to the initial ground state, and thus re-enter the main cooling cycle.

Slowing lasers for the iqClock system

The lasers required for slowing are the main slowing laser, which provides the optical force to retard the atoms, and repump lasers necessary to keep the main slowing cycle going. In the strontium electronic structure seen in figure 3.1 there are potential dark states that electrons in the cooling cycles can fall into, i.e. the cooling cycle is not completely sealed. An atom that falls from the $^1P_1$ to the $^3P_2$ or $^3P_0$ state will no longer be stimulated by the $461nm$ first stage cooling laser. Although the chance per cycle that an electron falls into one of these long lived dark states is low, if it occurs that atom can no longer be interacted with by the cooling laser and will experience

no more slowing. As there are millions of atoms experiencing many many cooling cycles the number of atoms that get trapped into these dark states is significant. In order to keep electrons from being trapped in these dark states, and to thus improved the efficiency of the slowing process, additional repump lasers are used to promote electrons out of these states and back up to the excited state of the cooling transition. These repumps promote atoms from the $^3P_2$ and $^3P_0$ up to the $^3S_1$ state via a $707nm$ and $679nm$ laser respectively. The lasers needed to drive these cycles can be seen on in figure 3.1.

3.4.3 Zeeman slowers

The manipulation of atomic energy levels to keep them on resonance with the laser is commonly achieved through use of a Zeeman slower. A Zeeman slower, as the name suggests, uses the Zeeman effect to keep the atoms on resonance with the laser [107]. The Zeeman effect is the removal of degeneracy in atomic states with different magnetic moments under the application of an external magnetic field. A description of the shifts caused by the Zeeman effect is shown in section 2.2.1. For the Zeeman slower on the system energy shifts caused by the first order Zeeman effect are of interest, the second order shifts being much smaller with the magnetic fields produced by a Zeeman slower. A Zeeman slower is a device added to a cold atoms system to increase the slowing of an atomic beam through application of the Zeeman effect. The Zeeman slower provides a spatially varying magnetic field across the slowing region, ensuring that the laser remains on resonance with the atoms at all points [109].

With this energy shift induced from the Zeeman effect, the force on the atoms is dependant on the magnetic field along the beam path, $B(z)$, as well as the velocity of the atoms.

$$F = \frac{\hbar k \Gamma}{2} \frac{S(z)}{1 + S(z) + 4(\delta_0 + kv + \mu' B(z))^2/\Gamma^2} \tag{3.5}$$

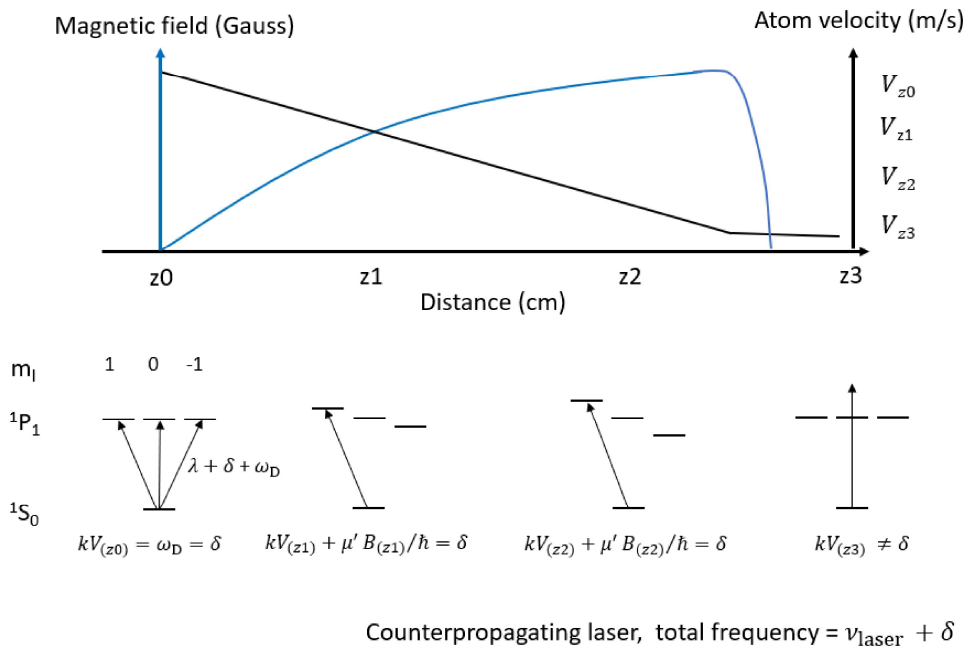

Figure 3.4 A diagram showing the splitting of the $^1P_1$ state under a magnetic field and how the splitting keeps the atoms on resonance with the slowing laser as they are slowed. At the end of the slower the atoms abruptly come out of the magnetic field and and out of resonance with the laser, this prevents them from being pushed back up the slower by interactions with the laser.

Where μ' is the effective magnetic moment. As seen earlier, in order to have the maximum slowing force on the atoms it is required that $\delta_0 + kv + \mu' B(z) = 0$. If the detuning δ_0 is kept constant the changing magnitude of $\boldsymbol{k}.\boldsymbol{v}$ as the atoms slow can be compensated for by changing the splitting effect $\mu' B(z)$ by adjusting the magnetic field.

By applying a spatially varying magnetic field over the slowing region the atoms will experience different magnitudes of Zeeman splitting at different points along the slowing path, this is calculated to offset the decrease in Doppler shift and to keep the laser on resonance with the slowing atoms, a diagram for this concept is presented in figure 3.4. An ideal magnetic field profile for a Zeeman slower is given in figure 4.7a.

The deceleration possible in the Zeeman slower is not the maximum calculated in

3.4. If the maximum force is applied to the slowing it makes the slowing process unstable [110]. As the beam of atoms is not at a perfectly homogeneous velocity at any point, any atoms that reach a point with a velocity higher than the beam is tuned to will not feel the full decelerating force, leading to atoms being lost from the slowing lasers influence, potentially taking other atoms with them. To create a more stable slowing with higher efficiency an acceleration $a = \epsilon a_{max}$ where ϵ is a factor between 0 and 1 used to reduce the force on the atoms is used. When ϵ is 1 maximum slowing occurs, but the process is unstable, by reducing this to between 0.75 and 0.6 much more stable slowing is achieved, without sacrificing too much of the deceleration. At this new value of deceleration any variants in the atomic velocities present at any point are compensated for by varying deceleration's at different points [108], [111].

From equation 3.5, the maximum force on the atoms is present when the total detuning given by $\delta_0 + kv + \mu^{'} B(z)) = 0$, giving a maximum deceleration as given in equation 3.4. By setting up the factor epsilon to produce more stable slowing a deceleration of $a = \epsilon a_{max} = \epsilon \frac{\hbar k \Gamma}{2m} \frac{S(z)}{1+S(z)}$ is achieved. Assuming that this deceleration is constant the length of the slower necessary to slow the atoms from initial velocity v_0 to a trappable velocity can be calculated:

$$L = \frac{v_0^2}{2a} = \frac{v_0^2}{\epsilon \frac{\hbar k \Gamma}{2m} \frac{S(z)}{1+S(z)}} = \frac{m v_0^2 (1 + S(z))}{\epsilon \hbar k \Gamma S(z)} \tag{3.6}$$

From this and the deceleration value the velocity at any point along this slowing length assuming maximum deceleration can be described.

$$v(z) = v_0 \sqrt{1 - \frac{z}{L}} = v_0 \sqrt{1 - \frac{z \epsilon \hbar k \Gamma S(z)}{m v_0^2 (1 + S(z))}} \tag{3.7}$$

From this calculation of the velocity at each point the amount of Doppler shift compensation required at each point along the slower can be calculated to keep the atoms at the chosen deceleration value.

$$kv(z) = \pm \mu^{'} B(z)/\hbar \tag{3.8}$$

$$B(z) = \pm\frac{\hbar k}{\mu'} v_0 \sqrt{1 - \frac{z\epsilon\hbar k\Gamma S(z)}{m v_0^2 (1 + S(z))}} \tag{3.9}$$

With this new value of the deceleration resonant velocity at each point along the slowing axis can be calculated as

$$v_{res}(z) = \frac{(\mu' B(z))/(\hbar - \delta_0)}{k} \tag{3.10}$$

This then feeds into how much force is needed to slow the atoms,

$$kv(z) = kv_{res}(z) - \frac{\Gamma}{2}\sqrt{(1 + S(z))\frac{1 - \epsilon}{\epsilon}} \tag{3.11}$$

Which leads to the deceleration being,

$$a(z) = \epsilon\frac{\hbar k\Gamma}{2M}\frac{S(z)}{1 + S(z)} \tag{3.12}$$

By using the above equations a magnetic field profile can be designed with accompanying laser power and detuning necessary to slow the atoms to a level where they can be efficiently trapped, an ideal Zeeman slower profile can be seen in figure 4.7a. Although it is possible to trap atoms without use of a Zeeman slower, as was done in the MiniClock experiment at Birmingham [112], if the experimental structure allows it is desirable to install one in order to trap atoms more efficiently. Once the atoms have been slowed, with or without the use of a Zeeman slower, they can then be trapped. The designs for the iqClock system Zeeman slower can be seen in chapter 4.

3.5 Trapping and cooling of atoms

The need for cold atoms comes from the desire to increase measurement times, reduce Doppler shifts, and reduce inter atom collisions in atomic experiments. This technology is key not just in clocks but in other areas of quantum technology such as computing or interferometry.

3.5.1 Magneto Optical Traps

Once the atoms are slowed via laser slowing they need to be confined within a volume of space to allow interrogation with probe lasers. The trap works by having a velocity dependant aspect to the trapping force, along with a position dependant aspect. The velocity dependant aspect is provided by interaction of the confined atoms with a laser field, with the position dependant aspect coming from an quadrupole magnetic field placed over the trapping region. The Magneto Optical Trap (MOT) uses both of these forces to confine the atoms and is a key technology in capturing atoms for further cooling and interrogation.

Velocity dependant force- Optical Molasses

The velocity dependant aspect is formed by the overlap of three orthogonal counter-propagating laser pairs detuned from the $1S^0 - 1P^1$ trapping transition. If the atoms are moving towards a laser, then the Doppler shift will cause that laser to be in resonance with the atoms and a force will be felt slowing their progress away from the centre of the trap. However if the atom is not moving at the an interact-able velocity then the atoms will experience no force from the laser and will drift out of the trapping region. This set up is called an optical molasses, as it only slows the atoms rather than providing a restoring force back to the centre of the trapping region. To calculate the velocity damping of an optical molasses equation 3.3 can be applied to two counter propagating circularly polarised beams so that $F_{OM} = F_{Rad\sigma+} + F_{Rad\sigma-}$. Assuming that by this point the atoms have been slowed then $kv << \Gamma$ and the following equation is gained:

$$F_{OM} \approx \frac{8\hbar k^2 \delta S v}{\Gamma[1 + S + (2\delta/\Gamma)^2]^2} \tag{3.13}$$

When the lasers are detuned below the atomic transition (δ is negative) the atoms experience a damping force on their motion, but are not yet truly trapped, as there is no restoring force. The optical molasses force will act on the atom only as long

as the Doppler shift caused by the atoms motion brings the atomic transition into resonance with the detuned laser, once this shift has been changed by the slowing of the atom the force F_{OM} will be lost. This means that an atom travelling slowly enough to not interact with the lasers would eventually find itself drifting out of the trapping region. A diagram of this process can be seen in figure 3.5.

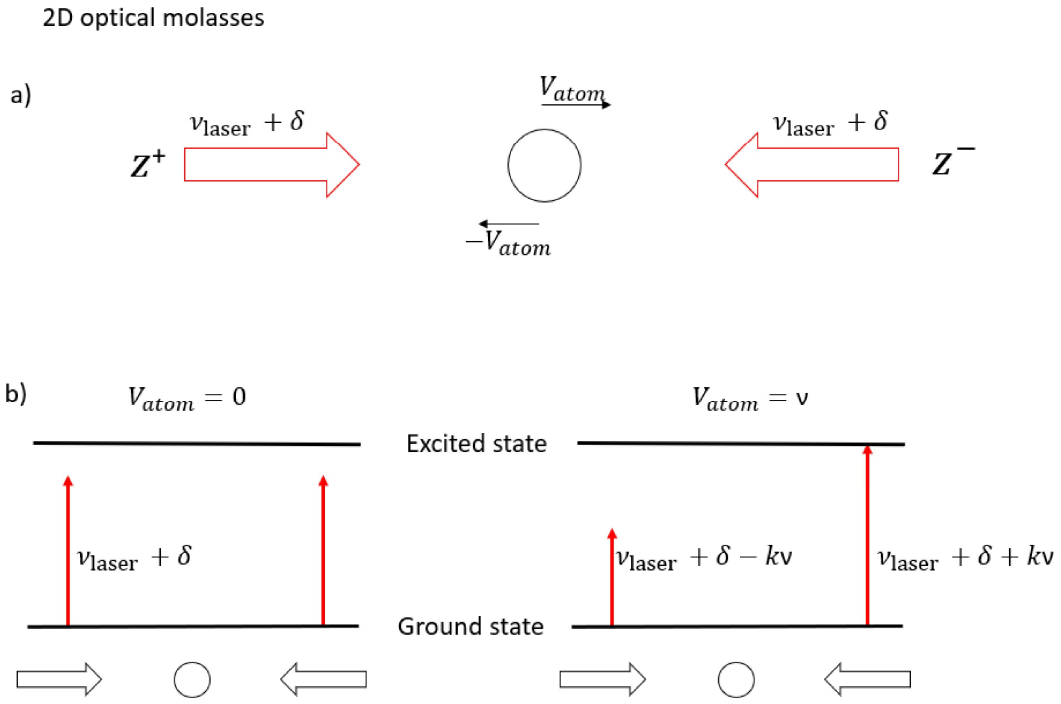

Figure 3.5 Diagram of a 2D optical molasses. a) shows the set up of the molasses, with an atom being illuminated by a pair of counterpropagating beams along the z axis. In this set up only velocity components along the z axis would expreience F_{OM}. In order to slow velocity components along the x and y axes additional laser pairs along those axes woulf be installed, making a 3D molasses. b) shows the process by which an atom with a positive velocity component along the z axis will find itself only interacting with the counter-propgating beam.

Formation of a MOT

To provide true trapping a position dependant aspect is required. A quadrupole magnetic field is applied over this optical layout, this magnetic field removes the

degeneracy of the Zeeman sub-levels and shifts the energy levels more the further the atom drifts from the centre of the trap. Thus as the atom moves from the centre, no matter its velocity, at some point it will hit resonance with the trapping laser and be pushed back to the centre of the trapping region. The layout to produce this can be seen in figure 3.7. If an atom is moving out of the trap centre towards the $\sigma-$ beam, the increase in magnetic field as the atom moves from the centre will shift the $m = 0 - m = -1$ transition such that it will begin interacting with the laser. At the same time, this splitting is moving the atom further from resonance with the $\sigma+$ beam parallel to the atoms motion. This leads to unbalanced forces between the two lasers that moves the atom back into the centre of the trap. This process is analagous to the process by which the Zeeman slower works.

Including the magnetic term in 3.3 returns:

$$F_{\sigma+,\sigma-} = \pm\frac{\hbar k\Gamma}{2}\frac{S}{1+S+[2(\delta \mp kv \mp \mu' B(z)/\hbar)/\Gamma]^2} \tag{3.14}$$

Where the effective magnetic moment $\mu^{'}$ is given by $\mu^{'} = g_e m_e - g_g m_g$. g_e and g_g are the Lande factors for the excited and ground states respectively, with m_e and m_g being the magnetic numbers of those states. As with equation 3.13, assuming that the splitting given by $\mu^{'}B/\hbar$ and kv are small compared to δ then:

$$F_{MOT} = -\beta v - \frac{\partial B}{\partial z}\frac{\mu'\beta}{\hbar k}r \tag{3.15}$$

where $\beta = \frac{8\hbar k^2 \delta S}{\Gamma[1+S+(2\delta/\Gamma)^2]^2}$. This force is what returns atoms to the centre of the MOT should they begin to drift. MOTs are ideal for capturing atoms out of an atomic beam and cooling them to μK temperatures, but they are unsuitable for the interrogation step of the clock cycle as the presence of magnetic fields causes Zeeman shifts in the clock transition [113].

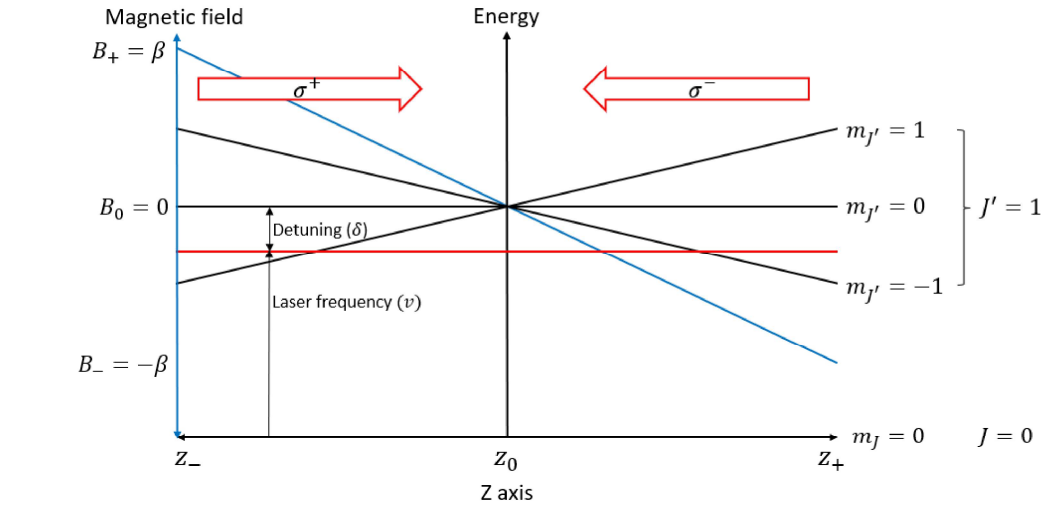

Figure 3.6 A diagram showing the energy levels in a simplified 2D MOT. As the magnetic field varies with z so does the splitting on the J' state. The larger the value of z the larger the magnetic field and thus the magnitude of the splitting. A magnetic field of β will cause the same magnitude of splitting as a field of $-\beta$ but with the order of the $m_{J'}$ reversed, with the $m_{J'} = 0$ level experiencing no shift. As the magnetic field is zero at z_0 the $m_{J'}$ states are degenerate. The shifting of the $m_{J'}$ levels with B_z is what causes the position dependant aspect of the trapping.

3.5.2 Laser orientations

For a 3D MOT setup three pairs of counter propagating beams are required, but how to reach this is up dependant on the purpose of the system. Many older systems use three beams that are then retro reflected through a quarter wave plate to form the counter propagating beam pairs. Although this works well, it can be cumbersome to set up and align the beams to cross correctly, a viualisation of the necessary beams optics can be seen in figure 3.7. As machining technology has improved however there are other methods to get a usable beam layout. One is to use a large single beam to illuminate four prism mirrors to form a MOT in the centre of them, as shown in figure (3.8)The benefits of such a MOT layout is the requirement for only one laser beam, as the rest of the beams are provided by reflections off the prism mirrors. This is a naturally much more compact system, and is thus suited for portable and transportable systems where space is at a premium. The potential rigidity of the system is also higher, as the mirrors are fixed in place within the vacuum system, making misalignment's less likely to occur; the downside of this is of course that any misalignment of the mirrors that does occur cannot be corrected without breaking vacuum [114]. One of the detractors of prism MOTs is that any laser light that does not fall onto the mirrors is lost, making it fairly inefficient in terms of optical power. Additionally this method does require that the mirrors are placed within the vacuum system, which means methods of mirror mounting and potential adjustments once in place must be considered. For example, special vacuum screws and glues would have to be used to hold them in place which are vacuum safe. For systems that need to get even smaller, chip scale MOTs have been realised with the use of diffraction gratings. These function similarly to a prism MOT with a single laser reflecting off a diffraction grating forming the necessary overlapping beams to create the necessary beam pairs. Grating MOTs show great potential for future work in miniaturising optical atomic clocks [115], [116].

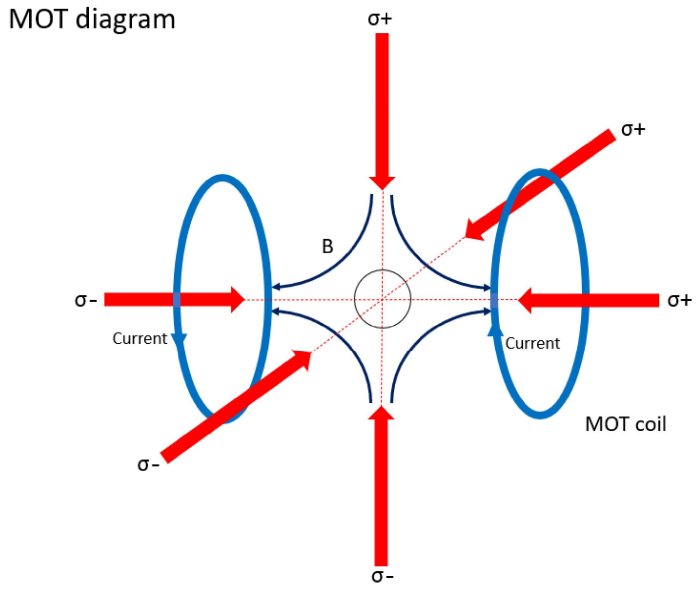

Figure 3.7 Schematic of the optical beams and the coils required for the formation of a Magneto Optical Trap

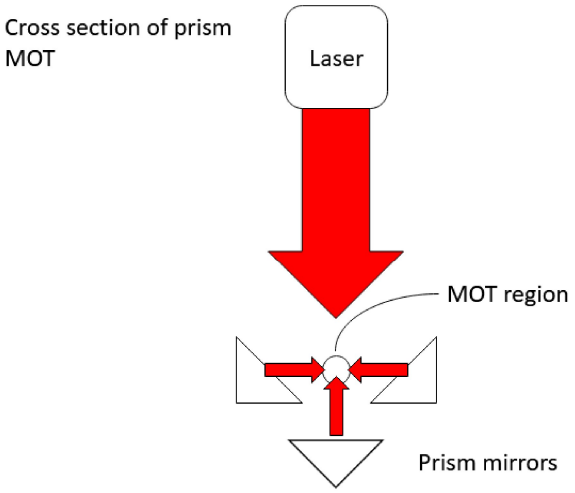

Figure 3.8 A basic 2D visualisation of the laser beam orientation in a prism MOT. The reflection of the beam on the mirrors causes a swap in the circular polarisation forming the necessary beam pairs needed for a MOT. Not seen on this diagram are two more prism mirrors that would form the beams into/out of the plane of the diagram.

iqClock MOT design

As the iqClock is not intended to be a portable or transportable system the miniaturisation benefits of the prism and grating MOT designs are not so important. Although it may be bulkier to set up three counter-propagating laser pairs from six laser outputs it is cheaper and quicker to do it this way as it does not require any in-vacuum mirror optics or unique gratings to be machined. A photograph of atoms captured in the iqClock MOT can be seen in figure 3.9.

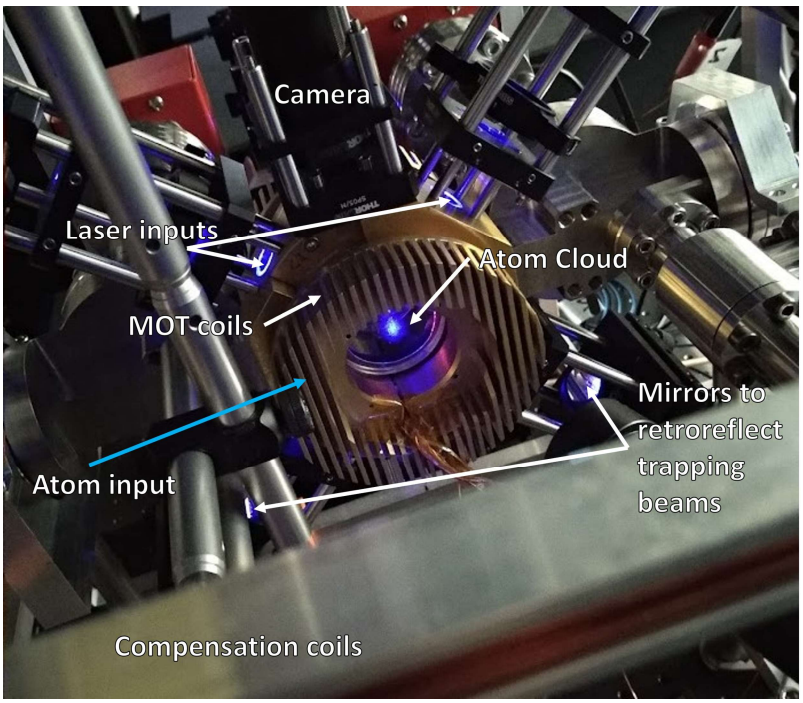

Figure 3.9 A photograph taken by the author of a cloud of strontium atoms captured in the iqClock system. Two of the laser pairs forming the optical molasses portion of the trap can be seen diagonally facing into the system, the final laser pair being into and out of the plane of the photograph. The gold coloured components with heatsinks are the magnetic coils used to form the quadrupole magnetic field, characterisation of these coils can be seen in chapter 5. The two large red boxes behind the MOT are the ion pumps used to keep the system under UHV conditions. The telescope directly above the system is to allow a camera to observe the MOT for characterisation purposes. Finally the beam in the forefront of the photograph is part of the set of compensation coils set around the system to help keep the suppress any stray magnetic fields that might be present in the region.

3.5.3 Further cooling

There are limits to the temperature that such a trap can achieve. The Doppler limit describes the cooling limit achieved through laser cooling. During the process of laser cooling the atom emits a photon to return to its ground state, this emission comes with a momentum kick in the direction opposite to the direction of photon emission. These emission momentum kicks form a minimum amount of kinetic energy held by the atoms known as the Doppler limit. This limit in the is described by the equation

$$T_D \approx \frac{\hbar \cdot \Gamma}{2k_B} \tag{3.16}$$

Where Γ is the linewidth of the excited state of the atoms. This Doppler limit is for a specific atomic transition, so moving to another atomic transition can lower the temperature of the atoms. Thus by replacing the blue lasers of the MOT with a superimposed set of red lasers, a different transition can be accessed with a lower value of Γ, resulting in a lower T_D. This is especially useful in alkali earth elements such as strontium as the ${}^1S_0 - {}^1P_1$ has a high T_D around the mK level [53]. In the iqClock the first stage MOT uses the $461nm$ cooling transition used to initially slow the atoms, this is known as the blue mot stage after the colour of the cooling laser. The second MOT stage is the red MOT, using a $689nm$ laser (labelled (2) in figure 3.1 . This transition has a narrower linewidth that allows the red MOT to cool the atoms further than the blue MOT is able to. By using the narrower ${}^1S_0 - {}^3P_1$ μK temperatures can be approached. This process does not cool the atoms below T_D, but instead lowers the value of T_D itself. To get lower than the Doppler limit one has to use sub Doppler cooling methods.

3.5.4 Sub Doppler cooling

These are techniques used to bring the temperature of the atoms below T_D. The first inclination that this was possible was found in 1988, when an experiment with MOT's was found to have cooled the atoms below the expected temperature [117].

This suggested that one of the following processes was at work cooling the atoms within the MOT past the Doppler limit.

Polarisation gradient cooling

Polarisation gradient or Sisyphus cooling is the process through which atoms can be divested of energy through interaction with two counter propagating lasers. The lasers interact with each other forming a series of potential peaks and troughs, a standing wave. Atoms lose kinetic energy moving from an area of low potential to an area of high potential, at the peak of potential optical pumping is then used to remove the gained potential energy from the atom and move it to a less energetic state [107], [113].

Evaporative cooling

Evaporative cooling reduces the average temperature of atoms confined in a a lattice site by allowing the most energetic atoms to escape, to "evaporate" out of the potential well into the chamber. This is achieved by momentarily lowering the potential of the lattice sites allowing the hottest atoms to escape [107]. As the atoms exchange energy through collisions the atoms that escape have a much greater energy than the average atom in the potential well, thus each atom that evaporates out reduces the average energy of the confined atoms considerably.

3.5.5 Lattice

A purely optical lattice requires the atoms to have been cooled as much as possible before loading, as the depth of the trap potential is much shallower than that present in a MOT. However confining in an optical lattice has major benefits over confinement in a MOT. It removes the magnetic field, meaning no Zeeman shifting of atomic energy levels; and if a magic wavelength exists then at this lattice wavelength the

energy shift due to interaction with the optical field is equal for both the ground and excited states of the clock transition, resulting in no net change of transition energy [118].

The lattice consists of multiple closely spaced potential wells formed by the standing wave formed by interaction of counter propagating laser pairs. The simplest form of this trap is one dimensional, but through the addition of more laser pairs a three dimensional trap can be constructed. The potential wells formed by the standing wave are the lattice sites where the trapped atoms congregate. A greater number of trapped atoms gives a better signal to noise ratio, but the more atoms there are in each lattice site the more inter-atom interactions there will be- increasing the uncertainty on the value of the transition.

For two counterpropagating beams of the same intensity I the potential depth formed by the resulting standing wave is:

$$U_0 = -\frac{8\pi}{c}\alpha I \tag{3.17}$$

Where α is the polarisability of the atom. Each atom contained within this potential experiences a potential of:

$$U_{(r,z)} = U_0 \exp(-2(r/w(z))^2) cos^2(2\pi z/\lambda) \tag{3.18}$$

Where r and z are the position of the atom radially within the beam and along the beam path respectively. $w(z)$ gives the beam waist at a point z along the beam path, and λ is laser wavelength.

As long as the value of α is greater than zero, the atoms contained in this 1D lattice remained trapped, as the atoms are pushed towards the maximum intensity value. If α is negative then the atoms will escape the lattice sites as they are pushed towards intensity minimas. As the atoms are attempting to escape radially then the application of perpendicular beams to the 1D trap will keep them confined, forming a 3D lattice [119]. The interaction of the trapped atoms and the probe laser would usually impart a momentum kick to the atoms, $p = \hbar\nu_{probe}/c$, which would perturb

the clock frequency. To avoid this the atoms can be kept within the Lamb-Dicke regime [120]. In this regime the recoil energy of the atoms is less that the spacing between the harmonic levels in the lattice potentials, thus the atoms do not change their motional energy level despite the imparted energy. The recoil energy caused the probe laser must be much less that the harmonic level spacing at the bottom of the lattice potential wells:

$$\hbar\nu_{harmonic} = \frac{2\pi}{\lambda}\sqrt{\frac{2U_0}{M}} \tag{3.19}$$

Where M is the mass of the atom. The process outlined above is only the first half of any clock experiment. The slowing, cooling and trapping of atoms is only the first half of the process in creating an atomic clock. Once the atoms have been trapped the probing of the cooled sample and extraction of the signal are the next steps, as a usable clock signal has not been gained from the cooled and trapped atoms.

3.6 Interrogation of the atoms

Once the atoms are cooled and confined within an optical lattice the next step is to interrogate them with the clock laser. The extraction of a usable clock signal from the atoms is as follows, the clock laser is set to the clock transition frequency of the atom and then pulsed across the sample. In the case of Rabi spectroscopy there is only a single pulse of light, if Ramsey spectroscopy is to be used two pulses separated by a dark stage are used. The Ramsey scheme first excites ground and excited states of the clock transition, bringing them into coherent superposition. This superposition is allowed to evolve during the dark stage. When detection of the atomic population is measured after the second pulse, the effects of interference from the second pulse can be seen, information which is not present in the Rabi method. The benefits of using the Rabi method is that as there is only a single pulse the set up for the experiment is less complex, especially beneficial in a portable system, and

reduced laser intensity is needed, which reduces stark shifts from interaction with the probe laser. However, in the same interrogation time as the Rabi scheme the use of the Ramsey scheme affords a narrower linewidth; additionally if the time of each pulse is shorter than the time of the dark stage then the atoms remain sensitive to the excitation lasers for a longer duration [118]. Once the atoms have been through this process of excitation pulses the population of excited atoms is measured through stimulated emission of the excited states, in a process called electron shelving [121]. This method creates a large number of fluoresced photons, giving a large signal to noise ratio, but also destroys the coherence of the atomic sample at the same time. The destruction of the atomic sample means that every measurement has to wait for a new group of atoms to be cooled and trapped. Whilst waiting for this new sample the laser must rely only on the cavity to keep its frequency, before being able to "relock" onto the clock transition during measurement. Thus any method that decreases the time between the atomic measurements will increase the stability of the clock. For instance non-destructive population measurements of the sample will allow the same atoms to be interrogated without the need for preparation of a new sample [122].

3.6.1 Frequency combs

Frequency combs are the technology that perhaps has most facilitated the jump to optical frequencies. First developed around the turn of the millennium, frequency combs allowed the measurement of optical frequencies which are around 100 000 times faster than the speed with which modern day electronic systems can react [28]. Before the development of frequency combs a "chain" of well known elemental frequencies would have to be used to try and determine an unknown optical frequency. Starting with a known atomic frequency, the frequency chain multiplies the previous frequency and mixes it with the next known frequency. In this fashion a starting microwave frequency can be multiplied up in steps to reach an optical frequency, which can

then be determined by the multiplication factor needed to travel up the chain. The major issue with this method was it required multiple frequency standards to form the links of the chain, and this was incredible complex to build and run [107].

The frequency comb bridges the gap between electronic response time and optical frequencies more elegantly than the frequency chain method, allowing the measurement of the clock frequency with digital electronics. Although currently there are multiple ways to generate a frequency comb, such as fourwave mixing and periodic modulation of a continuous wave laser, the first devices used a phase stabilised mode locked laser to produce the necessary modulated pulses to form a "comb". This laser now contains both an optical frequency in the light and a microwave frequency in the pulse repetition rate, by locking the phase between them a "ruler" for mapping optical frequencies to microwave ones can be created [85].

The "comb equation" can be seen in equation 3.20[123] and shows how the frequencies of each of the teeth of the comb, ν_N, are formed from the laser pulse repetition rate f_r, and the frequency offset f_o.

$$\nu_N = f_o + N f_r \tag{3.20}$$

N is an integer that multiplies f_r to the optical regime from the microwave regime - usually in the range of 10 000- 100 000. Each of the optical nodes are separated in frequency space by the pulse frequency, $f_r = 1/T_r = v_g/2L$. T_r is the time between each pulse, v_g the cavity pulse group velocity, and L is the optical path length in the cavity. By adjusting v_g and L you shift the spacing between the teeth of the comb. The offset frequency is needed to ensure that each pulse of the laser is the same length and is in phase with every other pulse. The offset frequency relates the optical phase of the laser to the carrier envelope phase, where $f_o = 1/2\pi \frac{d\phi_{CEO}}{dt}$, with ϕ_{CEO} being the phase of the carrier envelope. Both f_o and f_r are controlled through physical manipulations of the frequency comb cavity. A diagram showing how the laser frequency can be determined with a frequency comb is shown in figure 3.10.

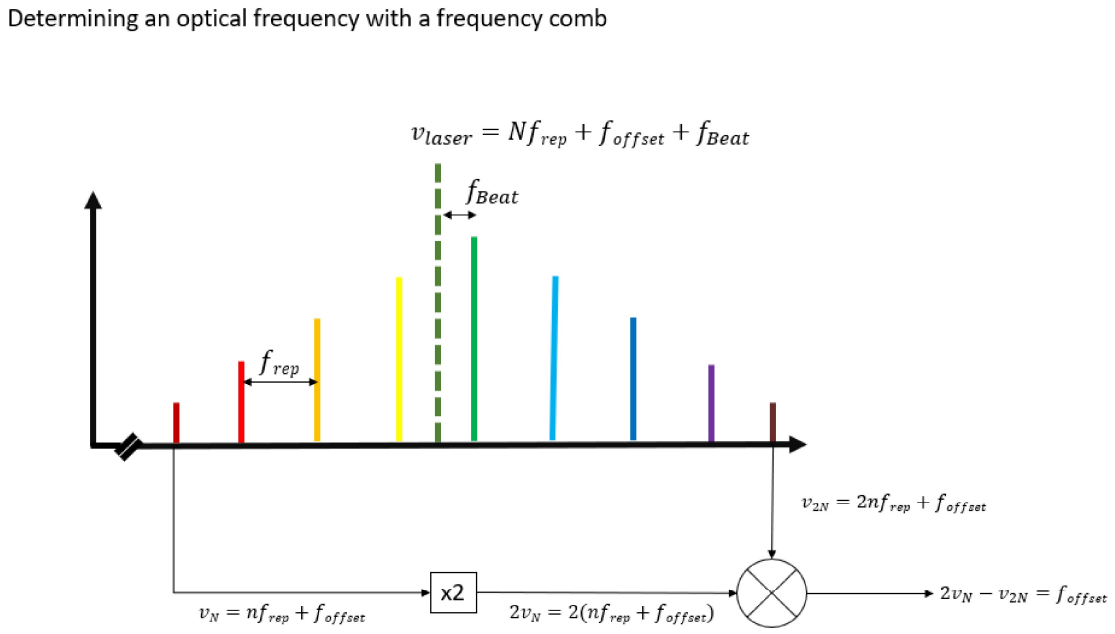

Figure 3.10 Diagram showing how the frequency of a laser ν_{laser} is determined from a frequency comb. In order to determine the laser frequency f_r, f_o and f_{beat} must first be determined. f_r and f_{beat} can both be measured directly but f_o has to be determined by the process shown at the bottom of the figure. By comparing the doubled frequency of an optical node at position N and beating it against the frequency of an optical node at $2N$, the offset frequency f_o is found.

Current frequency combs are rather large, which limits the portability of any devices built with them. The miniaturisation and environmental proofing of frequency combs is therefore a key area of research at the moment. The miniaturisation of combs with the end goal of mounting on a satellite is needed for the upgrading of GPS satellites for instance [30]. Other avenues currently under investigation for the creation of miniaturised frequency combs include whispering gallery modes in micro resonators [31], [124], silicon semiconductor lasers, electro optic combs, and super continuum lasers [28].

The applications of frequency combs extend beyond the internal use in the clock. They are also key to comparing clocks running on different atomic species, for instance comparing the absolute frequency of current standard Cs clocks to the newer

alkaline earth metal devices. Frequency combs can also be used to synchronise clocks through connected networks, generation of microwaves, spectroscopy, calibration of astronomical spectrographs, and LIDAR distance measurements [28].

3.6.2 iqClock testbed

The iqClock testbed system follows the steps of the clock system outlined above. Although their presence is useful for increasing the efficiency of the atomic slowing process and capturing more atoms in the MOT, an optical atomic clock system can function without a Zeeman slower. This was proved in the Miniclock experiment at Birmingham. For the iqClock system an investigation was carried out into the feasibility of mounting a Zeeman slower on the system and the effect that it would have. This investigation is carried out in chapter 4.

Chapter Four

The iqClock Zeeman slower

4.1 Zeeman slower designs

The theory behind Zeeman slowers has been introduced in chapter 3 of this thesis, and here is presented the different designs of Zeeman slowers that can be built and the rationalisation for choosing them in the iqClock system. The Zeeman slower is part of the atomic package in the block diagram in figure 3.3, and aids in the slowing of the atomic beam.

4.1.1 Method of field generation

In order to apply a magnetic field over the slowing region there must of course be someway to generate the magnetic field. An obvious choice would be a solenoid. By varying the number of turns in the coil along the length of the solenoid the magnetic field can be exactly designed to provide the correct amount of Zeeman splitting. A solenoid is an ideal choice for a static system which does not care about power requirements or potential requirement for additional cooling systems. It also has the benefit that the field can be on and off at will, this means that the magnetic fields required to help slow the atoms are no longer active when it comes to trapping and interrogating the atoms. An example of a solenoidal design for Sr is given in [108]. The other method for applying the magnetic field is by use

of permanent magnets [125]–[128]. Using permanent magnets has several benefits over the solenoidal method: it means no power source is required, and therefore no cooling whilst also reducing the power requirements for the system; it also allows easier access to the slowing region, both optically and physically, as once installed a solenoid cannot be removed without breaking vacuum or breaking the solenoid. The draw back to permanent magnets is that, as the name suggests, the magnetic field will always be present, this means that some form of shielding or compensation is necessary to account for the field in the trapping and interrogation chamber. A benefit of solendoidal designs over the permanent magnet designs is that that the magnet field can be remotely controlled by changing the current supplied to the solenoid, potentially allowing the same solenoid to function for different atomic species, and the field to be optimised on the fly. With a permanent magnet system in order to change the field without rebuilding the system the magnets must be physically moved to provide a new field profile. A method for achieving this can be seen in [129], but this removes the "no power required" benefit outlined earlier. What can be seen from these generation methods is that permanent magnet Zeeman slowers are generally more suited for systems that are designed not for ultimate accuracy and stability but for portability and reduced resource consumption.

4.1.2 Magnetic field orientation: Longitudinal or Transverse?

When designing a Zeeman slower the orientation of the field is an important consideration, as it will effect the amount of stray fields in the rest of the system and the polarisation of the lasers necessary for slowing. With a solenoidal slower wrapped around the the propagation axis of the atoms the field will be parallel to the atoms direction of travel. This is called a longitudinal magnetic field [125], [127]. Longitudinal slowers have the advantage of requiring less powerful lasers to operate as all of the power of the circularly polarised beam is interacting with the atoms at any one time. However the magnetic fields in longitudinal Zeeman slowers do extend

further from the ends of the slower, deeper into the rest of the system, this means systems that wish to run at a very high precision require more shielding when using a permanent magnet longitudinal slower to reduce these stray fields [62].

Transverse slowers have the magnetic field perpendicular to the propagation of the atoms. This magnetic field orientation is more difficult to achieve with electromagnets, but can be preferable for permanent magnet designs. The transverse design has less magnetic field leakage from the ends of the slower, and as the orientation of the magnets is N/S rather than E/W more of the magnetic flux from each magnet flows across the region of interest, necessitating less magnets to get the same strength field. The draw back of a transverse slower is that it requires linearly polarised light, both $\sigma-$ and $\sigma+$ components are required to interact with the atoms, but only one of them is interacting at any one time. This means that twice as much beam power is required from a laser in a transverse slower set up, as half the beam power is lost [111], [130]. A visualisation of the longitudinal vs transverse magnetic field set ups can be seen in figure 4.1.

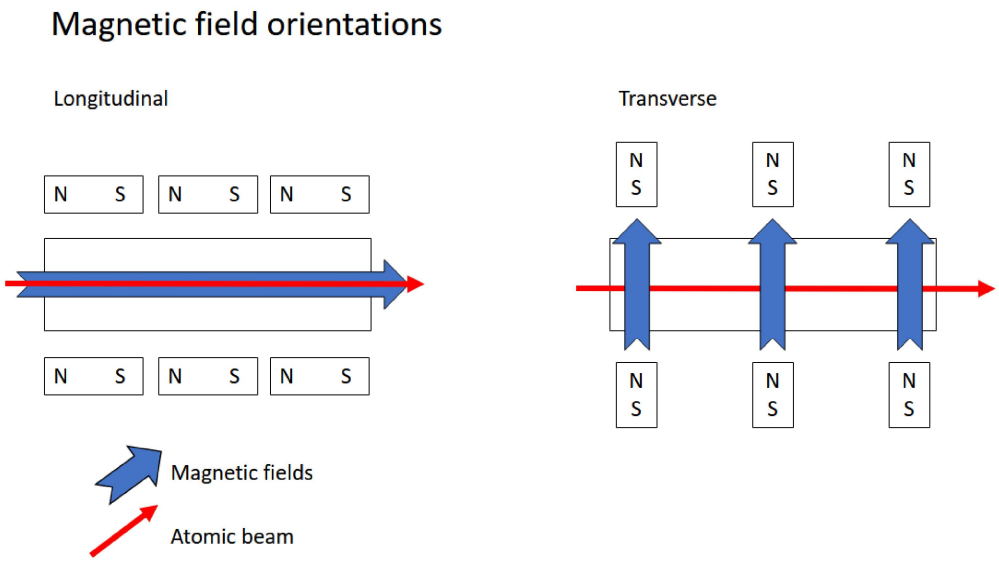

Figure 4.1 A visualisation of the orientation of the magnetic fields across the atomic beam. A representation of the magnets required to produce such a field is also present on the image, although this North/South orientation of the magnets is not necessary for the longitudinal/ transverse field to form. For the transverse field it is important that the magnets across the beam are oriented so that a North face and South face are facing each other, or the fields will repel each other and a smooth profile will be much more difficult to attain. For the longitudinal case all the magnets must be facing the same direction along the atom beam path (North/South or South/North doesn't matter), or again the individual magnets field will work against each other.

Forming a transverse field

The obvious way to form a transverse magnetic field is the one given in figure 4.1, with pairs aligned magnets facing each other across the atomic beam path. This method has been successfully utilised previously in Zeeman slowers on clock systems in [129], [131]. As it is a transverse field naturally there are reduced stray magnetic fields from the end of the slower compared to a longitudinal design, but to the sides of the slower relatively large fields emanate from the magnetic poles not facing the atomic beam. An alternative to this magnetic set up is to arrange the magnets in a Halbach formation. A Halbach formation of magnets is an arrangement of magnets that produces a high strength field on one side, whilst producing a very low field

on the other [132]. Halbach slowers [133]–[135] reduce the stray fields present in the rest of the system through the use of this magnetic configuration. The Halbach slowers tend to be somewhat larger than traditional style transverse systems, and are less configurable on the fly; but the reduction in stray fields is something that all permanent slowers must contend with so the use of this configuration would reduce the need for magnetic shields and other magnetic field suppression methods. Simulated magnetic fields for a Halbach array and a cross section of a Halbach cylinder are presented in figure 4.2. Some investigations into making a Halbach slower for the iqClock system were looked into, but ultimately the constrained space around the system made these designs unsuitable. The initial measurements are presented in section 4.2.5.

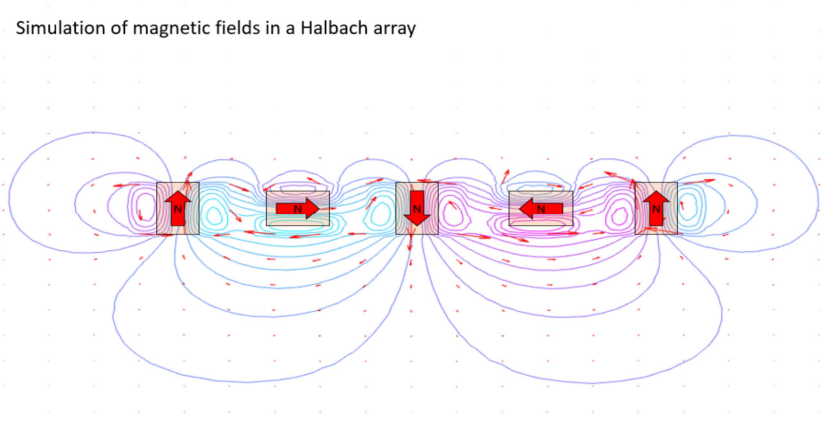

(a) Simulated magnetic fields for a Halbach array. It can be clearly seen that this arrangement of magnets creates a strong magnetic field profile on one side whilst suppressing it on the other. This array can be though of as similar to a row of horseshoe magnets.

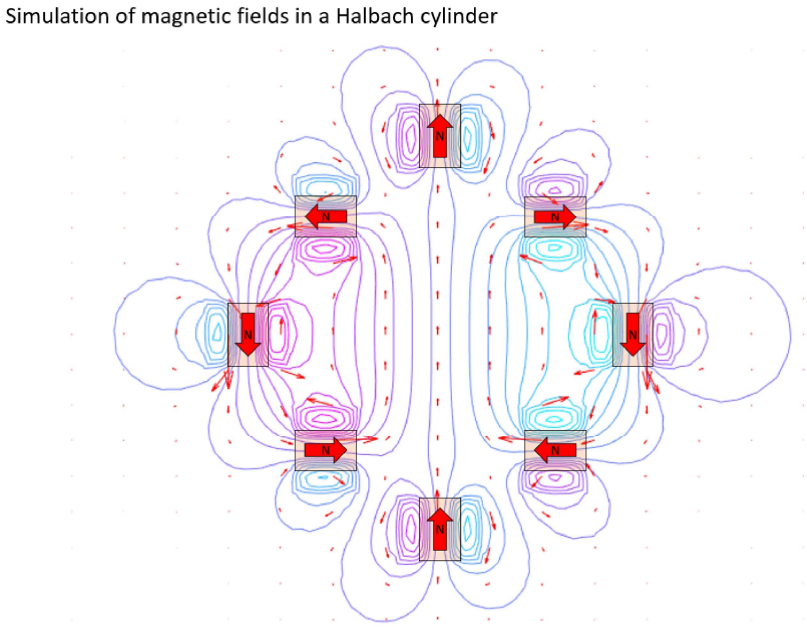

(b) Simulated magnetic field of a ring of magnets arranged in a Halbach configuration. By extending the ring out of the plane of the image a cylinder could be formed that would create a transverse field suitable for creating a Zeeman slower.

Figure 4.2 These simulations were done in MATLAB using the in-built graphical 2D PDE solver to illustrate the effect of the Halbach array on the magnetic fields in two dimensions. Individual bar magnets were simulated by mapping the interaction of two magnetic fields formed by two opposing currents travelling through identical conductors into/out of the plane of the page. Whilst not a representation of a real set up, they clearly illustrate the magnetic field suppressing effects of using a Halbach array. For more accurate 3D modelling of magnetic fields a program such as ANSYS could be used.

4.1.3 Direction of field gradient

The direction of the gradient of the Zeeman slower is a factor in determining the efficiency of the slower. If the gradient is falling (i.e the atoms enter in into a high magnetic field and exit into a low field) it is known as a $\sigma+$ slower, conversely entering a rising gradient (i.e enter at low field, exit at high field) is known as a $\sigma-$ slower. Both a $\sigma+$ and a $\sigma-$ slower can have the same magnitude of magnetic field, but the detuning of the laser will have to be set at different points. For $\sigma+$ the laser detuning is set to interact with the atomic transition when the atom is moving very slowly. However as the atoms are moving slowest as they exit the slower where the magnetic field is at minimum, this can cause an issue in that the atoms do not decouple from the laser field as they exit the slower. This leads to some atoms having their velocity reversed and being sent back up the slower. For this reason the $\sigma-$ slowers are more efficient, with the laser detuning being set to interact with the fast moving atoms out of the oven, this means when the atoms move out of the slower from the magnetic field maximum they immediately decouple from the slowing laser, and no longer interact with it [136]. A diagram of the magnetic field profile of a $\sigma-$ slower is seen in figure 3.4.

When using permanent magnets one of the limitations is the magnetic field strength of each individual magnet. The construction of high field strength Zeeman slowers using permanent magnets is quite problematic, as very high strength permanent magnets are difficult and potentially hazardous to work with. In such cases where the atomic species require such a high field, a magnetic field that travels through zero can achieve the same effect as a very high strength field.

As seen in equation 2.4 and 3.8 the amount a m_l level shifts is directly proportional to the change in magnetic field, with the direction of the shift being dependant on the polarity of the magnetic field. Thus a field strength change from -500 G to 500 G results in the same magnitude of energy shift as a field strength change of 0 G to 1000 G. This "spin-flip" or "zero-crossing" method allows us to cause the same

amount of energy level shift without needing such high magnetic fields [126], [137], [138]. This method will always give good decoupling at the end of the slower as there will be a non-zero magnetic field at the end of the slower. The draw back comes from the interaction of the atoms at the zero crossing point, at this point all the atomic energy levels are degenerate- no Zeeman splitting is occurring at this point. This degeneracy can lead to electrons falling into optical dark states, no longer in the correct cooling cycle; without the use of re-pump lasers to excite the atoms back into the main cooling cycle such atoms would be lost from the slowing process. A side by side comparison of the profiles for a $\sigma+$, $\sigma-$, and spin-flip slower are presented in figure 4.3.

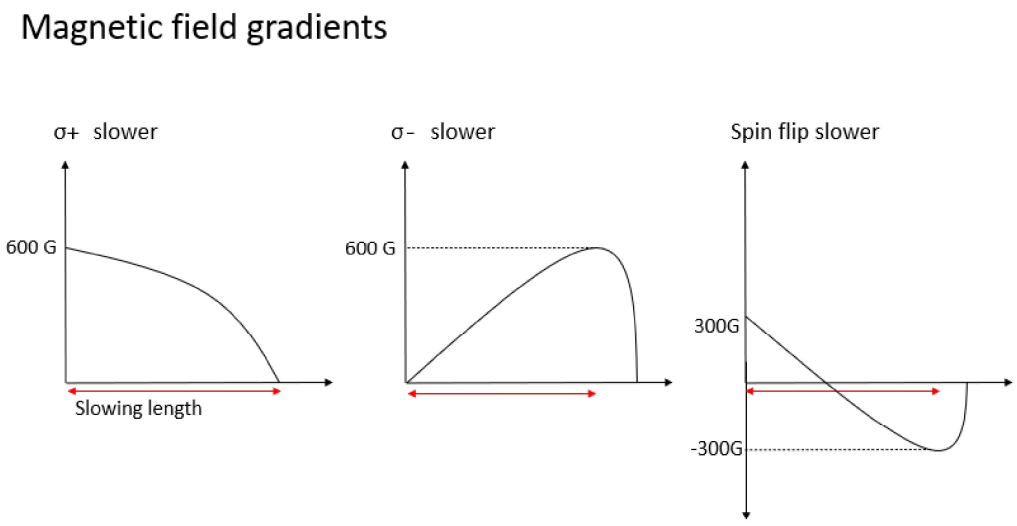

Figure 4.3 Illustration of the three potential magnetic field magnitude profiles for Zeeman slowers. These slowers can be either transverse or longitudinal. When making a permanent magnet slower it can be difficult to achieve high field magnitudes, as strong permanent magnets are difficult and can be dangerous to work with. By passing through a zero field strength region, the spin-flip design gives the same Zeeman splitting as the $\sigma+$ and the $\sigma-$ designs without having to reach such a high field magnitude, making it attractive for permanent magnet systems. Both the $\sigma-$ and spin-flip designs both have a sharp drop in the magnetic field at the end of the slowing region. This sudden change in the magnetic field at the end of the slower means the atoms rapidly move off of resonance with the slowing laser and are no longer interacted with. Thus the system can be designed to slow the atoms to the desired trapping velocity, and then cease interactions to prevent atoms slowing too much to reach the MOT region or being pushed away from the MOT region by the slowing laser.

4.2 The iqClock slower

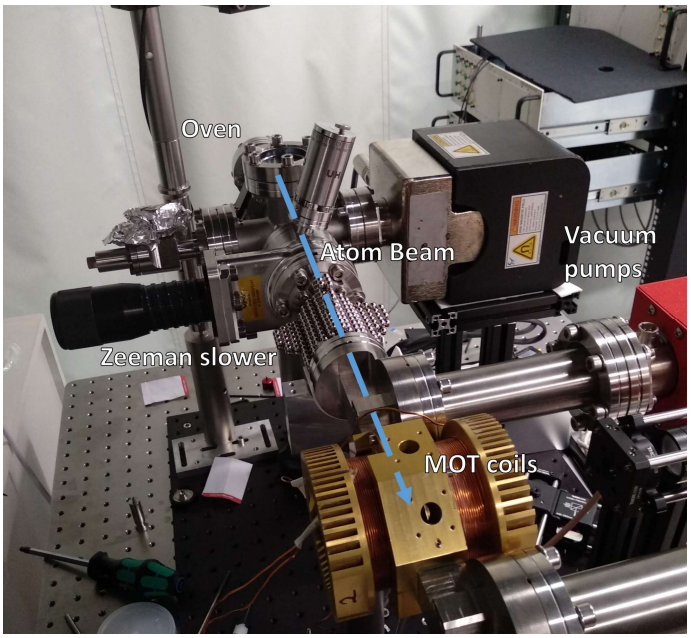

Figure 4.4 A photograph taken by the author of the iqClock slower mounted on the system with the MOT coils. The laser systems for the clock are not yet mounted in this photo.

4.2.1 Design choices

The design for the iqClock slower is an iteration upon a design used in the construction of another experiment in the Birmingham Sr team, the Long Range Interaction experiment. This slower is a "self assembled" design. The term "self assembled" means that there is no external frame or fastenings in the slower, it is entirely held together by the magnets that also provide the magnetic field profile. These magnets are 5mm diameter neodymium spheres, the spherical nature of which allow building in two configurations. In this description a "chain" of magnets is a singular row of magnets attached to each other north to south. Square packing where the magnetic poles of adjacent chains of magnets are antiparallel to each other; and triangular packing, where by offsetting each adjacent chain all the magnets field lines face the same direction. A visual description of this can be seen in figure 4.5a, and an image of those principles being used to form the slower in figure 4.5b

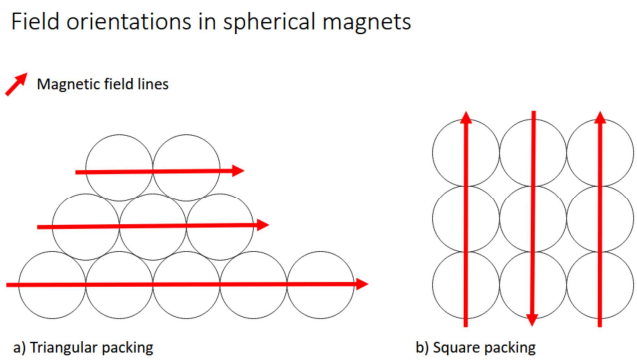

(a) A visual representation of the magnetic field in the triangular and square packing formation available when working with spherical magnets. The triangular packing configuration is used to form fins of parallel field, with the square packing being used to form an adhesive layer of net zero magnetic field upon which to attach the fins.

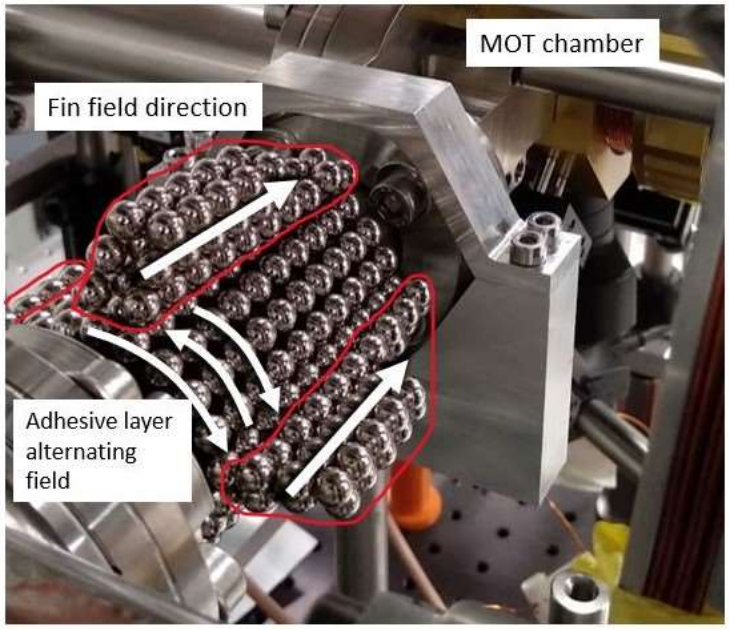

(b) Photograph taken by the author of the iqClock Zeeman slower on the system, the arrows depict the direction of the magnetic fields of each of the components. As the fields adhesive layer is square packing configuration, the magnetic fields of each neighbouring row around the circumference cancel each other out. The fins are constructed in triangular configuration, and thus all rows of magnets sum their fields. Two fins can be seen clearly, the third and fourth are directly opposite the ones labelled in the photo.

Figure 4.5 Images illustrating the square and triangular packing configurations possible with spherical magnets and the different uses of these magnetic configurations when building a Zeeman slower.

These configurations of laying the magnets allow the construction of a base or "adhesive layer" of magnets that is placed around the atomic beam axis. By using the square packing configuration a layer of magnets can be made that has no net magnetic field along the atomic beam path [125]. This layer is called the adhesive layer as it then allows fins made in the traignular configuration to be mounted on it with no glues or extra parts, the magnets of the adhesive layer will attract the magnets of the fins and hold the fin in place. It is these fins that provide the magnetic field profile such as the one laid out in figure 3.4, as long as all the fins are placed evenely around the circumference and have their constituent magnets aligned with each other fin. A more detailed explanation of this set up can be found in [139] and can be seen in figure 4.6 below.

Spherical magnets are used over the more commonly shaped cuboid magnets in the self assembled design for two major reasons. Firstly a single chain of spherical magnets can be wrapped around to form a ring, by placing multiple rings of the same length next to each other and alternating the direction of the field through them (as seen in 4.5b) the adhesive layer is constructed. This cannot be achieved with cuboid magnets as they will not naturally sit with only corners touching, instead rearranging themselves to be connected by the north/south faces. The second reason for using spherical magnets is due to the need to have parallel chains of magnets in the fins. With the triangular packing allowed by spherical magnets parallel chains of magnets can be stacked on each other to add their fields together to form the Zeeman slower profile. This is possible as the shape of the spherical magnets allows the parallel chains of magnets to tessellate slightly, allowing the north pole of the magnets in the row above to interact with the south pole of the magnets in the chain below, this tessellation can be seen in 4.5a. With cuboid magnets where this tessellation between chains is impossible the chains will not naturally sit parallel to each other without being constrained by cases or gluing.

For the iqClock testbed there was considerably less space to play with than the LRI experiment, constraining the size of the slower and the position it could be placed in. In order to create a large enough magnetic field to be useful in Zeeman slowing it was decided to increase the number of fins from three to four. The profile of the new shorter iqClock slower can be seen in figure 4.6b in comparison to the LRI slower in figure 4.6a.

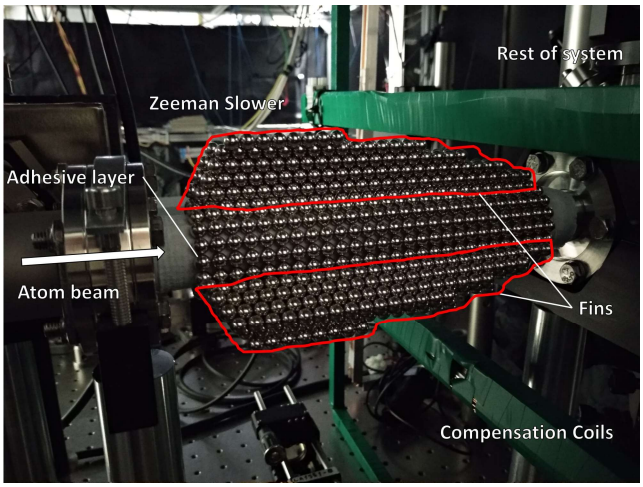

(a) The Zeeman slower for the LRI experiment at University of Birmingham mounted on the system.

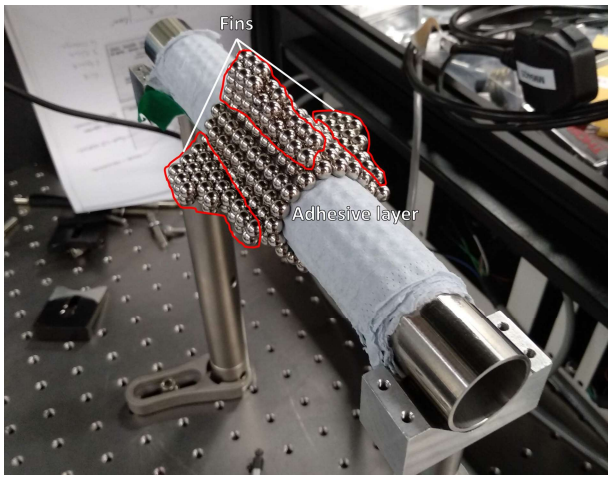

(b) The iqClock Zeeman slower mounted on a pipe used for testing the magnetic field.

Figure 4.6 Comparison of the relative sizes of the LRI and iqClock Zeeman slower, each slower is aiming to produce a magnetic field with a 600 G difference between maxima and minima, but the available space differs greatly between the two experiments. In order to help produce the field for the smaller iqClock slower an additional fin was added to increase the magnetic field strength in the centre of the slower. Both photos were taken by the author.

The reduced length of the slower means that the power of the laser will have to be greater for the iqClock slowing beam over the LRI one, as in order to get the same total reduction of speed more interactions per unit distance along the length of the slower are required.

Physical considerations

The reduced length of the iqClock slower presents some physical challenges not present in the LRI design. Using spherical permanent magnets there is a minimum limit of triangular close packing that can be formed as at too short a length the magnets reorient themselves to square packing. The fins of the slower are therefore limited in both maximum and minimum number of magnets that they can hold, by available space and by this minimum stable length. It is difficult but possible to make a fin pair of 3 magnets length (6 in total) without the magnets flipping and orienting into the more favourable square packing formation, but so far it has proved impossible to make a fin length of 2 or less magnets. From some brief experiments with small cuboidal magnets it is not possible to form the triangular geometry necessary with non-spherical magnets, as they do not interlock making the triangular packing impossible to create without gluing the magnets in place. Thus the self assembling Zeeman slower design must have fins constructed from the spherical magnets, and will therefore be somewhat limited in the minimum layer length of a fin.

4.2.2 Suppression of magnetic fields

Both the LRI and the iqClock slowers are longitudinal spinflip designs, meaning that there are considerable stray magnetic fields that exit the end of the slower and pass through the MOT region. For the LRI system the slower is sufficiently far from the MOT region that the stray fields do not require suppression to prevent them interfering with the formation of the MOT. However for the iqClock system this is not the case. With no suppression the stray fields from the iqClock slower

were measured to be around 5 G in the MOT region, more than what the current compensation coils on the system can account for, as seen in figure 4.9b. Usually such stray fields would be attenuated through the use of magnetic shields, however the geometry of the iqClock system is such that the shields required for reduction of the magnetic field would be too bulky to mount without drastic redesigns of the system. A redesign to a transverse Zeeman slower would have required a redesign of the laser systems, and a shift away from the self assembled system of building the Zeeman slower. A brief attempt to make a transverse self assembled slower was attempted, but the physical stability of the slower was very poor. In order to reduce the magnetic fields small cuboid magnets were used that had previously been bought for a prototype Halbach slower design. The aim of these magnets were to "guide" the magnetic field away from the MOT region and back towards the slower.

In order to mount these magnets specialised mounts were designed to fit the existing iqClock atomic chamber, within these mounts the cuboid magnets could be arranged transverse or anti-transverse across the path of the atoms. These mounts can be seen in figure 4.10b The aim of these guide magnets is to reduce the stray magnetic fields in the MOT chamber without affecting the profile of the slower itself in such a way as to reduce the slower efficacy.

4.2.3 iqClock Zeeman slower results

The iqClock Zeeman slower was designed using the program in appendix .1. It was found that a slower with 4 find placed equally around the adhesive layer provided the profile closest to figure 4.7a considering the restraints on space on the iqClock system. Each fin was comprised of 44 magnets, with the bottom layer comprising two rows of 8, the next two rows of 6, the next two rows of 5, and the final layer two rows of 3 magnets. An image of the slower can be seen in figure 4.6b with the calculated profile in figure 4.7b. Due to constraints on the length of the slower the gradient of the profile is much steeper than the one seen on the LRI slower, and

thus the slowing potential is much lower. For this particular profile a red detuning of around 400 MHz from the slowing transition of 461 nm is required was calculated to be most effective using the code in appendix .1 .

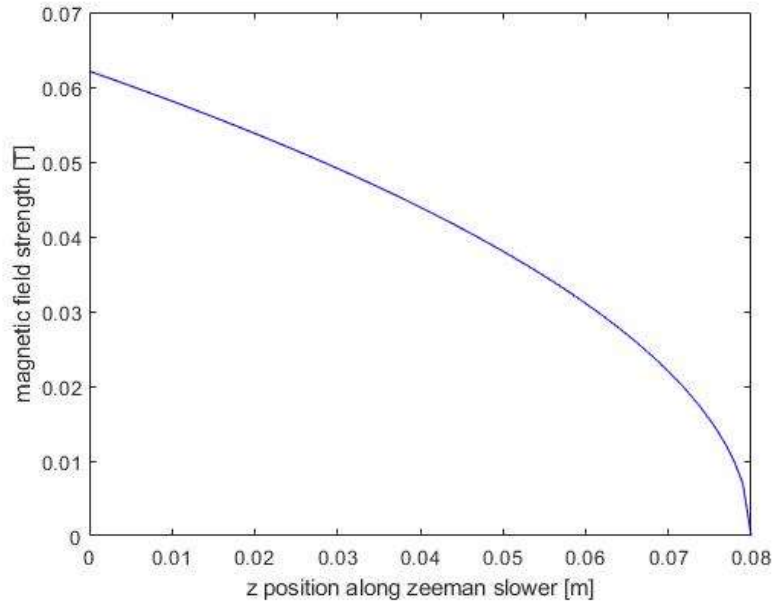

(a) A simulation of the ideal Zeeman slower profile over the region available on the iqClock testbed system. There is a total 600 G difference between the maxima and minima, this difference is required to provide enough Zeeman splitting to cover the range of atomic velocities along the length of the atomic slowing region for strontium.

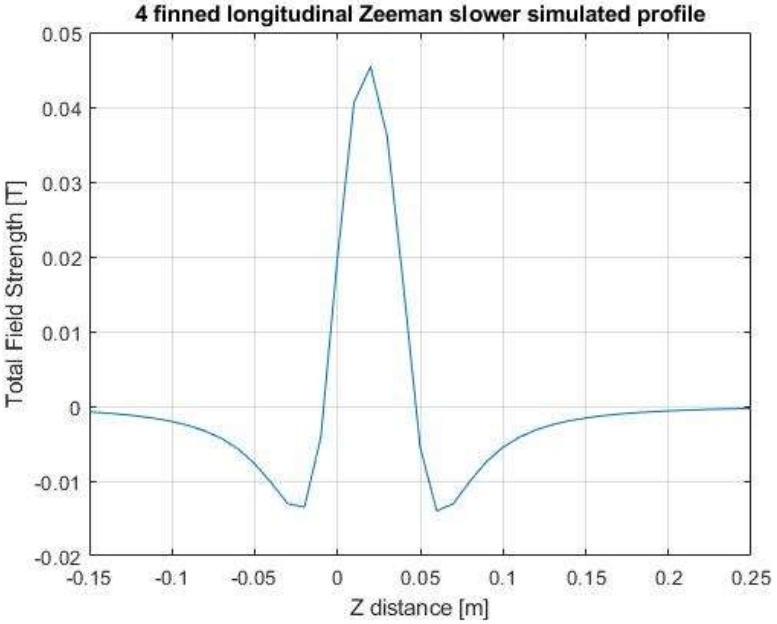

(b) Simulated profile of the iqClock Zeeman slower. The first magnet in the Zeeman slower is placed at the 0m mark, with the slowing region being between 0.02 and 0.06 m.

Figure 4.7 A comparison between ideal Zeeman slower profile over the slowing region, 4.7a, and the profile of the slower that best fits that profile using the self assembled magnet method of constructing a Zeeman slower, 4.7b.

As can be seen from figure 4.7 the ideal profile extends over the full 8cm region available to mount the slower, whereas the simulated slower only has a useful gradient between 0.02 and 0.06 m. This is due to the way the slower forms the magnetic field; the useful region of the profile formed is not the whole length of the slower, reducing the length within which the atoms can be slowed. Although the gradient of the slowing region is not as long as one would hope, the 600 G range is present and means that the slower can still be used, but will require higher optical power than a slower that conforms to the ideal profile seen in 4.7a. One of the key differences between the ideal and simulated profiles is the position of the magnetic field relative to zero, the ideal profile is purely positive, whereas the simulated profile passes through 0 to provide both positive and negative values. This difference is not a hugely problematic alteration however, as described in section 4.1.3, spin flip slower can provide some useful benefits over purely positive magnetic fields, especially when using permanent magnets. The key aspect of the ideal profile is the 600 G difference, with the position of the field relative to zero being a question of laser detuning.

The projected atomic capture range can be visualised from a set of MATLAB scripts previously written in the group. With these scripts the effects of changing the slowing laser detuning and power as well as the effect of changing the magnetic field can be simulated. Increasing the power of the laser increases the number of interaction that the atoms go through when travelling toward the MOT region. This power increase will increases the maximum velocity of atoms that can be caught but slows atoms towards the lower end of the velocity curve too much and they do not reach the MOT region at all. Comparisons between changing power, detuning and magnetic field can be seen in figure 4.8.

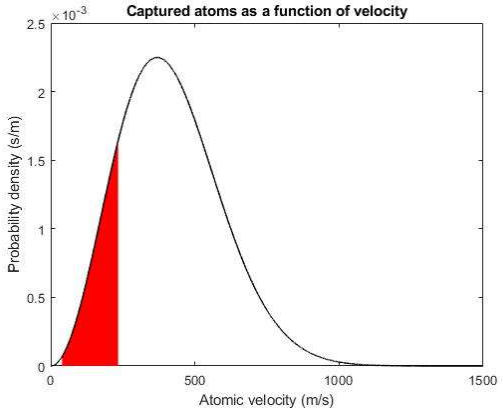

(a) iqClock slower at 450MHz detuning 16mW beam power. 16mw of power is the maximum power the lasers can provide to the Zeeman beam in the lab.

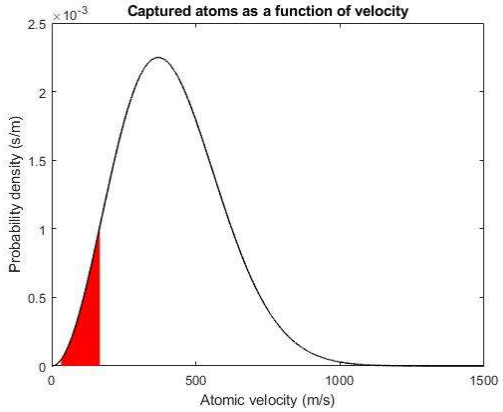

(b) Effect of no Zeeman slower, at 450MHz detuning, 16mW beam power. Only the slowest atoms are caught in the trap

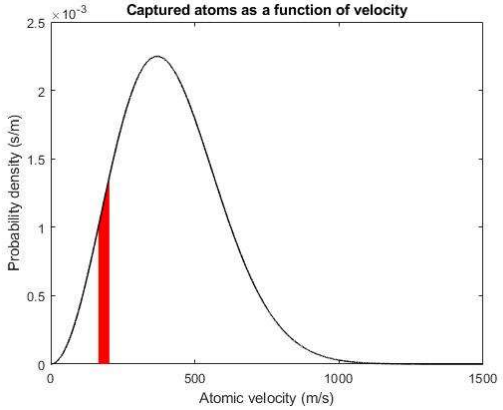

(c) Detuning reduced to 300 MHz, much reduced range of atoms captured

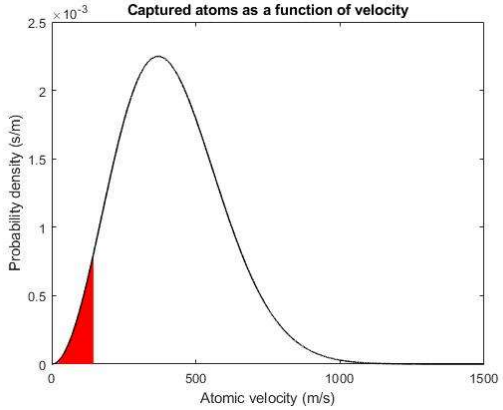

(d) Reduced power of beam to 1mW, detuning at 450MHz, only the slowest of atoms are caught in the trap.

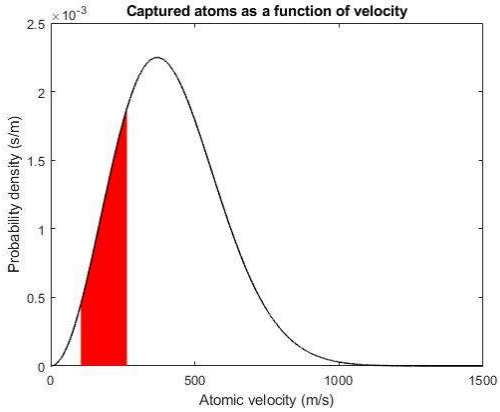

(e) Increased power to 50mW, 450MHz detuning, the slowest atoms drop out of the beam before reaching the MOT, but faster atoms are now able to be caught.

Figure 4.8 Comparisons of changing variables in the MATLAB scripts to find the optimal set up for the iqClock Zeeman slower. The red area under the curve represents the atoms captured by the MOT after they have passed through the Zeeman slower. The velocity distribution of atoms is calculated from an oven at around 450 Celsius. These graphs were generated using code found in appendix .1.

The measured profile of the Zeeman slower simulated in figure 4.7b can be seen in figure 4.9a. The measurement was performed with a Hall probe, the Zeeman slower was mounted on the set up seen in figure 4.6b and the Hall probe was inserted along the centre of the tube to measure the magnetic field. Two washers were 3D printed to keep the Hall probe at the exact centre of the tube where the atomic beam would be travelling were the Zeeman slower mounted on the real system. The measured and simulated profiles match each other well, with a small discrepancy in the height of the maxima of around 30 gauss. Other than this the shape and the total between maxima and minima agree well with each other. The discrepancy could be due to one of two factors. The difference could lie with the code not taking into account a disruptive magnetic field from the adhesive layer, or the point dipole approximation not being comprehensive enough for this simulation. Alternatively the discrepancy could be down to the magnets no longer being at the same strength as stated by the manufacturer. Repeated impacts will disturb the magnetic domains

within permanent magnets and will cause them to slowly lose their strength over time. It may be a good idea for an experiment determining the robustness of these magnets to repeated impacts to see how quickly their strength degrades.

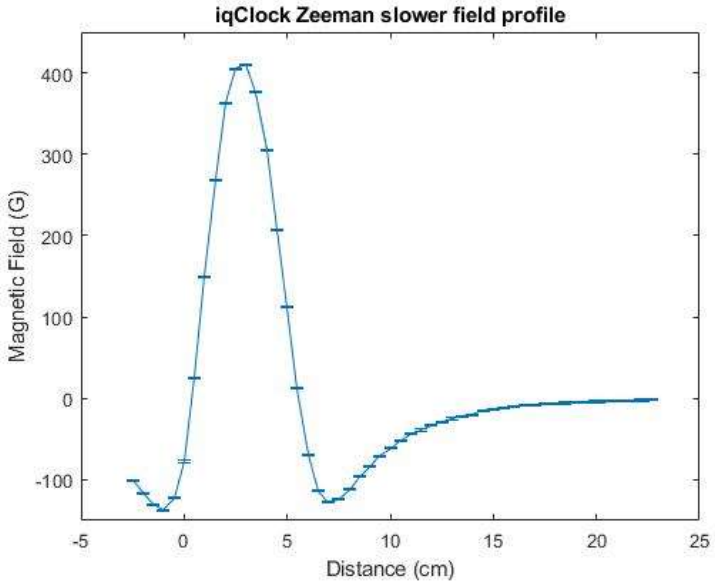

(a) Measured profile of the iqClock Zeeman slower. Profile matches the shape of the simulated profile given in 4.7b fairly well, but does not quite reach the same maxima. Error on the measurement is +/- 1 G as at these magnetic fields the Hall probe used did not measure digits lower than a gauss.

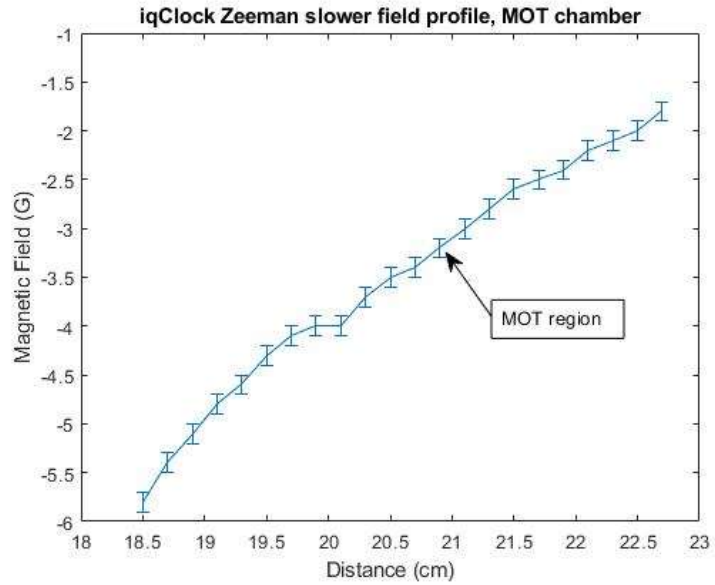

(b) Magnetic field over the area where the MOT is to be formed in the clock system with the un-shielded Zeeman slower. Error on the measurements is +/- 0.1 G, at these low magnetic fields from the Zeeman slower other fluctuating background fields in the lab prevented more accurate results.

Figure 4.9 Measured profiles of the iqClock Zeeman slower with no shielding on the system. The magnetic field at the MOT region caused by the stray fields from the end of the slower is too large to be effectively suppressed by the magnetic compensation coils have available.

This profile of the iqClock slower does have an issue that can be difficult to see from figure 4.9a. A clearer picture of this issue can be seen in figure 4.9b. Over the MOT region the residual magnetic field from the Zeeman slower is around 5 G, which is too much for the compensation coils around the system to effectively cancel out. This leaked magnetic field causes the MOT to form skewed or not at all.

The solution to this issue is the use of some form of magnetic shielding to reduce the stray magnetic fields over the MOT region. Usually magnetic shields are comprised of multiple layers of metal that redirect the magnetic fields away from the magnetically sensitive areas, however the size and layout for the iqClock system meant that there was no space for traditional shields of this type. Additionally shields work best when they completely enclose the source of the fields/ the area the fields are being shielded from. With the Zeeman slower being mounted on the route that atoms take to the MOT there is no way to completely enclose either the MOT region or the Zeeman slower, as they need to be connected by the route the Sr atoms take. In order to reduce the magnetic field over the MOT region a magnetic field transverse to the path of the atoms was applied to "guide" the stray fields away from the MOT region and back towards the Zeeman slower. The positioning of these guide magnets can be seen in figure 4.10a with an image of the setup in figure 4.10b. The guide magnets were held in place with a 3D printed clamp placed over the chamber component. The guide magnets themselves are small cuboid magnets, stacked together to give the desired magnetic field orientations. For the final set of tests a total of 36 guide magnets were used, 18 in each side, arranged in two rows of 3x3 magnet columns.

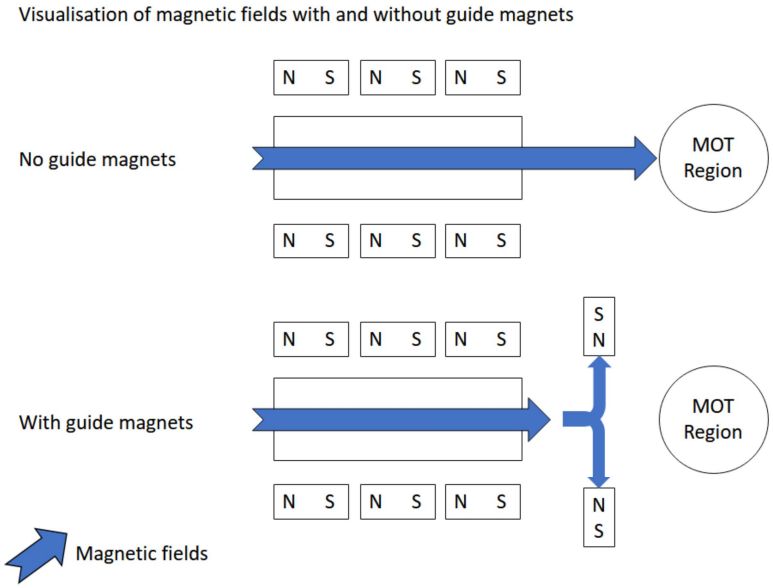

(a) A basic schematic of the system used to produce the magnetic fields across the path of the atoms. The stray fields from the south end of the Zeeman slower are interfering with the production of the MOT, by placing magnets in either side of the atom path, it was hoped stray fields could be guided away from the MOT region.

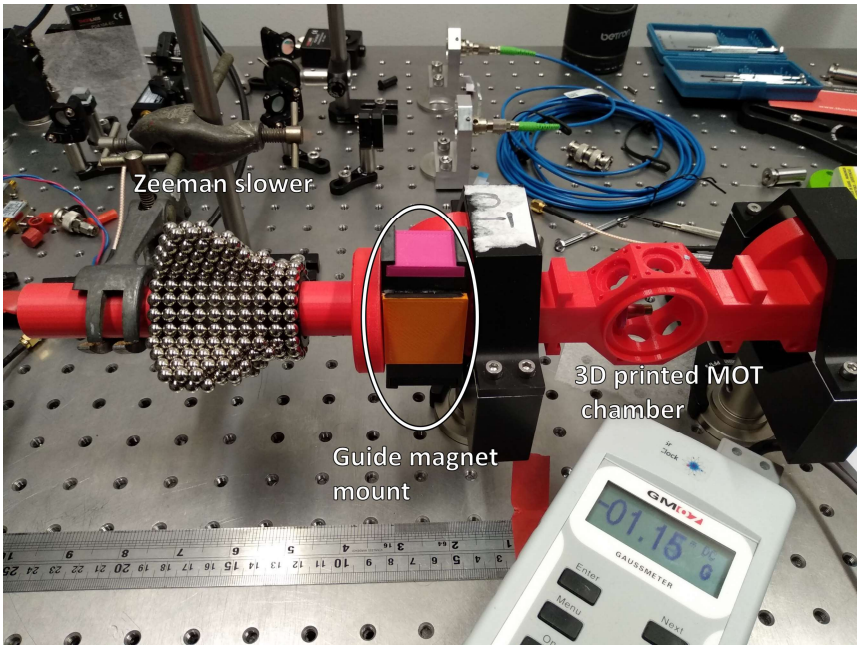

(b) Photograph taken by the author of the setup used to test the guide magnets. The guide magnets are held in place on in the black/pink/orange construction mounted on a 3D printed version of the iqClock testbed chamber.

Several orientations of these guide magnets were tested to see which gave the best

suppression of magnetic fields in the MOT region. Taking the Zeeman slower to be pointing South along the direction of atomic flux the transverse magnets were tested in parallel and anti parallel orientations. The results can be seen in figures 4.13, 4.12, and 4.11. The titles of the graphs describe which faces of the guide magnets were facing each other across the atomic path. Ideally the guide magnets would not interfere with the Zeeman slower profile over the slowing region, but would only reduce the magnitude of the magnetic fields over the MOT region.

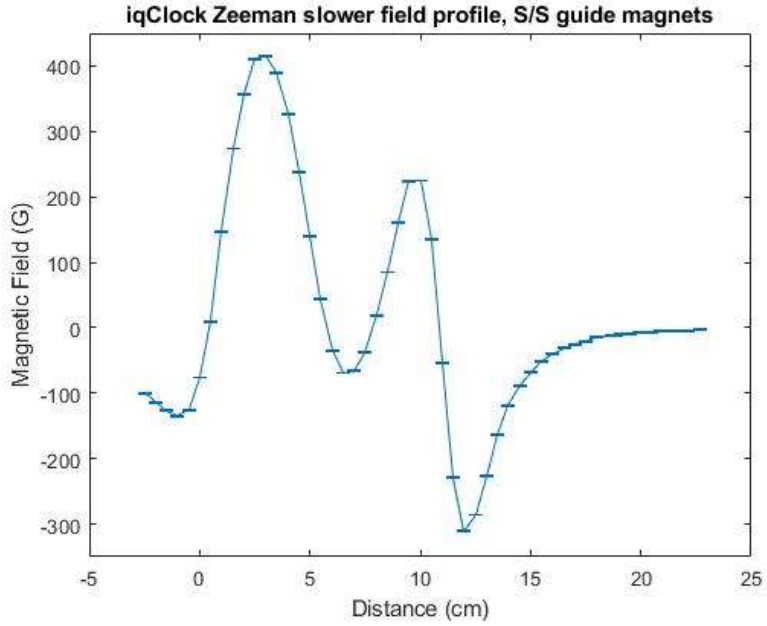

(a) Full profile of the iqClock Zeeman slower with anti-transverse guide magnets with the south poles facing each other over the atomic path.

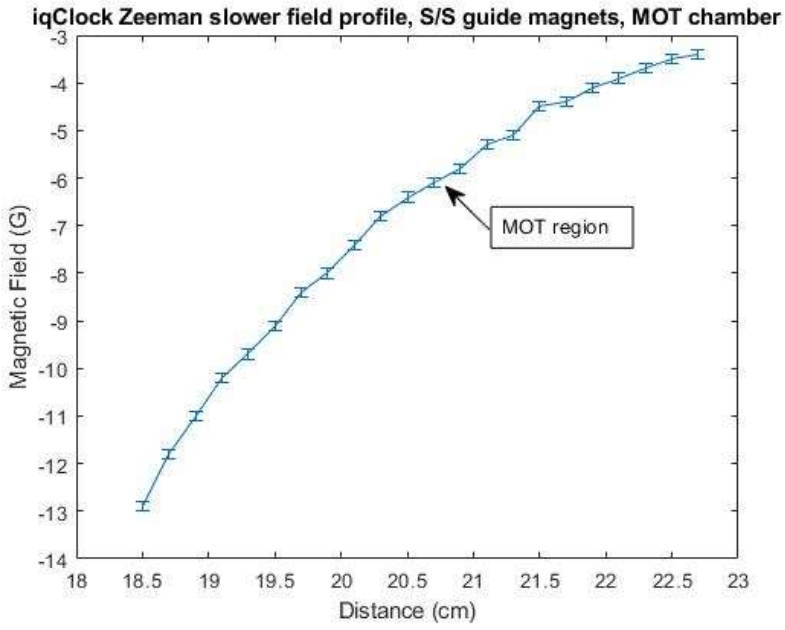

(b) Magnetic field over the MOT region for the S/S facing guide magnets

Figure 4.11 Overall profile of the slower seen in figure 4.11a is quite severely changed, with two regions that could be considered for slowing, a 409 to -74 G drop from 3 to 6.5 cm and another potential gradient from 225 to -311 G over the 10 to 12cm range. Neither region reaches Δ 600 G, and both have very steep gradients. Moreover the magnetic field over the MOT region seen in figure 4.9a is actually higher with this configuration of guide magnets, making it doubly unsuitable for use. The errors seen in these figures match the ones seen in 4.9a, with +/- 1 G and +/- 0.1 G respectively.

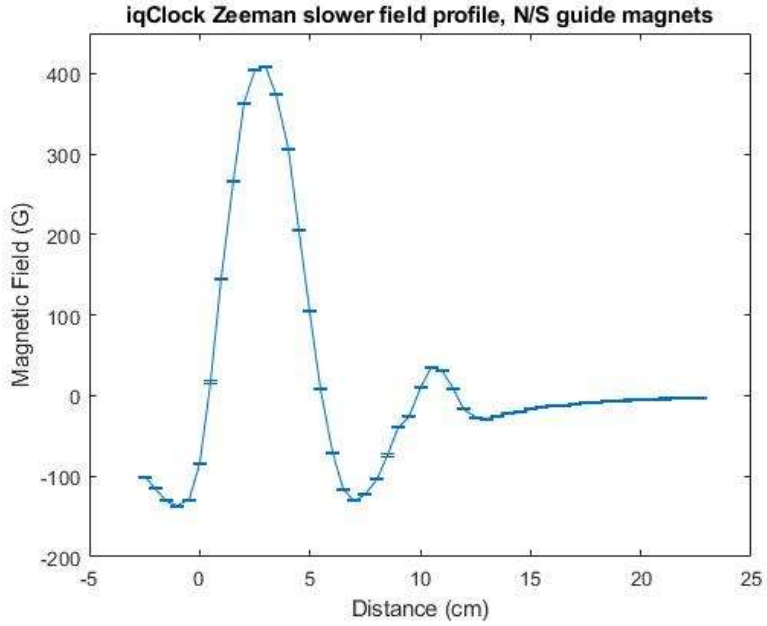

(a) Full profile of the iqClock Zeeman slower with transverse guide magnets oriented with north pole - south pole facing each other over the atom axis.

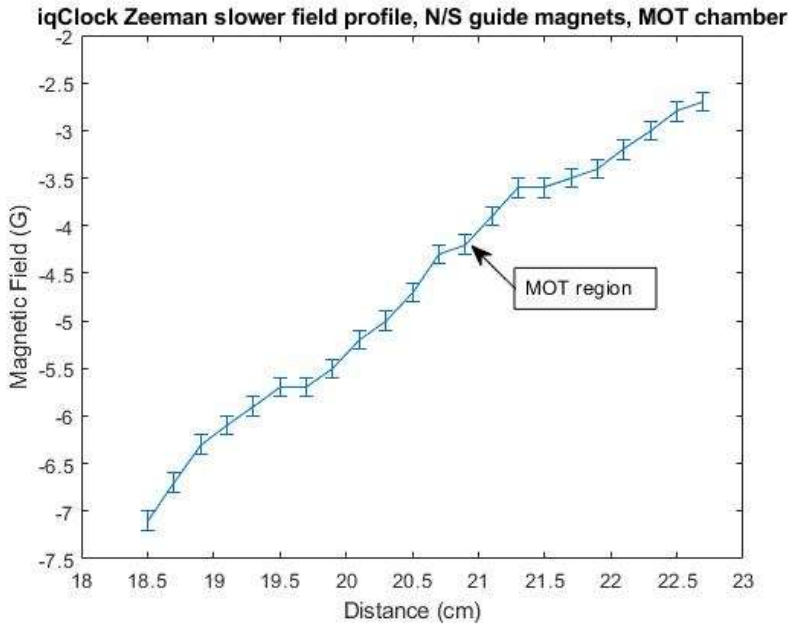

(b) Graph of the MOT region with the guide magnets in the transverse orientation

Figure 4.12 With the guide magnets in the transverse orientation the least deviation from the original magnetic field profile is seen, but also see very little improvement of the magnetic field in the MOT region is present. Flipping the transverse orientation makes no difference to the profile, i.e. having the magnet faces opposite each other over the beam be N/S is the same as S/N. The errors seen in these figures match the ones seen in 4.9a with +/- 1 G and +/- 0.1 G respectively.

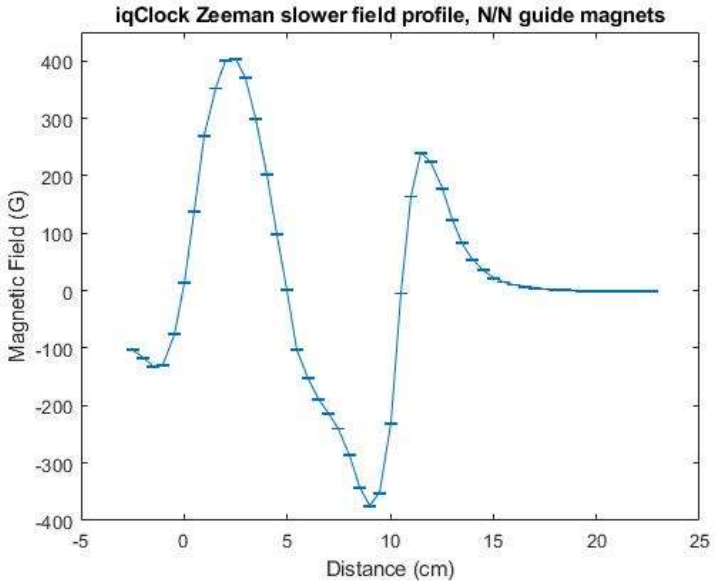

(a) Profile of the Zeeman slower with the guide magnets oriented with their north faces facing each other over the atomic path.

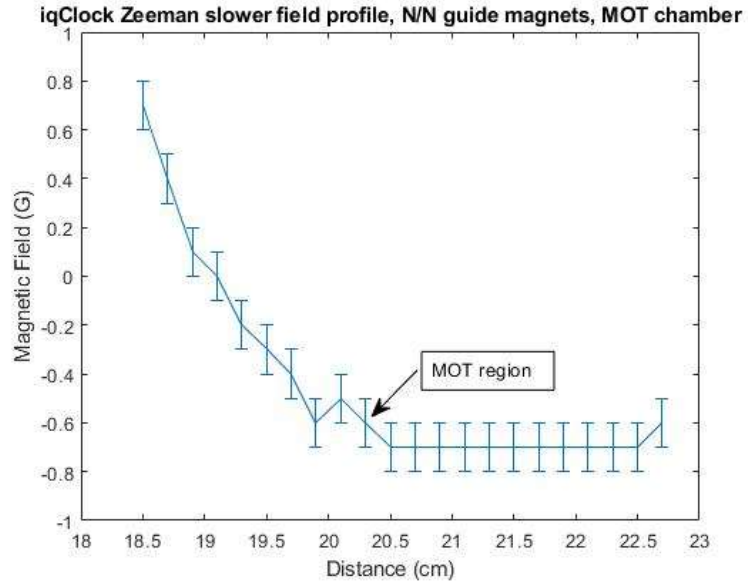

(b) MOT region with the north/ north facing guide magnets

Figure 4.13 Profiles of the Zeeman slower with the north facing anti-transverse magnets show quite a lot of distortion to the Zeeman slower profile, however this distortion does provide a longer slowing region than the other designs, and the gradient remains fairly stable despite the bigger change in magnetic field. The reduction of the magnetic field in the MOT region for this design is also the best out of all designs tested, reducing the magnetic field at the centre of the MOT to less than one G. The errors seen in these figures match the ones seen in 4.9a with +/- 1 G and +/- 0.1 G respectively.

4.2.4 Effect of Zeeman slower on the atom capture number

Initial simulations of the number of captured atoms against the detuning suggested that with the guide magnets on a detuning of around 450 MHz would yield the largest percentage of atoms captured. In order to test this the power of the Zeeman detuning beam was set to its maximum stable value of 17mW and varied the detuning to determine the value for the maximum atom number. This test was performed for a bare chamber, the Zeeman slower with no guide magnets, and the Zeeman slower with the guide magnets installed. These results can be seen in figure 4.14

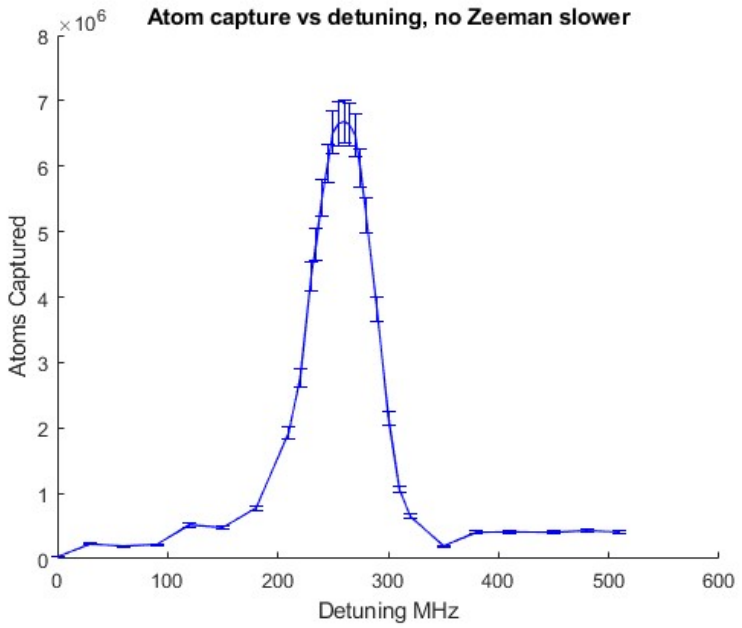

(a) Atom number vs detuning graph for the plain chamber. Without a Zeeman slower the curve is at its smoothest but also relatively narrow.

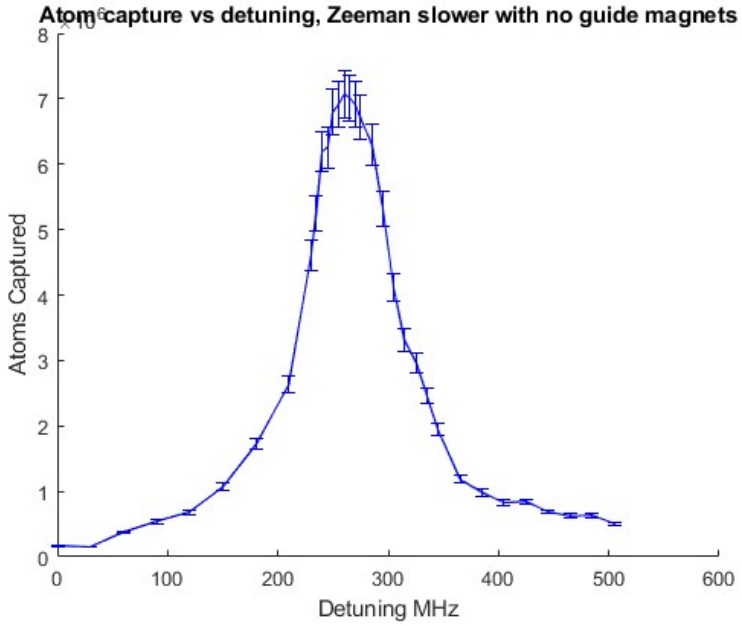

(b) The atom number vs detuning curve for the Zeeman slower is very similar to the curve on the plain chamber, the Zeeman slower curve peaks at a slightly higher atom number, at just over 7 million atoms. The curve is also broader, suggesting that having the Zeeman slower in place would be beneficial if the detuning cannot be precisely locked.

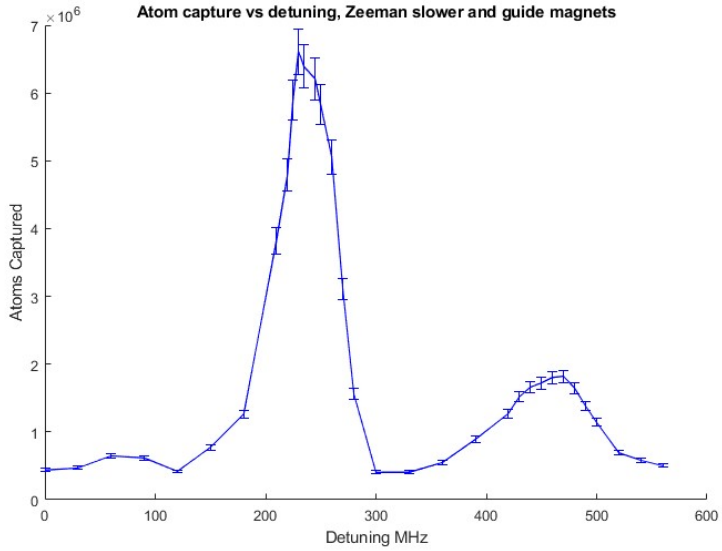

(c) Atom number vs detuning for the setup with guide magnets mounted to the setup. Two peaks can be seen in the graph, not seen in either of the other plots. This is likely due to the greater magnetic field profile seen in figure 4.13a interacting with the beam at two separate detuning ranges.

Figure 4.14 A comparison of the atom number vs detuning curves for the iqClock system MOT with various combinations of the Zeeman slower and the guide magnets installed. Each curve peaks around 7 million atoms, with the presence of the plain Zeeman slower increasing the caught atom number over the other two configurations. The presence of the guide magnets causes a large amount of perturbation to the curve. Each data point for the atom capture number is an average of many readings at the same detuning, taking the standard deviation of these readings gives an error of 5%.

The presence of the guide magnets on the system causes the detuning curve to have an extra peak not seen in either of the other two curves. This is most likely due to the extra peak that is formed in the profile with the guide magnets installed, which can be seen on figure 4.13a. The guide magnet system tested also fails to capture more atoms than either the Zeeman slower with no magnets or the system with no slower installed at all. Between the plain system and the Zeeman slower with no guide magnets there is an increase of around half a million atoms going from the plain system to the Zeeman slower system. Whilst this proves that the Zeeman slower is beneficial in capturing more atoms, the issue of the stray magnetic fields has not been solved satisfactorily. Therefore there are three ways for the project to continue in regards to the Zeeman slower. Firstly the project can continue with no Zeeman slower, this will reduce the number of atoms caught, but the system will still function. Secondly a new design of Zeeman slower could be designed, built, and tested. Using a transverse or design could reduce the stray fields in the MOT region, but would require more laser power. Thirdly the guide magnet system can be iterated upon and perfected. As seen in figures 4.11, 4.12, and 4.13 the use of guide magnets does successfully reduce stray fields in the MOT region. If the affect of the guide magnets on the rest of the Zeeman slower profile could be reduced then the combined Zeeman slower/ guide magnet system would provide increased capture rate and lower stray fields.

4.2.5 Prototype Halbach slowers

As mentioned earlier in this section Halbach arrays present an opportunity for building permanent magnet Zeeman slowers that naturally suppress stray magnetic fields. In order to test these some measurements were taken to determine the difference between the "strong" and "weak" sides of a Halbach array formed of neodymium cuboid magnets held in place with a 3D printed frame. The frame consisted of a bar of plastic with individual slots for each magnet, with a lid that could be slid in place

over the top. This was necessary as the magnets do not want to sit at 90 degrees to each other, and without the frame they would flip and stick together. The lid was found to be necessary as without it the magnets would flip out of the slots to stick together. This data is presented in figure 4.15.

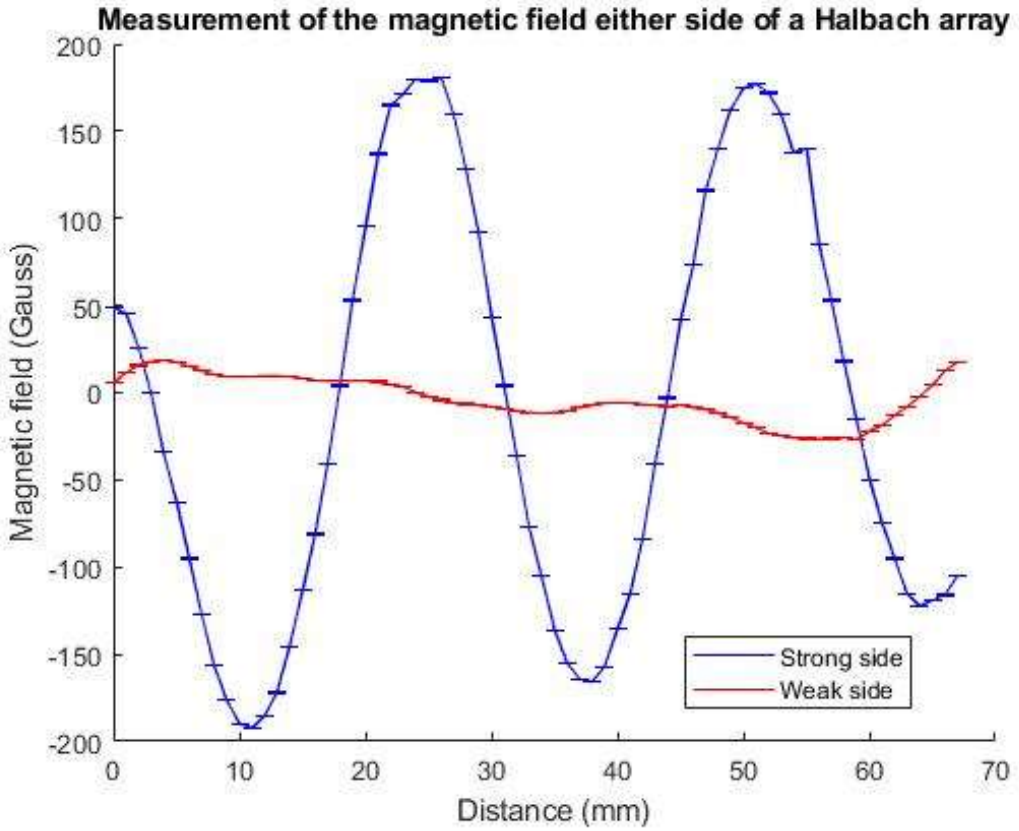

Figure 4.15 The measured magnetic field of the strong and weak sides of a single Halbach array. The measurement was taken at a constant 1cm distance from the array of magnets. It can be clearly seen that the strength of the magnetic field varies drastically from one side to the other. The oscillating quality of the magnetic field is due to the rotating orientation of the individual magnets comprising the array. The error of +/- 0.1 gauss stem from the hall probe used to measure the magnetic field.

The oscillating quality of the magnetic field in figure 4.15 does pose a problem from constructing Zeeman slowers out of individual Halbach arrays. As the magnitude of the field oscillates it means that during the region between one maxima and the next the atoms will be out of resonance with the laser, meaning the slower will have to made considerable longer to have the same slowing effect. Instead the design

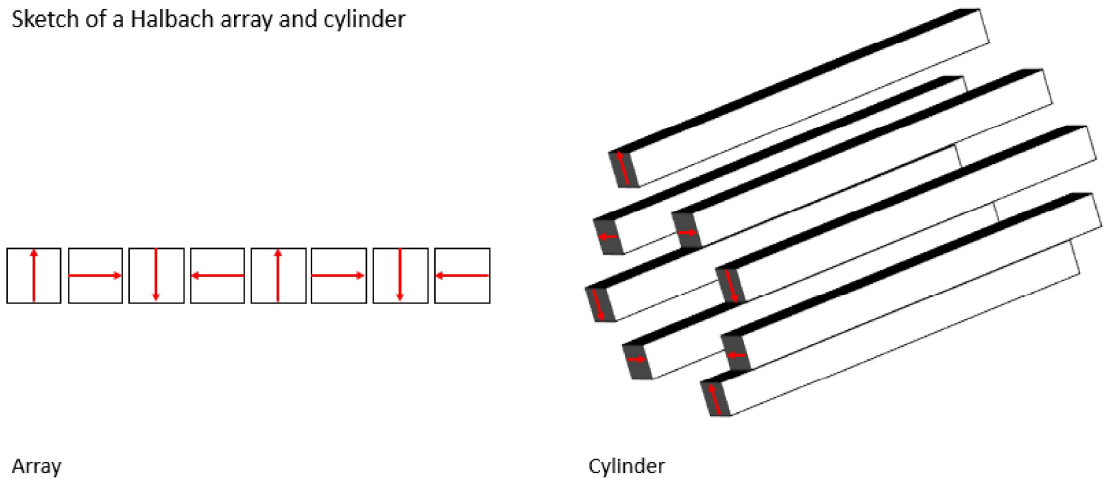

Figure 4.16 Sketch of a Halbach array and how this is looped to form a Halbach cylinder. The red arrows denote the magnetic field flux from south to north through the magnet. The Halbach cylinder will form a transverse field between the top most and bottom most bars of the cylinder. A slice through a Halbach cylinder and the fields formed is seen in figure 4.2b.

is to take a Halbach array and bend it into a loop, and then extend this loop to form a cylinder. A visualisation of this can be seen in figure 4.16.

As a test a Halbach cylinder was constructed, using the same 3D frames as and the magnetic field through it measured. This data is presented in figure 4.17.

The benefits of spin-flip slowers have been outlined in section 4.1.3, and in order to make one with a Halbach cylinder two cylinders would be required. The cylinders would be rotated in relation to each other so that the transverse field flux across their diameter flowed in opposite directions.

Whilst this shows promise for future Halbach designs, on the iqClock testbed system the lack of space severely prevented any further investigations. The self assembled design has the benefit that it requires no additional support structures to keep it in place, being entirely held in place by the magnets that comprise its form. A Halbach slower would require a frame to keep the magnets in place, the added bulk of which would be difficult to fit on the iqClock testbed architecture. An attempt to make a Halbach cylinder mounted on the adhesive layer unfortunately did not work as the

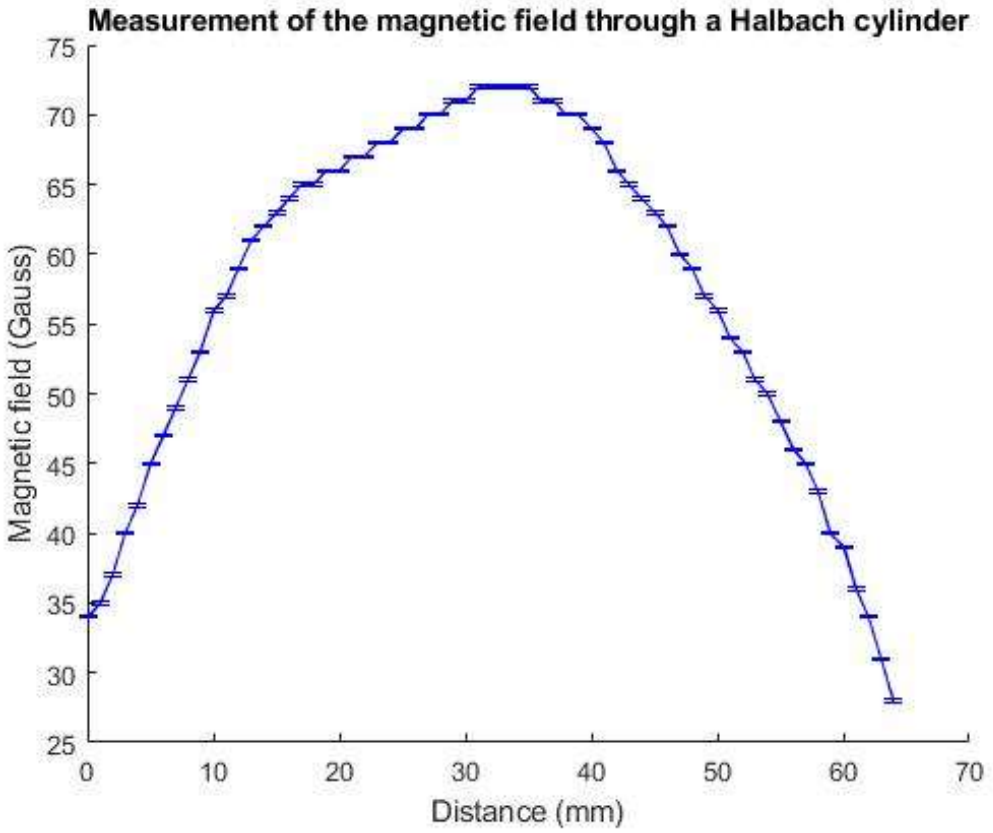

Figure 4.17 The magnetic field through the centre of a Halbach cylinder. As expected for a transverse field the magnetic field drops sharply at the ends of the cylinder. The profile shows that the field through a parallel Halbach cylinder remains steady in the centre and only drops off towards the exits. Error of +/- 0.1 gauss from the Hall probe.

cuboid magnets used would flip themselves round to more favourable positions. A more traditional transverse design such as the one presented in figure 4.1 is much smaller than a Halbach cylinder, as it only requires two rows of magnetic material placed wither side of the slowing axis, rather than the eight rows for the Halbach cylinder design. Should the system architecture allow a project to design a Halbach slower for the iqClock industry system would present an intriguing opportunity.

4.2.6 Conclusions

Utilising spherical permanent magnets a Zeeman slower can be relatively simply simulated, built, and characterised. Proof of concept for the stray field attenuating guide magnets has also been achieved, although there is further work to be done to perfect this technique and to incorporate it into the simulations for the magnetic field profile. Future projects wanting to use the self assembled Zeeman slower technique will have to account for the stray fields by ensuring that there is enough space between the end of the Zeeman slower and the MOT region to either install magnetic shields or guide magnets, or let the magnetic fields attenuate naturally as in the LRI experiment [139]. As the iqClock system is already under vacuum and taking it apart would cause massive disruption to the experiment the installation of a solenoidal Zeeman design is not desirable. Thus any future work on Zeeman slowers for the iqClock testbed would have to look into transverse permanent magnet designs to reduce the stray fields in the MOT region. As mentioned in section 4.2.5 above, the system architecture for the iqClock testbed is too cramped to allow a Halbach cylinder design. Thus any transverse system would not benefit from the self suppression of magnetic field present in the Halbach designs. A transverse system would however mean that a redesign of the laser systems would be required to interact with the transverse fields as outlined in section 4.1.2. Ultimately the iqClock can form a MOT of around 7 million atoms with no Zeeman slower in place, and thus future work in the group on Zeeman slowers would be concentrated on the to be built iqClock industry system

or as a replacement for the self assembled system on the LRI project.

Chapter Five

MOT coil eddy current investigation and characterisation

As part of a 3D MOT system it is necessary to have 3 counter-propagating laser pairs, produced either through individual beams or through other methods such as prisms or optical gratings. These lasers provide the optical velocity dependent component of the trap. To create the magnetic position dependent element of the MOT two coils are used oriented in an antihelmholtz configuration. This produces the quadrupole magnetic field necessary for trapping the atoms. The iqClock requires rapid changes of the magnetic field between stages in the clock process, for this it is necessary to install fast switching circuits in place on the coils, and that the induction of magnetic fields caused by the current in the coil in the rest of the system is limited. The coils are solenoids wrapped around metal formers to keep their shape, and as the flow of current generates heat large heatsinks were built onto the side of the formers to keep the coils cool. These MOT coils are part of the atomic package seen in the block diagram in figure 3.3, and are mounted around the MOT and trapping region.

5.1 Eddy currents

Eddy currents are looped electrical fields induced into conductors by a nearby changing magnetic field. These eddy currents flow in a closed loop in an conductor, and

through Lenz' law, produce a magnetic field in the opposite direction to the one that formed them. These eddy currents will persist for some time after the removal of the magnetic field.

Whilst building coils for the iqClock MOT an investigation was done into the need to cut slits in the metal former that the wire would be wound around. Metal formers present the perfect conditions for eddy currents to form, as they are close to a changing magnetic field source, and the formers geometry lends itself well to a closed loop of current flowing through it. To prevent eddy currents from conducting around the circumference of the former a slit can be cut through the former to break the circuit. This doesn't remove the eddy currents, but by preventing the eddy currents from conducting around the circumference of the former the magnetic fields that are produced by the current are reduced.

The desire to reduce eddy currents comes from the need to have high levels of control over the magnetic field during the operation of the clock. In the final interrogation of the atoms the coils are quickly turned off to remove the magnetic field and allow magnetically unperturbed atomic transitions to be investigated. If eddy currents are present in the coil former however, the magnetic field switch off is not as quick, as the eddy currents only slowly decay in relation to the quick shut off of the coil. These eddy currents are therefore producing a decaying magnetic field past the time that the magnetic field from the coils has been removed, causing shifts in the transitions in the trapped atoms. This decaying magnetic field increases the dead time of the clock experiment, as whilst the field is present and changing no measurements can take place. The longer the dead time the more the clock laser can drift before the next set of measurements. By cutting slits in the formers the current that produces the decaying magnetic field should be suppressed. Images of the formers with and without the slit can be seen in figures 5.1a and 5.1c.

Former Designs

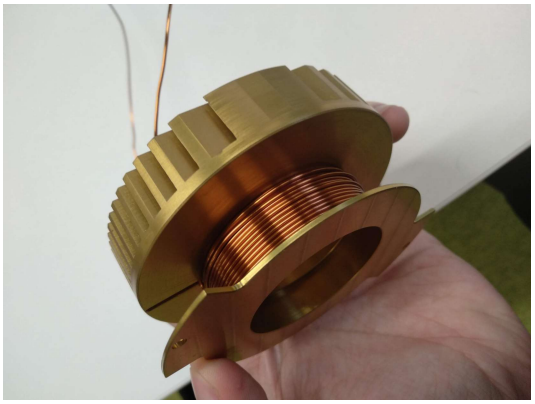

(a) Metal former as originally designed. There is a slot cut through the heat sink to allow the wire to be wrapped around the former neatly, but this slot does not go through the entire structure as in figure 5.1c.

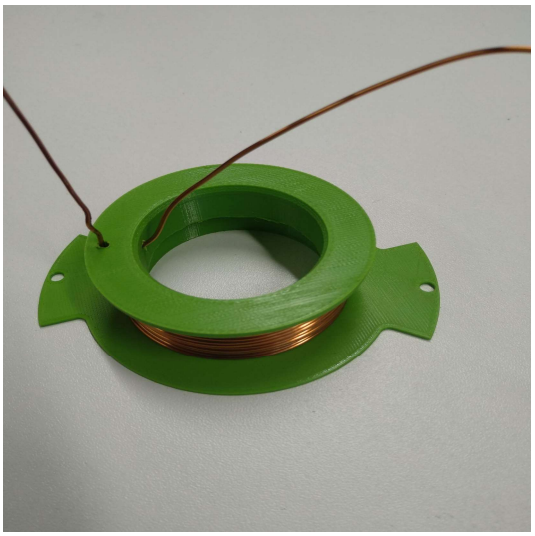

(b) Plastic former used to test against the metal formers.

Former Designs- continued

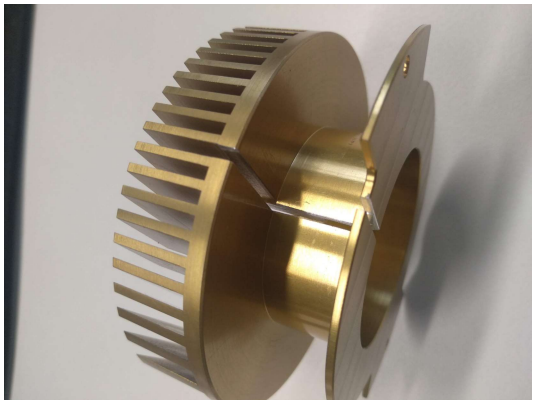

(c) Metal former with the slit cut through it.

Figure 5.1 Photographs taken by the author of the three former types used to test the impact of unconfined eddy currents induced by turning the MOT coils on and off.

The removal of eddy currents could also be achieved through use of a non-conductive former. A plastic former would meet this criteria, but another problem then would emerge. A plastic former would only be suitable for a low current coil, as it would not be able to transfer heat away from the coil. A buildup of heat within a coil changes the magnetic field it produces as the increasing temperature increases the resistance in the material, decreases the current that can flow through the wire. With no way for heat to escape, with a high current, the risk would be run of melting the wires at the centre of the solenoid or the former itself.

To test the impact on the magnetic response of having no slit in the former, a metal former with no slit in it was tested against a former constructed out of plastic. The magnetic field in the coil was drive by a square wave signal generator with a period of 1s. In order to ensure that the coils would follow the signal generator rapidly a basic fast switching circuit was constructed utilising a MOSFET chip.

Magnetic response times in a solid metal former.

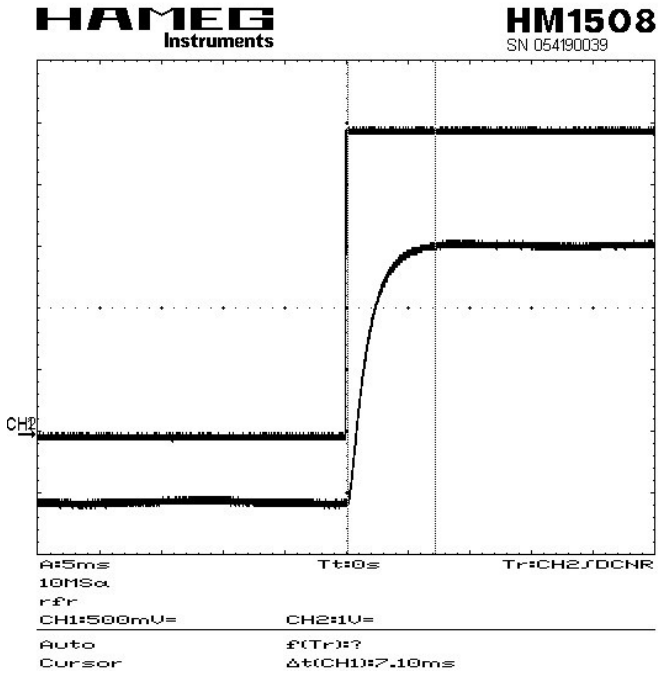

(a) The magnetic response to the turning on of the coils. The magnetic response (seen in the lower trace lags behind the driving signal by $\approx 7ms$.

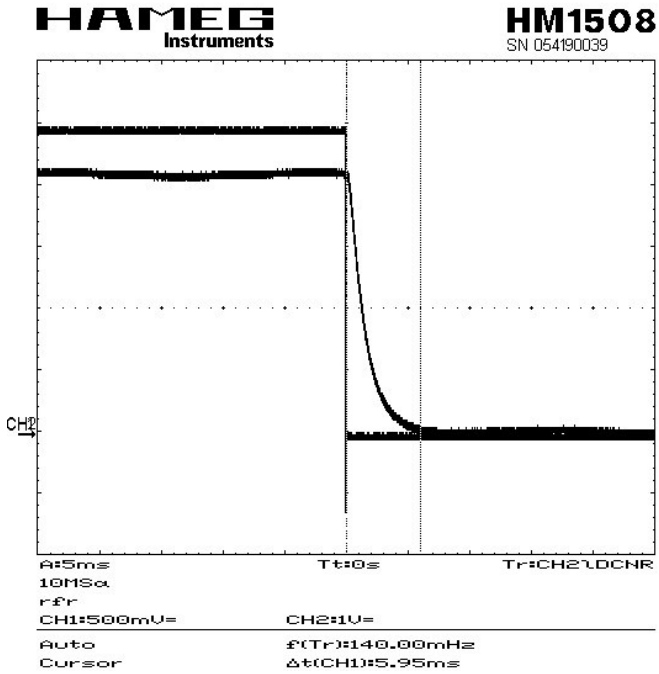

(b) The magnetic response to turning off the coils, the response lags behind the signal by $\approx 6ms$.

Figure 5.2 Oscilloscope trace of the effect of a non slit former on the eddy currents. The top trace shows the signal generator used to turn the coils on and off, whilst the bottom trace shows the magnetic response from inside the former.

Magnetic response times with a plastic former

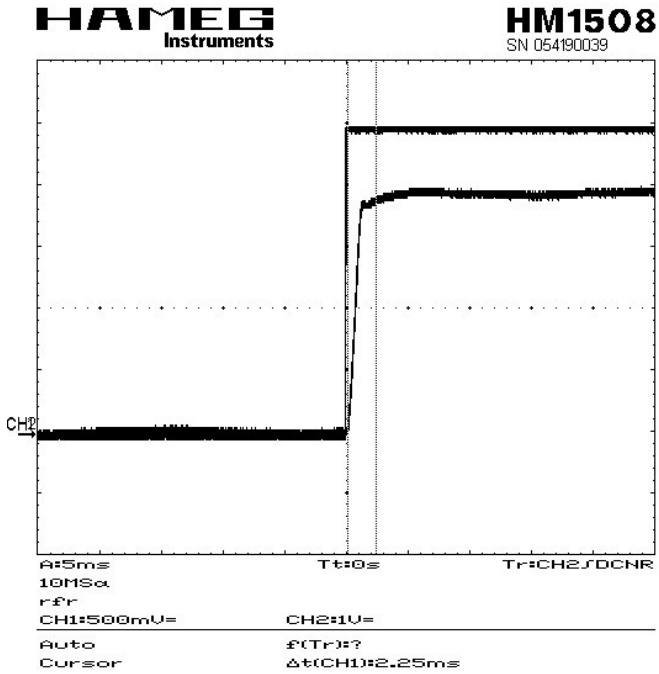

(a) The response as the magnetic field is turned on with a plastic coil former. There is a brief period of oscillation of less that $3ms$ before the magnetic field settles down.

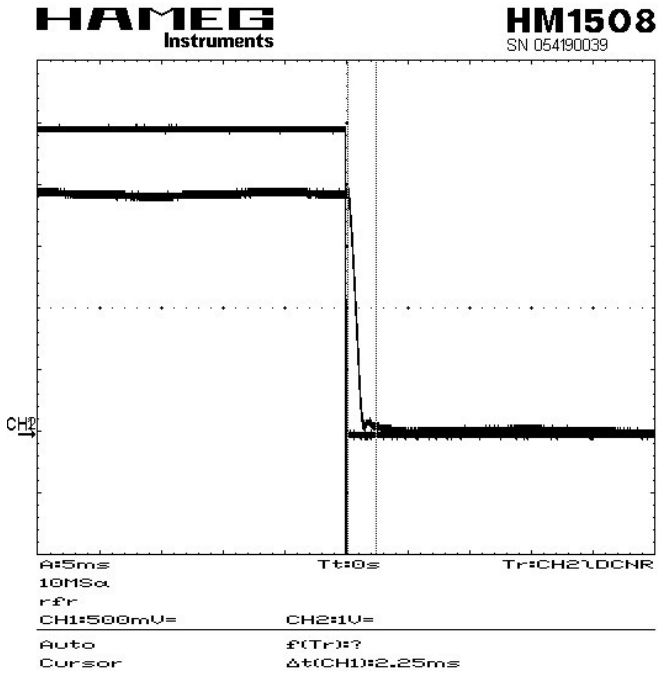

(b) Response as the magnetic field is turned off. There is another set of oscillations, which are more pronounced than in the turn on response. The effect subsides within $3ms$.

Figure 5.3 Oscilloscope traces of the magnetic response times with the coils wrapped around a plastic former. As an insulator no eddy currents can be induced in the plastic former. The oscillation of the field during the turn on/off process is likely due to a "bounce" present in the fast switching circuit constructed for this experiment.

For the coil former seen in figure 5.1a the field lags behind the signal generator by a considerable amount of time. The gradual rise/decay of the magnetic response compared to the driving signal is due to the eddy currents in the former existing beyond the time that the magnetic field exists.

The oscillations present in figure 5.3 before the magnetic field settles down are due to the fast switching circuit built for this experiment. With further work on this circuit this effect could be suppressed. The oscillations are most likely not seen in figure 5.2 as the large magnetic fields caused by the eddy currents are so large in comparison as to cover them completely.

The traces with the slit and plastic formers seen in figures 5.1c and 5.3 respectively, resemble each other much more than the smoother, longer magnetic field turn on/decay times seen in figure 5.2 with the solid metal former. As no eddy currents can form to circulate in the plastic former, this must be the "clean" response, with no induced fields. The magnetic field response times are on the order of 4 times shorter with the slit former, showing a great improvement over the solid former. Despite the potential for the formers to warp if they have a slit cut through them, the increase in performance allowed by the reduced eddy current flow is a much better trade off. Thus it can be determined that for the iqClock experiment the formers should indeed have slits cut through them to prevent the conduction of eddy currents and thus prevent decaying magnetic fields that would interfere with the formation of the MOT.

Magnetic response times with a slit metal former

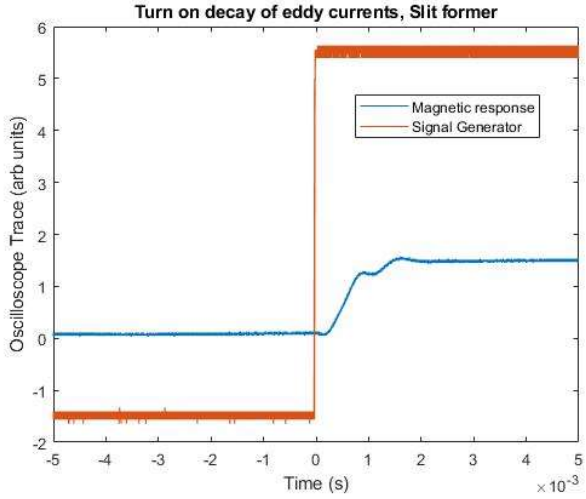

(a) The on response of the magnetic field with the slit former. Once again the oscillation from the fast switching circuit is present -suggesting no eddy currents. The response lags the signal by less than $2ms$.

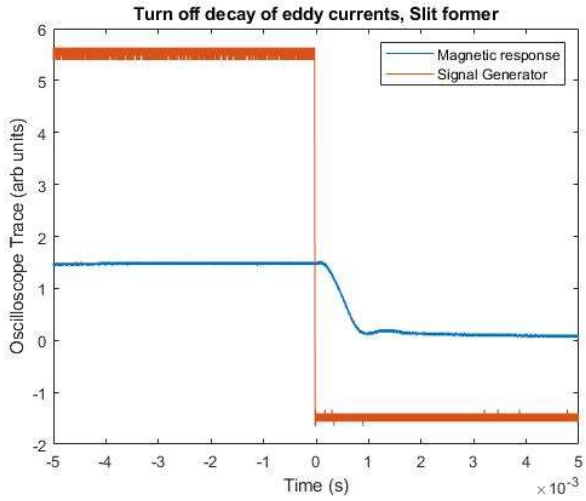

(b) The response time of the magnetic field when the coils are turned off. Much like the on response the magnetic field follows the signal within $2ms$.

Figure 5.4 This data was captured with a different Oscilloscope than the data in figures 5.2 and 5.3, hence the difference in graphical style. The major aspect of interest is that the traces in the above graphs much more closely resemble the traces of the plastic former in figure 5.3, indicating that the slit former does suppress the magnetic fields caused by eddy currents to a large degree.

From the data shown in 5.2, 5.3, and 5.4 it can be concluded that the addition of a slit into the metal former that holds the MOT coil is a necessary part of the

design. This slit drastically reduces the time that eddy currents are present in the system, thus reducing the presence of slowly decaying magnetic fields, which in turn reduces the dead time between measurements in the experimental cycle. The use of a non electrically conductive former would also provide the same benefits as the slit former, but the choice of material then becomes problematic. Most non electrically conductive materials also do not conduct heat well, such as plastics or ceramics. This would lead to heat building up from the coils and could warp or crack the coils or otherwise damage the experiment without external cooling systems. For the iqClock system the next stage is portability, thus the coils formers have been designed with heatsinks that passively conduct heat away from the coils without the need for active cooling systems. This requirement makes non thermally conductive formers unsuitable, and thus the slit metal former is the optimal solution to reduce the effects of eddy currents.

5.2 iqClock coils and characterisation

The coils for the iqClock system at Birmingham were built upon the slit formers investigated in section 5.1 of this chapter. The coils are comprised of coated copper wire, with 10 layers of 16 turns each. In order to construct the coils a winding device was used, as seen in figure 5.5. In between each layer of coils a coat of thermal paste was applied to help thermal conduction between the turns of wire. This is necessary as the central turns have no way of divesting heat other than transfer to neighbouring turns, if the thermal paste is not applied the coil can very quickly overheat and warp.

5.2.1 Temperature measurements

The temperature of magnetic coils is important to characterise as unregulated temperature increase can cause a multitude of problems. Firstly, and most drastically, if the temperature gets too high then damage can be done to the system itself. Secondly

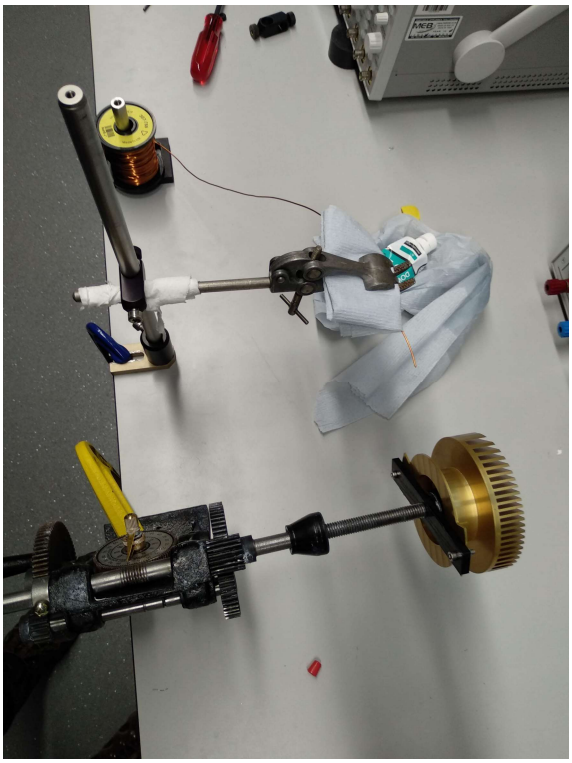

Figure 5.5 Photograph of the process for winding the MOT coils taken by the author. The clamp and blue roll set up was to keep the wire taught as the handle was wound on the winding device.

the increased temperature increases the resistivity of the wire forming the coils, this means that the current drawn by the coils increases and in turn so does the magnetic field.

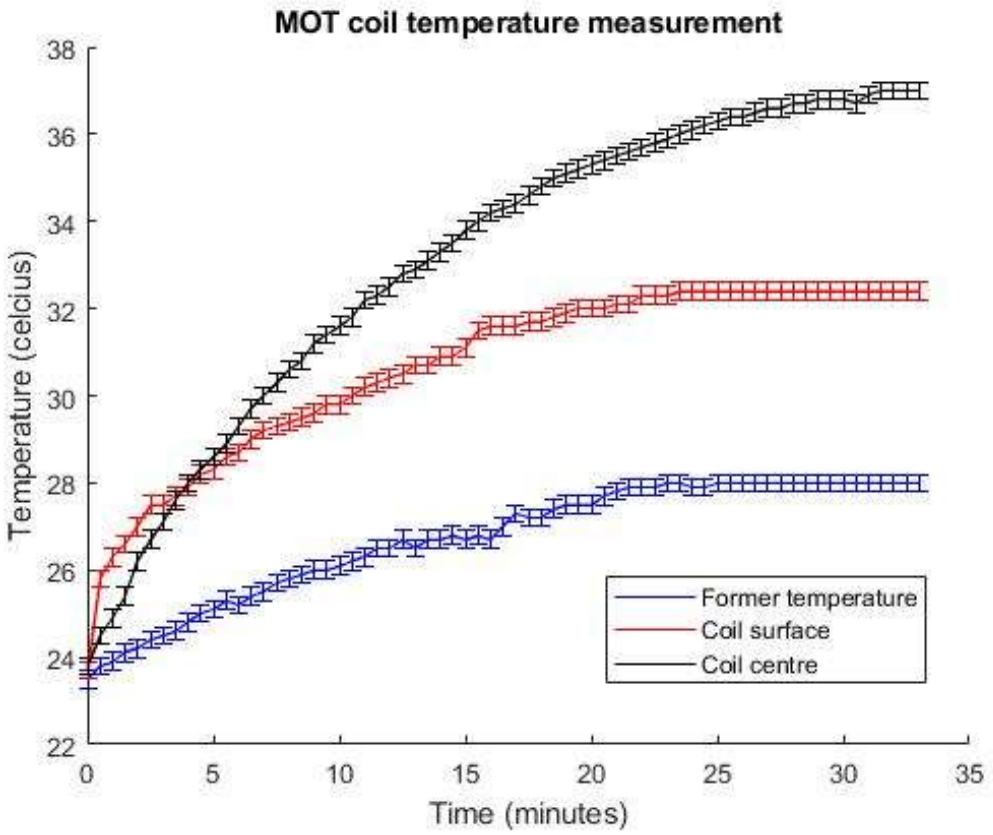

Figure 5.6 Graph of the coil temperature over time in the iqClock MOT coils. The current was kept at a constant 2.4 A. The temperature was sampled every 30 seconds, with the error on the measurement coming from the accuracy of the thermistors used at +/- 0.2 degrees.

5.2.2 Magnetic field measurements

Once the temperature response of the coils had been determined the magnetic field was measured to determine the profile of the magnetic field over the MOT region. The ideal current and profile for the coils had previously been calculated in the group and these measurements were taken to confirm that the built coils matched these simulations, as seen in figure 5.7.

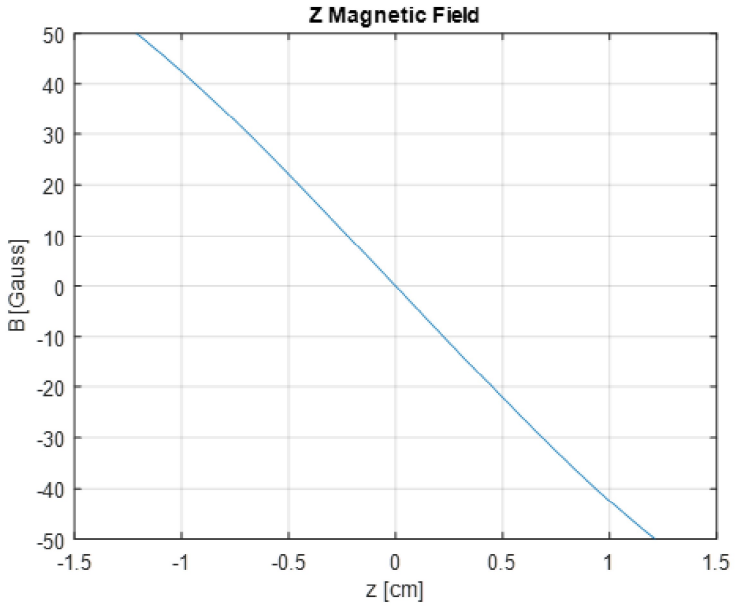

(a) The simulated magnetic field over the Z axis- along the path the atoms would take between the coils. The gradient of the magnetic field is -45 G/cm.

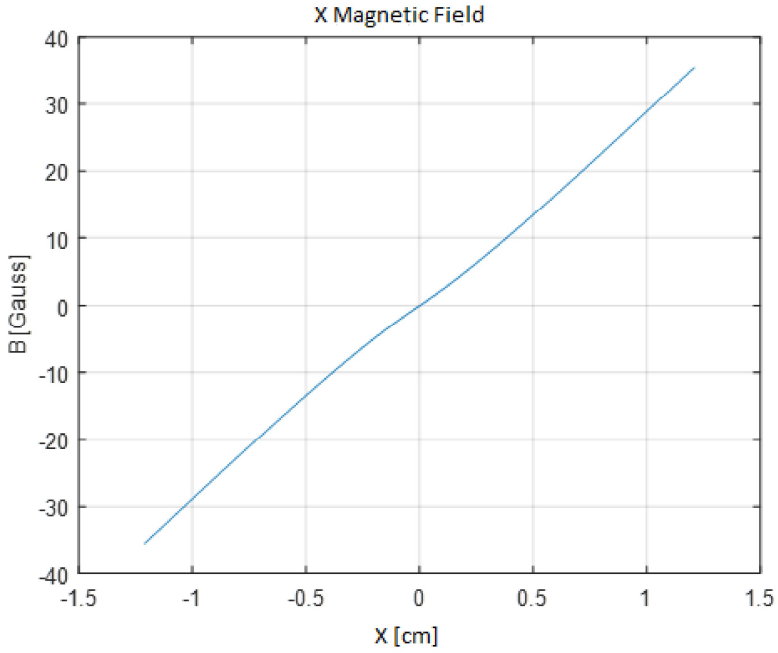

(b) The simulated magnetic field over the X axis- though the centre of the circumference of the coils. The gradient of the magnetic field is 23 G/cm.

Figure 5.7 Simulated magnetic field over the MOT region in the Z and X axes. This simulation shows the magnetic field produced with 3.8 W of power supplied to the coils.

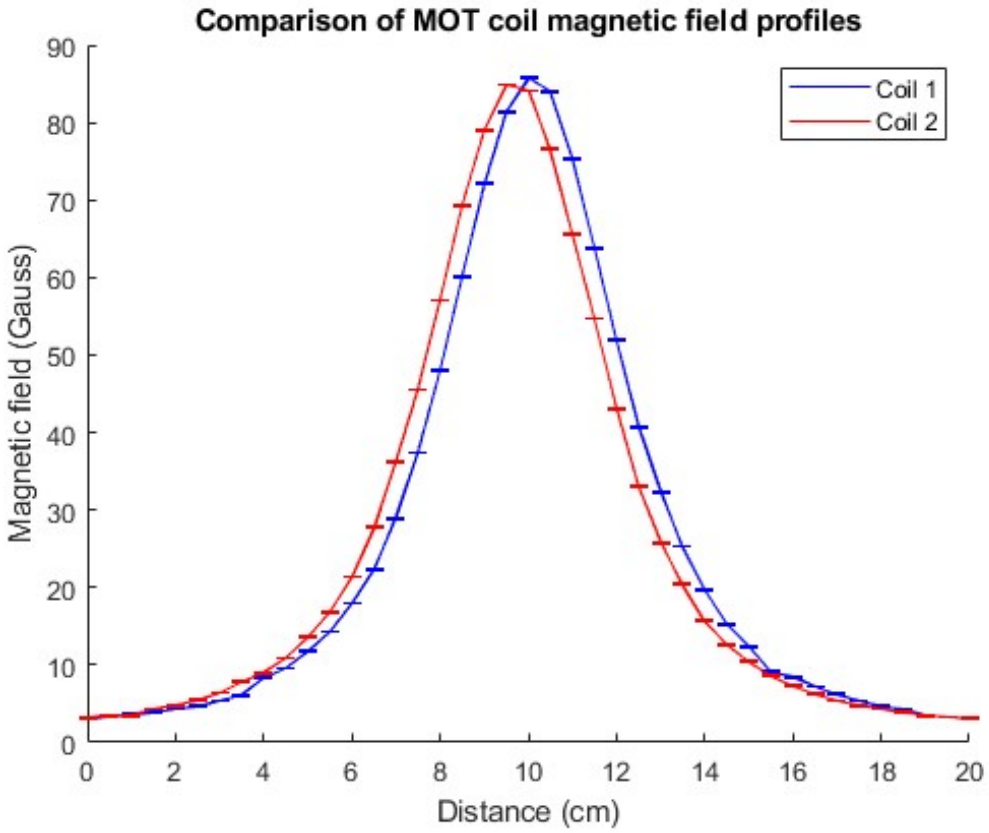

Figure 5.8 Measurement of each individual coils magnetic field taken through the centre of each coil, the offset between the two data sets is likely to be the result of a slight change in the position of the coil relative to the starting position of the magnetic probe whilst swapping the coils over. Otherwise, the magnetic field profiles match well. The errors in the data stem from the hall probe which at these magnetic field strengths is +/- 0.1 gauss.

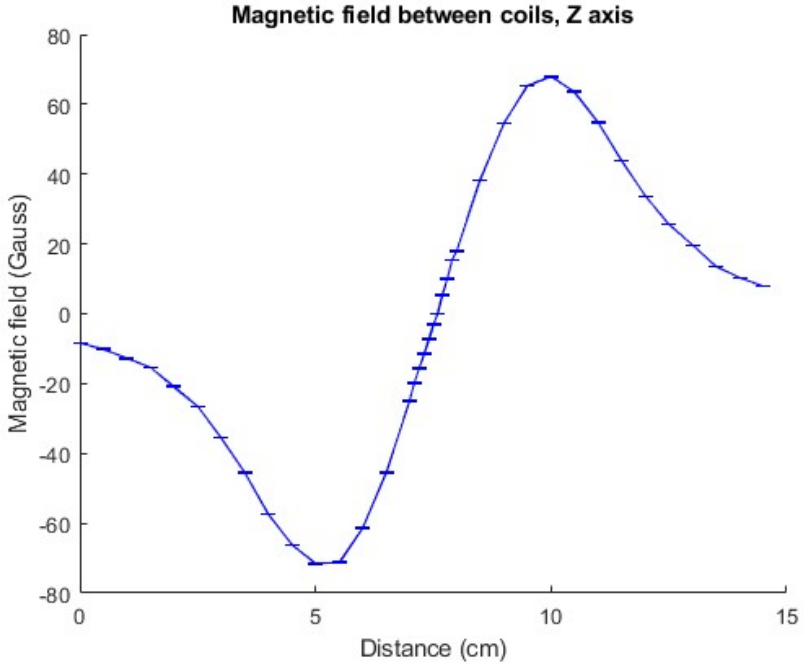

(a) Antihelmholtz configuration of the MOT coils at 3.8 W, 2.4 A, taken through the Z axis of the coils.

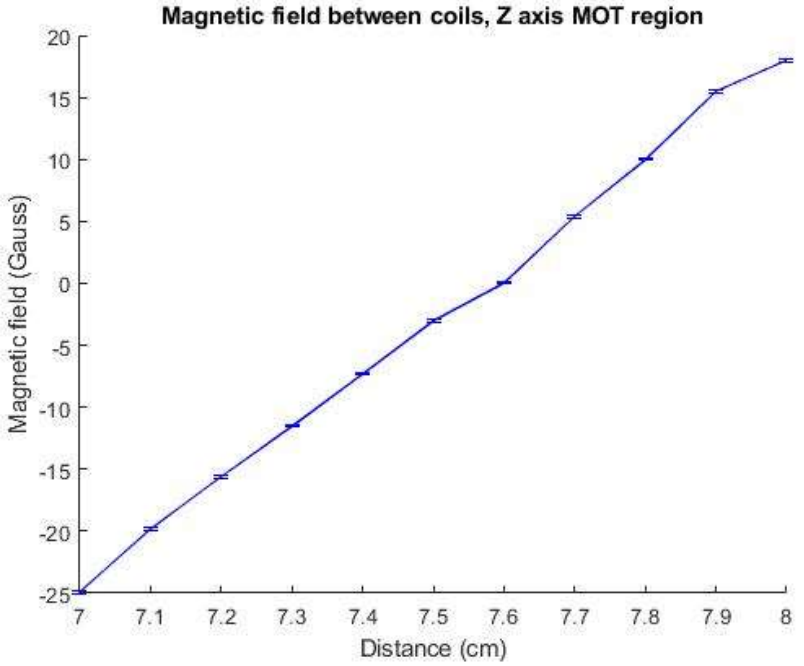

(b) Zoomed in image of the magnetic field over the MOT region, the centre of the MOT is at 7cm.

As can be seen from figure 5.10 for the time taken for the temperature of the coils to stabilise the magnetic field varies by less than 2 G. This means that the coils can be run for long periods of time without any major variations in the produced

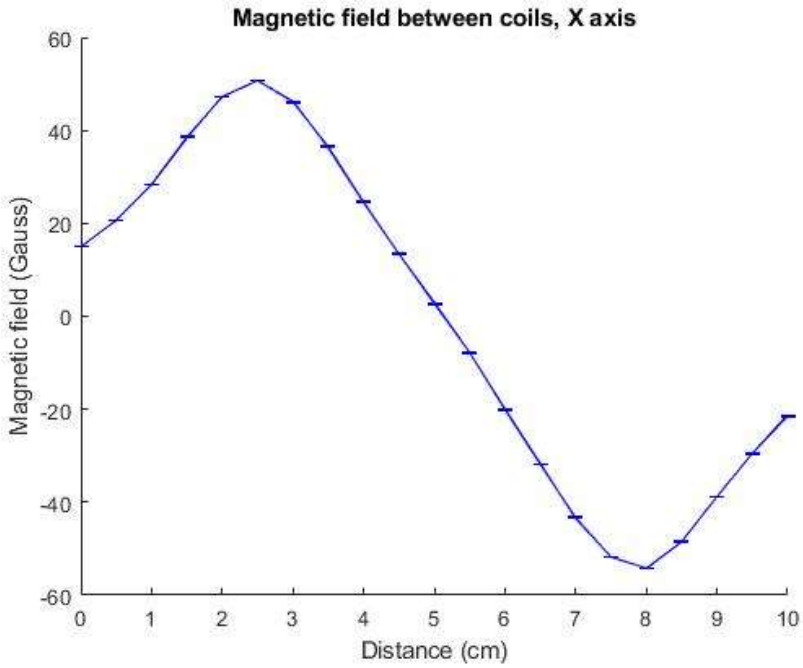

(c) X axis magnetic field over the MOT region between the coils, taken at Z= 7 in figure 5.9a. The MOT centre is at X=5cm.

Figure 5.9 The measured magnetic field of the MOT coils in situ on the system. The magnitude of the field gradient over the MOT region seen in figures 5.9b and 5.9c agrees well with the simulated field gradients seen in figure 5.7. The direction of the slope is not of great concern as this can easily be reversed by swapping the current inputs on the coils to make the direction of the gradient match the simulations. Error of +/- 0.1 gauss stemming from the hall probe sued to measure the magnetic field

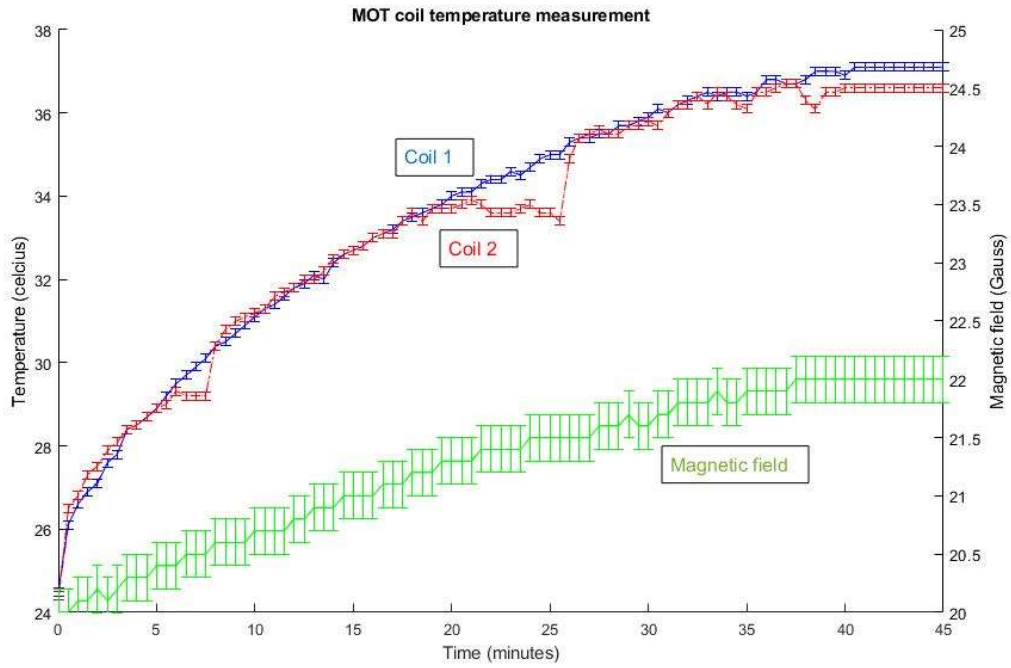

Figure 5.10 Graph showing the trend of the temperature for each coil and the effect on the magnetic field measured between them. The dip in the curve for coil 2 at the 26 minute mark occurred when the thermistor detached slightly from the coil. The thermistors in this test were placed in the same position as those measuring the temperature of the coil centre in figure 5.6. From this test it can be seen each coil has the same temperature response, and that it takes 40 minutes of constant use before the temperature stabilises at The The Y axes for the temperature and magnetic field are not in the same range to better show the details of each data set. The error present on the temperature data is +/- 0.2 Celcius coming from the accuracy of the thermistors. The magnetic field error is coming from the hall probe used which gives the same error as present in the Zeeman slower measurements in chapter 4 of +/- 0.1 gauss.

magnetic field. An image of a MOT formed in the iqClock system can be seen in figure 5.11.

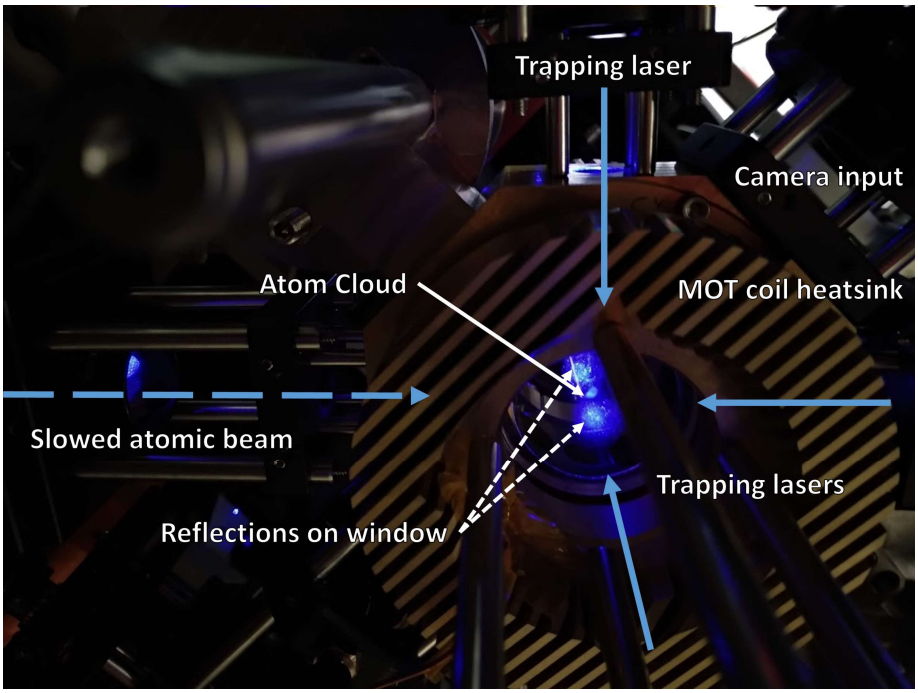

Figure 5.11 A photograph taken by the author of a successful blue MOT captured with the coils built in this chapter. The optical windows on the system are reflecting some of the laser beam power into and out of the plane of the image, but the MOT can be seen sitting between the the reflected spots. The coil former can be seen in the forefront of the image surrounding the optical window.

5.3 Conclusions

From the experiments detailed in this chapter it has been proved that the inclusion of slit formers in the design of the MOT coils reduces the magnetic fields that eddy currents induced into the system, and thus reduces unwanted decaying magnetic fields in the MOT region. Whilst this may reduce the structural strength of the system slightly this trade off is beneficial to the overall stability of the system. From the results presented in section 5.2, it can be seen that the coils are suitable for long periods of use without overheating and that they produce the required magnetic field for successfully trapping strontium in a MOT.

Chapter Six

Stabilisation of optical fibre connections for optical atomic clock systems

6.1 Clock Networks

A device used for the measurement of a dimension or value is limited in its use unless there is an external reference frame on which to compare its measurements. In terms of clocks this means that a system can be fantastically accurate and stable but it wouldn't be of much use unless its timing signals can be compared against similar standard clocks. By connecting spatially separated clocks via optical link, fibre, or portable clocks, a network of timekeeping devices is formed. Such networks have applications in measuring geodesy [18], [20], or to provide holdover systems in the case of a satellite failure for example. The need to accurately link timing systems is not just limited to the desire to create networks of such devices. In the iqClock testbed system the frequency comb necessary for the clock transition is located in a different lab to the atomic and laser packages due to space constraints. Additionally the iqClock testbed system is to be used as a standard to test the iqClock industry device against, these two devices will again need to be linked together in order to

characterise them. Eventually it is hoped to link the iqClock devices to clocks based at the NPL as part of efforts to make an optical atomic clock network. This link would take place on the rf output of the frequency comb seen in the block diagram in figure 3.3.

6.1.1 Methods of linking clocks

The connection between two clocks needs to reliably and accurately transfer the signal from one end of the link to the other. The method for doing so very much depends on the locations of the clocks in question. Free space links work best when disseminating signals between orbiting clocks, as there is no atmospheric interference. Additionally for networks that involve clocks in orbital or aerial platforms fibres are considerably less useful than free space links for obvious reasons. Atmospheric interference in a free space link ranges from the obvious weather issues such as rain and fog to more complex interference's. As the atmosphere is constantly in motion there is a considerable amount of perturbation introduced to any free space optical link. Atmospheric effects such as turbulence, temperature, and pressure can effect a signal in one of two ways. The first introduction of perturbations is due to scintillation and beam wander caused by atmospheric turbulence. This results in fluctuations in the beam intensity and can result in the signal fading in and out. For an optical frequency free space link any down time in the signal is a space of time where errors can creep into the the system, This effect is well documented in existing free space dissemination of microwave time signals Secondly shifting refractive indexes in the atmosphere due to atmospheric conditions will effect the optical path length of the link and introduce phase noise. On long time scales the temperature and pressure of the local climate will effect the atmospheric refractive index in much the same way as applying pressure or heat to an optically conductive material. On a shorter time scale the wind can introduce the "piston effect" which will also change the optical path length of the link and introduce jitters in the phase noise [140].

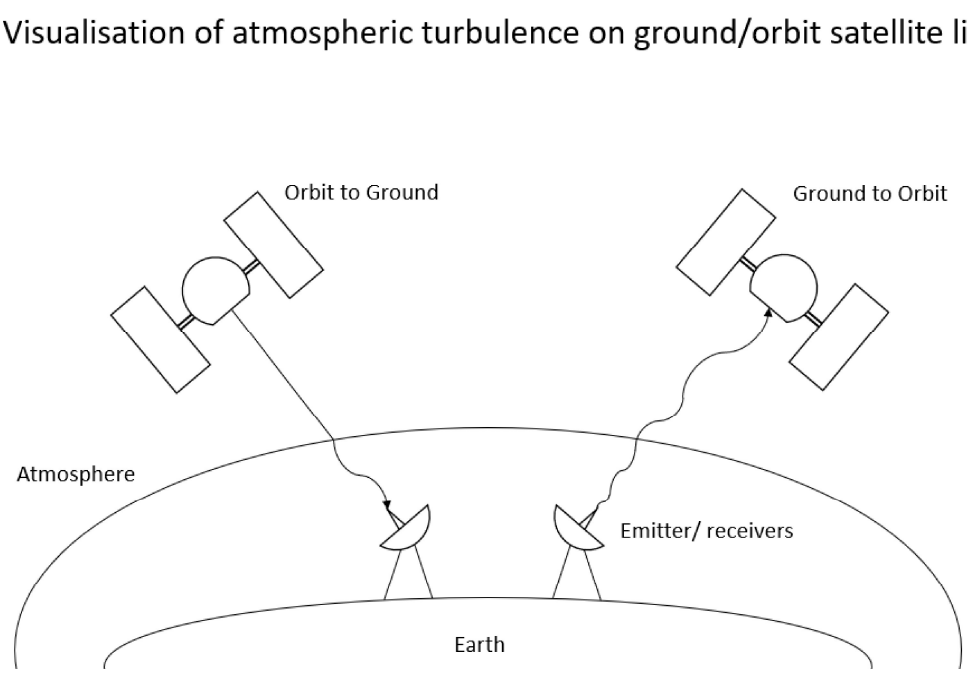

Figure 6.1 Visualisation of the effect on the atmosphere between space based and ground based emitter/receiver pairs. Any perturbations picked up in the atmosphere can propagate for a much greater distance in the ground to orbital case than in the orbital to ground case. The effect of the beams broadening is not shown in this image.

For an orbital to ground link the effect of the atmosphere is much greater going from ground to space rather than space to ground [141], as in the ground to space case the errors due to the atmosphere are allowed to propagate much further than in the space to ground case. A visualisation of this can be seen in figure 6.1. Other than the interference of the atmosphere in free space links the other major concern is the spread of the signal laser beam between the emitter and receiver over very long distances. From an engineering standpoint this means that any the satellites must be able to track each other to a high degree of precision and that the receivers must be able to detect a fraction of the beams initial power. Additionally if any particularly sensitive data were to be sent the broadening of the beam would allow for other satellite receivers to pick up the signals.

As part of a secondment at Mynaric [142] in Germany an investigation was undertaken to investigate optical links between satellites. As part of this investigation

was an overview of the QKD (Quantum Key Distribution) protocols used to prevent unwanted eavesdroppers from gleaning information from the beam spread between satellites; along with a quick look at the polarisation aberrations that are introduced to systems over great distances. Additionally a prototype system was designed to be placed on a satellite to ensure as much of an incoming beam could be caught and focused onto a fibre tip to convey to the rest of the satellites systems.

The fibre system was designed to replicate the collection of light sent from one satellite onto a receiver mounted on a second satellite. The first key point of this system is that as the beam from one satellite to another travels an incredible distance the expansion of the beam over that distance means that the intensity of the beam that strikes the receiver is of uniform intensity, rather than the Gaussian distribution usually seen in laser beams. Thus the beam is shaped into a flat intensity profile in order to properly simulate the collection of an inter-satellite signal, as any terrestrial lab will be far too small to do this by natural laser divergence. There are multiple methods for shaping the beam to give uniform power distribution across the beam diameter. Firstly, if a beam can be broadened considerably an aperture cutting away all but the centre of the beam would leave a roughly flat wave, but would also cause diffraction around the aperture edge, and would lose a considerable amount of power. Secondly an aspheric lens could be used, but this increases the complexity of the system and adds more components with focal length that will need to be taken account of. The final method considered was a top hat beam diffuser, although these can often leave the edges of the beam messy, an aperture could be used to remove this from the beam after passing through the diffuser [143].

As there can be many sources of light striking the satellite receiver, such as light form the sun, a narrow linewidth single mode fibre is the best choice for the collection fibre, as it will heavily attenuate photons from background sources whilst transmitting a high percentage of the incoming signal photons. The coupling of light into an SMF fibre is governed by the qualities of the incoming beam and the physical

properties of the fibre [144]. n_1 and n_2 are the refractive indices of the fibre core and the fibre cladding respectively; r_c is the core radius of the fibre; λ is the frequency of the light; ω_1 is the incident beam diameter, a is the focusing lens clear aperture; and f is the focusing lens focal length. Armed with these values the key values of the system can be calculated. The numerical aperture (NA) of a fibre is calculated by the following equation:

$$NA = \sqrt{n_1^2 - n_2^2} \tag{6.1}$$

The normalised fibre frequency ν_{fibre}:

$$\nu_{fibre} = 2\pi r_c NA/\lambda \tag{6.2}$$

The mode field radius of the fibre ω_0:

$$\omega_0 = r_c(0.65 + 1.619/\nu^{3/2} + 2.879/\nu^{6)} \tag{6.3}$$

Using these values a design parameter for the system χ can be calculated:

$$\chi = (\pi a \omega_0/\lambda f) \tag{6.4}$$

Using this parameter the coupling efficiency η [145] can be determined:

$$\langle\eta\rangle = \frac{2}{\chi^2}[1 - e^{-\chi^2}] \tag{6.5}$$

The maximum coupling efficiency is found to be $\eta = 81\%$ when $\chi = 1.121$ [146]. The reason 100% coupling is not possible is due to the mismatch between the incoming beam profile and the fibre coupling mode. In an SMF fibre the propagation mode is Gaussian, however as mentioned earlier the divergence of the beam due to the large distances between satellites means that the incoming beam profile is flat. This mismatch limits the coupling efficiency of the fibre [144].

The first iteration of the system was designed to be purely analog in its construction, with further iterations including servos and an FPA to keep the alignment at maximum efficiency. The designed system can be seen in figure 6.2.

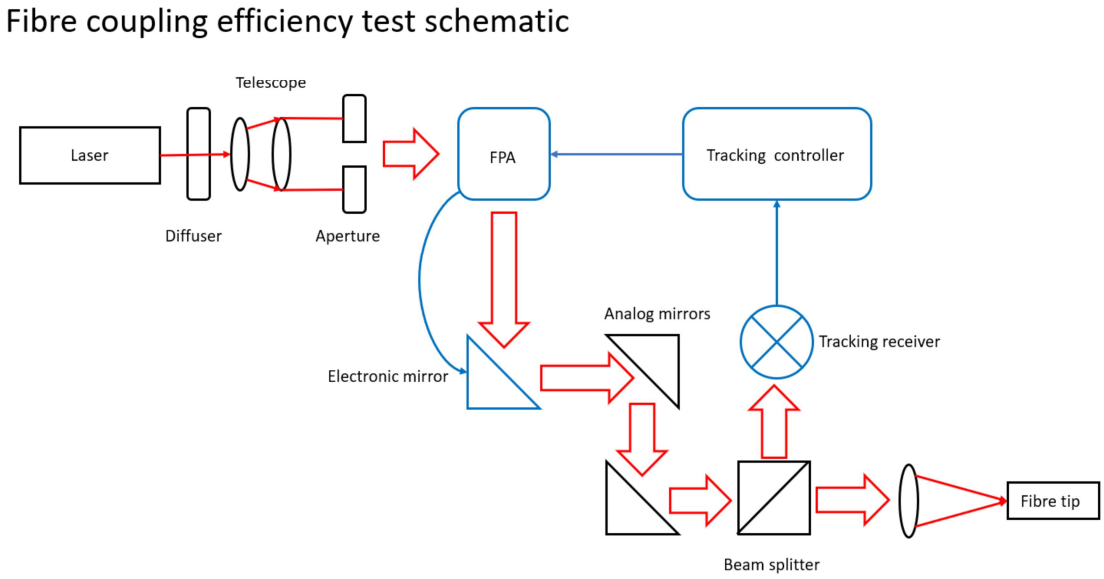

Figure 6.2 Proposed schematic to test the robustness of a fibre coupling system. The initial stages of the system simulate the beam as it would bee seen by a satellite, with a uniform intensity at all points across the beam diameter. The addition of two analog mirrors is purely to help with the initial alignment of the system. The weakness of the system in this current layout is that any errors that creep into the system after the beamsplittter cannot be measured by the tracking receiver. This can be mitigated by mounting the tracking reciver and the fibre end together in such a way that any adjustment in the system affects the beam striking each component in the same manner.

One of the limitations of this design is that once the beam has gone past the beam splitter on its way to the final focusing lens, there is no information on the system being fed back to the tracking receiver. This means that any misalignment that occurs between the beamsplitter and the fibre will not be detected and the coupling efficiency will suffer. As a solution the tracking if the tracking receiver and the fibre could be robustly mounted together then any misalignment in the final steps towaards the fibre will also be present on the tracking receiver. Additionally a power analyser mounted on the fibre would allow the system to flag if the power suddenly fluctuated, however this could not provide information on how to adjust the system to compensate for this. Unfortunately due to time and laser training constraints I was not able to put this system to the test.

Back on earth fibre optic cable do not require such a large amount of engineering to couple light into them as the beam powers are not so reduced by divergence over several hundred kilometres of free space transmission.

Fibre optic cables are ideal for terrestrial clocks as they do not require a direct free space optical path to the other end of the link, and are not subject to perturbations in the signal due to atmospheric effects. The environment may not have such a large effect on the noise in a fibre optic as it does on a free space signal but vibrations and temperature changes along the fibre path will still introduce perturbations. Vibrations caused by something as trivial as someone walking near the fibre connection will cause changes in the optical path in the fibre and introduce noise [147]. This sensitivity to environmental perturbations can be useful when designing sensors, but for sharing an accurate signal present a significant hurdle to be overcome. In iqClock the fibre linking the frequency comb lab and the testbed lab is run through the ceiling of the building over a distance of around $50m$. As the building the iqClock lab is situated in a busy work environment hosting many other groups there is a lot of vibration sources present in the building, from traffic outside, people walking through the corridors, slamming doors, and the vibrations potentially

caused by other experiments. These sources of vibration can all cause phase noise in the fibre linking the two labs. Fortunately for the linking of timing devices there are methods available to cancel or suppress the introduced phase noise.

6.2 Fibre phase stabilisation

The amount of phase noise introduced into a fibre is not necessarily stable over time. Changing environmental factors such as sources of vibration that are not time constant (e.g traffic) or temperature changes will both introduce differing amounts of phase noise over time. Every time a signal is passed along a fibre it will pick up some amount of phase noise δ. This phase noise is independent of the direction the signal passed along the fibre. Thus a signal travelling along a fibre from point A to point B will experience the same phase noise as counter-propagating signal travelling at the same time from point B to point A. As fibre optics allow for the transmission of two counter-propagating signals at the same time independently, a retro-reflected signal that has travelled along a fibre the signal received is identical to the emitted signal with 2δ of phase noise. Thus a signal emitted from a point A transmitted to a point B along a fibre optic will pick up a phase noise δ. If said signal is then retro-reflected at point B, when it re-emerges at A the total phase noise will be 2δ, this can be seen in figure 6.3.

In order to measure the value of the phase noise a known rf frequency 2Δ can be introduced to the signal at point B, upon retro-reflection this rf frequency will also be carrying twice the phase noise. By beating the emitted signal against the retro-reflected signal the injected rf signal is found. Dividing this by two gives the phase noise of a single pass at the emitter end of the system, point A. By injecting the signal at point A with $-\delta$, the signal coming out of point B is free of phase noise compared to the initial signal. As an alternative method the signal can be injected with Δ at point A. The signal will pass through this point again picking up an additional Δ

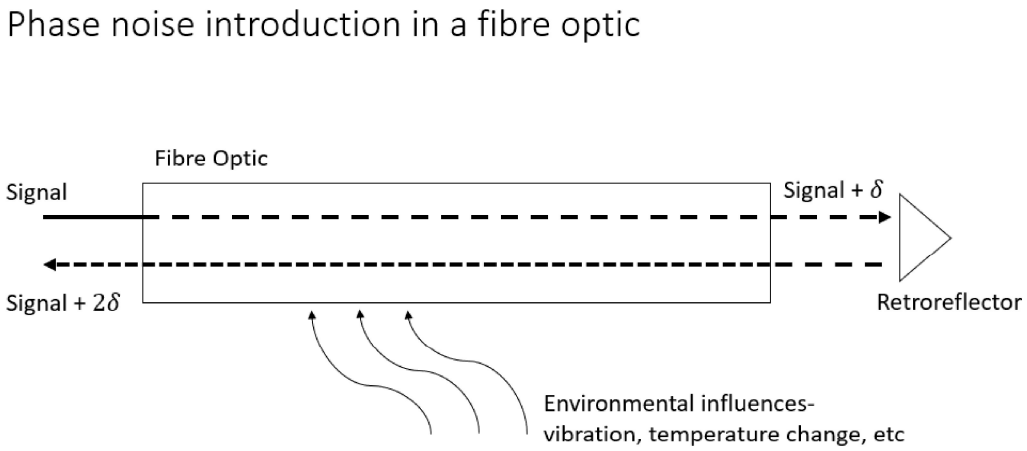

Figure 6.3 The introduction of phase noise into a fibre optic and the doubling effect on the phase noise provided by a second pass through the fibre.

just before the beat detection with the un-modified signal. This method allows all the electronics to be on one side of the fibre, and makes the creation of a PID loop to adjust the correction phase easier than having the electronic systems on either end of the fibre.

The limit to the speed at which the phase feedback loop can compensate for the noise is partially down to the length of the connection. The longer the fibre the greater the change in the phase noise that can occur between the signal leaving the emitter and being compensated for after the round trip. This limit on the suppression can be surpassed by using the method outlined in [148].

A passive method for remove the fibre phase noise is presented in [149], by using a post-processing method they are able to get below the limit on fibre stabilisation imposed by the travel time through the fibre.

6.2.1 Fibre stabilisation at Birmingham

As part of the iqClock testbed system a fibre was laid connecting two labs which will both contain atomic clock systems, namely the atomic package in one, and the clock laser and frequency comb in the other. In order to transfer signals between the labs

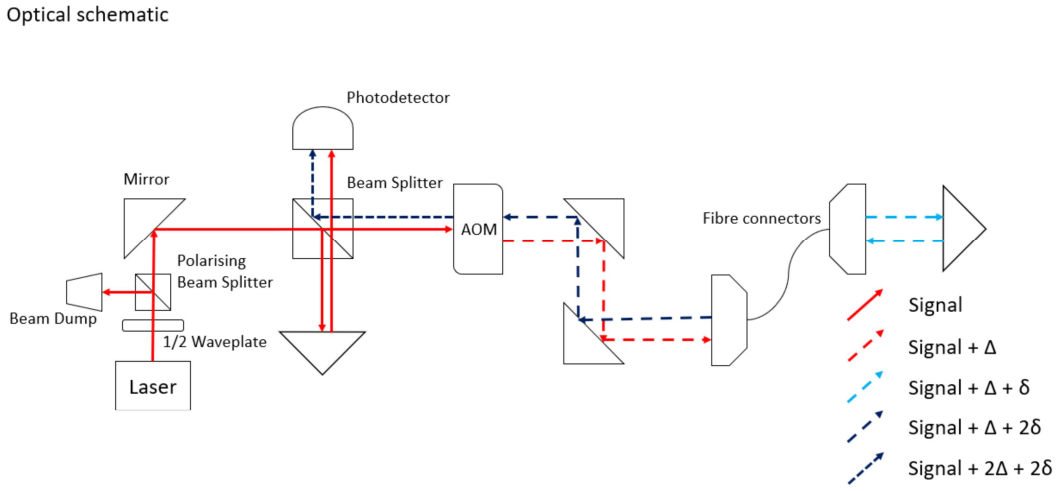

Figure 6.4 Optical schematic of the system used to cancel phase noise in a fibre. The prototype set up in the lab used only a 3m fibre for testing, but the actual fibre connecting the labs was on the order of 50m long running through the ceiling of the building.

the phase noise in the fibre must be compensated. In order to find the best method for compensating this phase noise several methods were attempted in parallel. An attempt using "off the shelf" stabilisation systems was made using a Stemlabs Red Pitaya system based off the method seen in [150], [151].

The optical layout for this system is shown in figure 6.4, in order to simplify the electronics needed it was decided to use a double pass AOM on the same of the fibre as the laser to introduce the rf 2Δ. As the laser output was in itself being carried by fibre optics from another bench in the lab a half wave plate polarising beam splitter combination was placed in front of the laser output in order to clean the beam polarisation and to maximise the power through the beam splitter.

As the aim was to build an "off the shelf" system electronic components from minicircuits along with a Red Pitaya were used in the system. The aim of this method was to provide a fibre stabilisation system at a considerably lower cost than other available systems and to investigate the usability of the Red Pitaya for further tasks in other systems in the lab. The electronics used to control this system can be

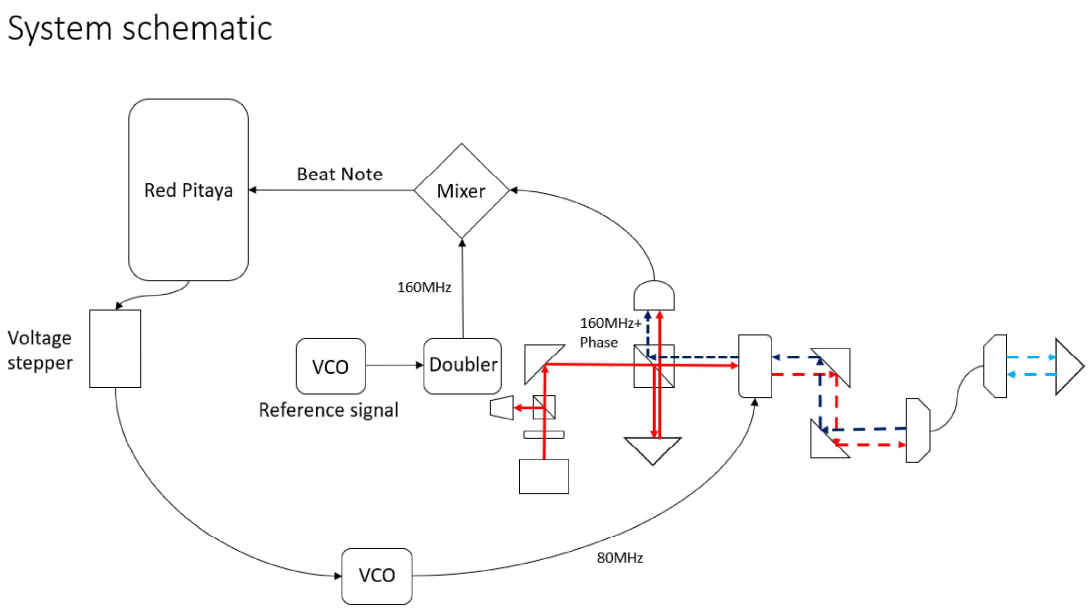

Figure 6.5 Overall schematic of the system showing the key electronic compoenets and circuits. VVA's and amplifiers have not been included for clarity of the image.

seen in figure 6.5. The reference frequency was provided by a VCO (VCO1) running at 9.4 V leading to a 80MHz output. This frequency is then doubled to be used as the "pure" 2Δ used to beat against the received signal after its pass through the fibre. The output of the redpitaya is used to control a VCO (VCO2) that in turn controls the AOM. Outputting 80 MHz from this VCO and taking the +1 order from the AOM gives a 2Δ value of 160 MHz. The returned signal is beat against the initial laser input on the photodiode producing a beat note at around 160 MHz. This beat note is mixed with the reference signal from VCO1 and fed into the Red Pitaya to form the error signal for the PID loop, the outcome of this loop will control VCO2 to adjust the frequency of the AOM in order to cancel out the induced phase noise in the fibre. In order to check the frequency at each stage of the circuit extra T connectors were installed in the BNC cables that would allow the signal to be picked off to measure using a frequency analyser.

Unfortunately this system came with a couple of unforeseen issues. Firstly the connection between the Red Pitaya and the computer that would control its interface

was only establish-able on certain devices, for reasons that were never ascertained. This limited the ease with which the Red Pitaya could be controlled and determine what was going on as signals were fed into it. Secondly the output for the Red Pitaya was not a high enough voltage to control VC02, so a beat note could be found between the input laser and the received laser, but the corrections to cancel the phase noise were not being implemented. In order to get around this issue a voltage amplifier circuit was built using operational amplifiers so that the output of the Red Pitaya would move around 9.4 V as necessary to control the output from VCO2 to correctly cancel the phase noise. The amplifier was was tested on a dummy circuit before installing it in the system. Lastly after the implementation of the voltage amplifier circuit the Red Pitaya stopped working briefly, and afterwards no sign was seen on the interface that suggested the Pitaya was receiving any signals at all from the mixer. This may have been due to some electrical fault in the voltage amplifier circuit that short circuited the system, and blew the input connection on the Pitaya. Unfortunately there was no time to order a second Pitaya to see if the fault was in the particular Pitaya in the lab or if there was an issue elsewhere in the system.

6.3 Conclusions

Accurately disseminating time signals between remote clocks underpins many of the applications that optical atomic clocks are designed for, such as geodesy and GPS. Presented in this chapter is a discussion of how the clock signal suffers over both free space and fibre links and two systems to help mitigate the issues that can arise. Whilst there were timing issues that meant the work could not be wholly completed over the course of the PhD, fortunately for the Birmingham team other methods of stabilising the fibre that were running concurrently met with more success. An experiment utilising a ABLNO crystal oscillator as the local oscillator with a DDS board to control the phase noise cancellation were successful in cancelling the phase

noise in the fibre to around 100 kHz, as was another system using a Toptica digilock 110. Red Pitaya systems have been successfully used to cancel fibre phase noise in other systems [151], so another attempt at making this system would be a useful task to be completed, as the components required are considerably cheaper than those incorporated into the other designs built at Birmingham. Additionally the Red Pitaya components are very versatile, and if they are successfully deployed in this system it opens the possibility to potentially utilise them in other parts of the system, such as timing controls for the MOT coils or repump laser stabilisation.

Chapter Seven

Outlook and Further work

7.1 iqClock testbed system

7.1.1 Magnetic systems.

The Zeeman slower designed and characterised in this thesis successfully formed a MOT as seen in 4, however the stray fields from the end of the slower would cause a shift in the clock transition of the trapped atoms. To try and mitigate this issue and set of guide magnets were installed to try and reduce the magnetic field at the centre of the MOT chamber. The integration of the guide magnets was successful in reducing the magnetic field, but had an adverse affect on the Zeeman slower profile, as well as the number of atoms caught in the MOT. Further work on this area of the system would focus on introducing the effects of guide magnets to the Zeeman slower profile code, and iterating on that combined Zeeman slower + guide magnet pair in order to more robustly design a system that reduces the stray magnetic fields whilst not perturbing the Zeeman profile. Alternatively a slower could be designed that would naturally reduce the stray magnetic fields without the need for guide magnets or magnetic shields. Further designs that could be tested include the design of a transverse system which would naturally reduce the stray magnetic fields over the MOT region, however without additional power to the slowing laser a transverse design could prove less efficient than the longitudinal design already in place. A sim-

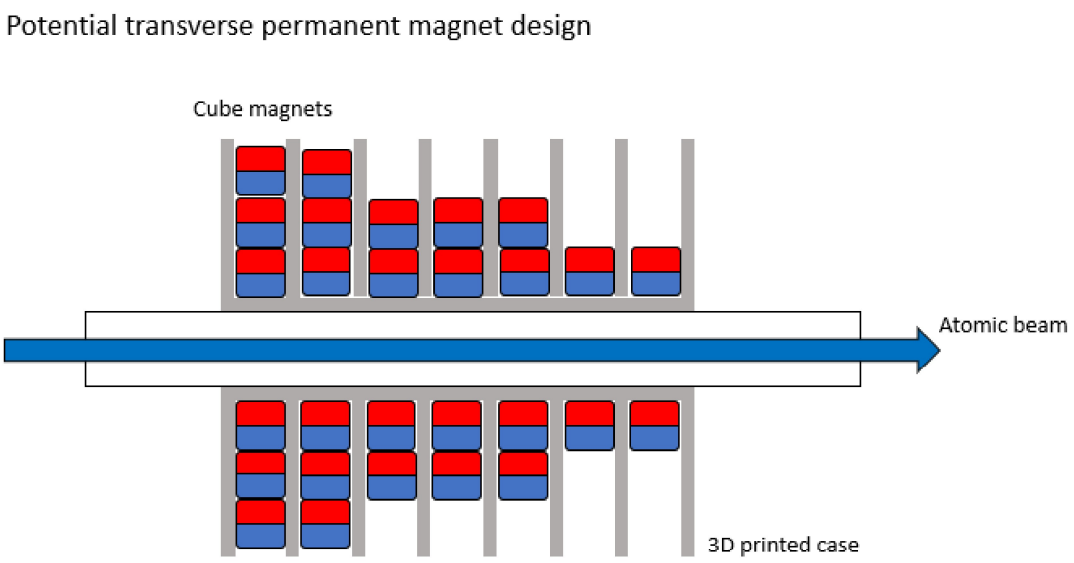

Figure 7.1 Visualisation of a potential transverse slower for the iqClock testbed system. By using columns of stacked transverse magnets the magnetic field profile can easily be adjusted by increasing or decreasing the number of magnets in said column. As found whilst making the guide magnets, the magnets do not like to sit in this formation with parallel columns right next to each other, which is why a case is required to prevent them from re-organising themselves into a more stable configuration.

ilar 3D printed bracket system similar to the one used for the guide magnets would make for an ideal starting point for any design of a transverse slower for the iqClock testbed system. The benefits of using a 3D printed skeleton to hold the magnets in place are the cheapness and speed of construction, although a more professionally produced non-magnetic metal skeleton would be preferable for any final product to ensure no material creep. A brief mock up of a transverse system taking inspiration from the easily configurable nature of the spherical longitudinal system could look like is presented in figure 7.1.

Although a Zeeman slower is not a necessary component in a working clock system, its inclusion would make for a more efficient system, and allow faster loading of the MOT. The faster loading of the MOT reduces the preparatory dark or dead time in the experimental cycle, reducing the time that the clock laser can drift and thus increasing the overall stability and accuracy of the system.

7.1.2 MOT coils

A set of passively cooled MOT coils were built and characterised, with an investigation into the affect of a slit cut into the former that the wire that comprises the coil is wrapped around, and is present in 5. The results of the investigation into eddy currents confirms the use of slits cut into MOT coil formers, the slits drastically reduce the time taken for magnetic fields caused by the switch off of the coils to decay. This allows the experimental cycle to more quickly reach the measurement phase, as waiting for the magnetic fields to decay is not required. As outlined above this reduces dead time in the experimental cycle and increases the stability of the overall clock system.

7.2 Signal distribution

The problem of distributing the measurement produced by the clock system is presented in chapter 6, along with designs for improving the collection of light between remote clock linked by a free space beam and a design for a system to cancel the phase noise that is introduced in long distance fibre connections. The building of the fibre phase noise cancellation system using a Red Pitaya was attractive as it presented a relatively simple and cheap way to cancel the phase noise; which is ideal for a transportable system and a boon when taking a system from an academic environment to a practical industrial one. This system was unfortunately not completed in the time scale of this PhD, but fortunately for the Birmingham group the simultaneous working on three fibre phase stabilisation system gave a degree of redundancy in case one of them failed to produce the wanted results. The inability to see any fibre phase stabilisation on the Red Pitaya system is most likely due to a mistake when installing a voltage amplifier circuit which may have short circuited some of the systems on the

Pitaya. Another attempt to retry this system would certainly be of a benefit to the group as the design would have many benefits such as relative cheapness and ease of use, but the existence of the more successful simultaneous experiments means this is not of primary importance. The next step is to test the fibre stabilisation systems on the testbed system proper, and to determine if the phase noise suppression can be further improved.

7.3 Next steps for the iqClock system

With the MOT successfully formed, the next steps of the experiment are making the optical lattice and the interrogation of the atoms. The formation of the lattice will be completed on the same system that the work in chapters 4 and 5, but the interrogation of the atoms will be more complicated. The measurement of the atoms requires the use of a frequency comb as detailed in chapter 3. Although the bulk of the iqClock testbed system is situated in one lab, due to space constraints the frequency comb was in a lab some distance away, thus necessitating the fibre phases stabilisation techniques seen in chapter 6. The frequency comb in question had not been operated for some time, so work was begun on getting it operational. To test the frequency comb a maser was installed in this lab to act as a stable reference. As mentioned briefly in chapter 1 Masers are a contemporary technology adjacent to atomic clocks. Whilst atomic clocks of various frequencies use lasers to stimulate the atoms, masers instead use microwaves to illuminate a trapped bulb of gaseous atoms. Masers have the advantages of relative simplicity over atomic clocks, and also boast high stabilities. The downside being that they have lower accuracy over the optical atomic systems. This maser is to be used as a reference device when first building the iqClock testbed system, as it is a very well understood frequency, it can easily be used to bench mark the testbed systems first measurements to ensure it is giving the correct results. In order to test the maser after installation a frequency comb

was required to take phase noise measurements from it. The phase data from the $5MHz$, $10MHz$, and $100MHz$ outputs from the maser is presented in figure 7.2.

The first step in testing the frequency comb system was to compare its stability against the masers in order to make sure that it had not been damaged during its long time turned off. After phase locking to the maser, the frequency comb will be locked to the clock laser to take the timing signals from the iqClock testbed system. Unfortunately the frequency comb was not operating as it should, and the Carrier Envelope Oscillator (CEO), was not functioning correctly. It was found that the issue was based in a photo detector that was not picking up a signal, whether this was due to the detector itself being faulty or the positioning electronics having broken has not yet been determined as it is locked inside a box only accessible by the manufacturer. The CEO is necessary to get working in order to properly set the values of f_r and f_o as described in section 3.6.1, without which optical frequency data cannot be taken. Despite this setback it was still possible to use the working elements of the frequency comb to take the phase noise data of the maser, and ensure that this was what was expected from the manufacturers specifications. However without the CEO the frequency comb phase noise stability cannot be compared to the masers.
Thus the next steps of the iqClock experiment will proceed along two tracks. The first track is concerns the atoms trapped in the MOT, the atoms need to be successfully taken from the blue MOT to the red MOT, and from there they need to be loaded into an optical lattice. The second track concerns the frequency comb and fibre stabilisation, the frequency comb needs to be brought back to full operation in order for the time signal to be produced, and the fibre phase stabilisation to carry the signal between labs.

7.3.1 Conclusions

Utilising the Zeeman slower designed and characterised in chapter 4 and the MOT coils built and characterised in 5, a blue MOT of around 7 million atoms has suc-

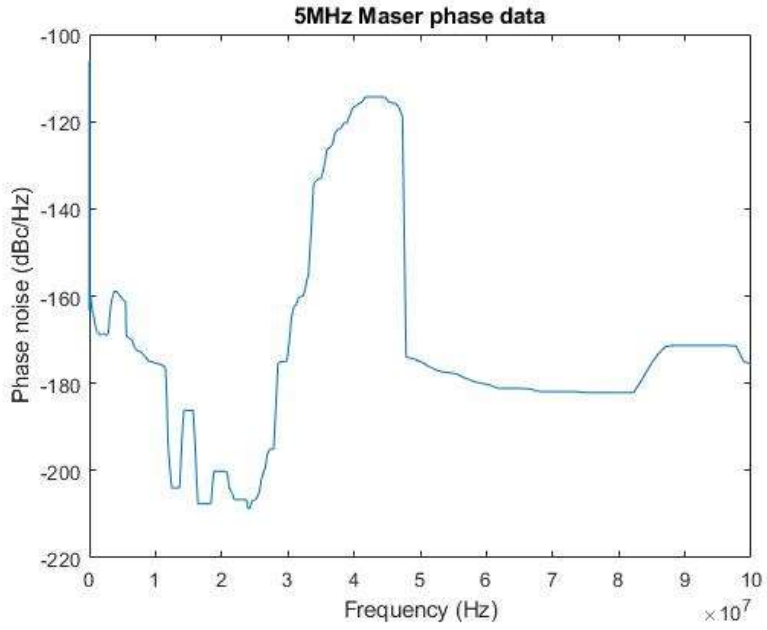

(a) Phase data from the 5 MHz output of the maser. The phase noise is not constant over the frequency range.

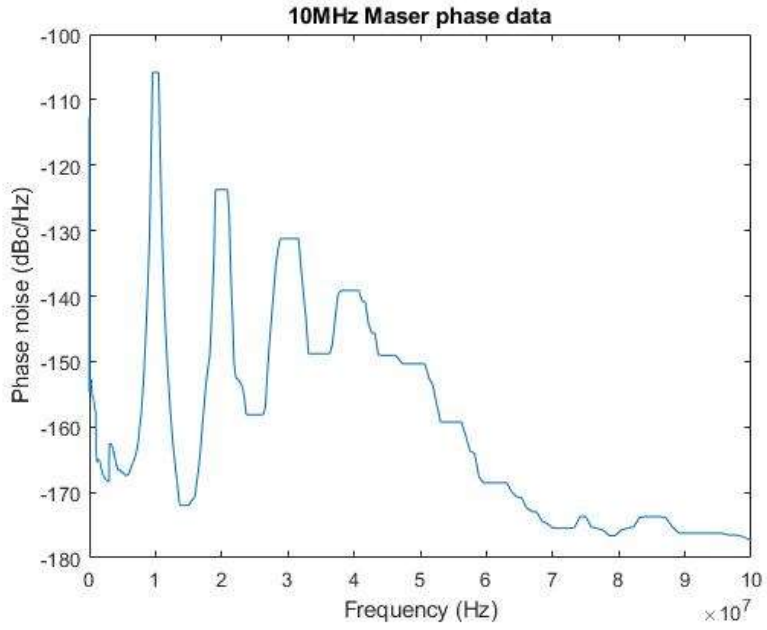

(b) Phase data from the 10MHz output of the maser. The phase noise decreases over the frequency range tested.

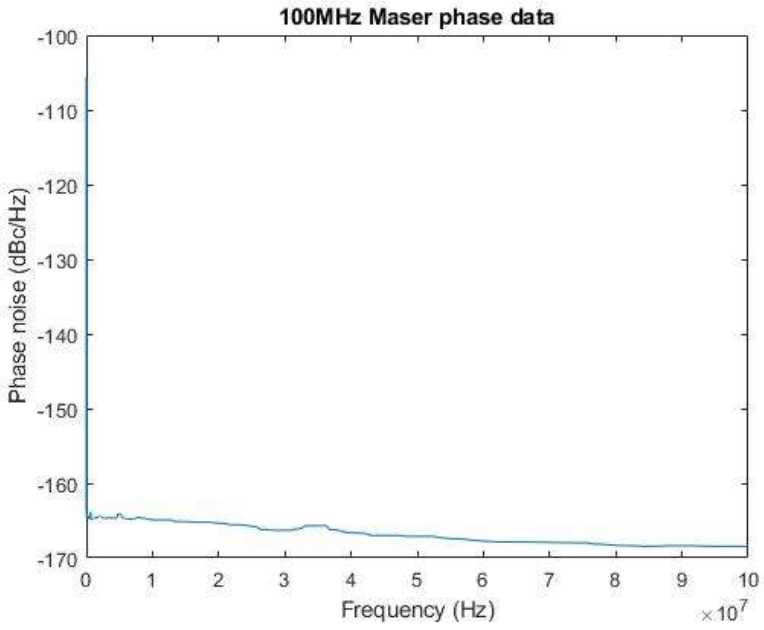

(c) Phase noise from the 100 MHz output of the maser. The phase noise from this output the lowest of the three outputs tested.

Figure 7.2 Phase data taken for three outputs of the hydrogen maser installed in one of the labs at University of Birmingham. The variation in the phase noise for each of the three outputs shows that the 100MHz output of the maser has the best stability.

cessfully been formed on the iqClock system. The next steps in this aspect of the experiment is to further cool the atoms from the blue MOT into a red MOT. This stage of the experiment can be tricky to achieve as the trapping potential of a strontium red MOT is lower than that of a strontium blue MOT meaning that a large proportion of atoms will be lost. It is for this reason that it is desirable to capture as many atoms as possible in the blue MOT stage. Using the guide magnets to reduce the stray magnetic field in the centre of the chamber where the MOT forms shows a lot of promise when designing longitudinal Zeeman slowers. By incorporating the guide magnets into the code used to simulate the Zeeman slower profile a more integrated Zeeman slower/ guide magnet set up can be designed to keep the desired profile and reduce the stray magnetic fields. Additionally investigations into potential transverse or Halbach designs would provide an interesting avenue of research within the group. The current technique of using spherical magnets is not suitable for these designs as the magnets do not have an easily identifiable north or south pole from simple visual observation and are liable to twist in place if placed in an unsuitable formation. However cuboid magnets are easily obtainable and would be able to be used in place of the spherical magnets for Halbach and transverse designs. A transverse magnetic field would require higher laser power, but the trade off of the reduced stray magnetic fields is attractive for moves toward portability.

The next steps after the MOTs are to achieve lattice confinement, and then to interrogate the atoms. This interrogation will utilise the fibre phase stabilisation system presented in 6 in order to transfer the signal to the frequency comb located in the neighbouring laboratory, and produce the timing signal. Once this system is shown to have worked then fibre links to other clocks in remote sites can be attempted, such a link to the clocks at the NPL in London. Within the lab the iqClock industry device will also need calibrating against the testbed system, which will also require a stabilised fibre link. With the success of the simultaneous fibre stabilisation projects, the main driving force for completing the system using the Red Pitaya is its relative

cheapness and lack of complexity. Both of which are desirable factors when keeping an eye towards transportability of the system.

Papers published by the group cover the iqClock testbed system and its place in the wider iqClock project [152], and a review of the desired traits for transportable systems [153]. Using expertise earned from the MiniClock system that was previously built at Birmingham a potential further step for the iqClock system would be to look into what steps would need to be taken to make the system transportable. As it currently stand the system takes the majority of one lab over two optical tables, as well as having components connected by fibre link in a lab across the building. This set up is clearly not conducive to portability, however the atomic package itself is relatively compact, with success in miniaturising the Zeeman slower and the passively cooled MOT coils contributing the compact size. The bulk of the work to miniaturise the system would thus be on the laser and electronic systems, and designing these systems to be reduced in size to be mounted within a considerable smaller volume than they currently occupy. Taking the lessons learnt and the systems investigated in this thesis the iqClock testbed system is in a good position to move to the next steps of the clock experiment, and is well positioned to develop towards a transportable system.

APPENDICES

.1 Appendix I

The code written to calculate the Zeeman slower profiles seen in figure 4.7b is presented below:

```
clear all; close all;

% Code to determine the magnetic field profile of a finned
    permanent magnet zeeman slower constructed out of
    spherical permanent magnets.

%The zeeman slower is constructed of three/four fins of
    spherical permanent magnets, placed around an adhesive
    layer (also contructed out of magnets) at regular
    intervals. The magnetic fields in the x and y directions
    are cancelled out by the equal but opposite contributions
    from the fins, leaving only the field along the z axis.
    The adhesive layer is constructed such that it has no net
    magnetic field at all, and thus does not contribute to the
     field.

%If another geometry of spherical magnet is used then adjust
    the values M,d, and ra accordingly, and recalculate the
    value of 0.0184 in ZdistXY to reflect the new adhesive
    layer

%If more layers are added to the fins then f, n_row, and
    n_layer need to be changed, the value of ii in the loop
    will also have to be changed to reflect the number of
```

```
    layers
10
11 %If more rows are added to a fin (fin becomes thicker) adjust
       n_layer
12 %If more magnets are added to the row (fin becomes longer)
    adjust n_row
13
14 %If fins are moved further from the z axis (adhesive layer
    diameter increase) the value of 0.0184m in ZdistXY will
    have to be recalculated to find the distance from the z
    axis of the first layer.
15
16 %The method for calculating this profile comes from 'Self
    assembled Zeeman slower based on spherical permanent
    magnets; V. Lebedev, D.M. Weld; Journal of Physics B:
    Atomic, Molecular and Optical Physics 47 2014; doi
    :10.1088/0953-4075/47/15/155003'
17
18
19 M=0.075;                          %magnetic dipole in Am^2
20 u0=1.257*10^-6;                   %permeability of free
    space in H/m
21 d=0.006;                          %magnet diameter (m)
22 ra=0.003;                         %magnet radius (m)
23 f=1:5;                            %fin layer, f=1 is
    closest to z axis.
24 ZdistXY=0.0184+f*(sqrt(d^2-ra^2)); %distance from the z axis
       in the xy plane, 0.0184 is the distance from the centre
```

```
    of the adhesive layer to the first layer of the fin for
    the LRI slower- will have to be remeasured for new slower
    geometries.
n_row=[26, 23, 19, 15, 8];                %number of magnets in
     each row of each layer of the fin (26x2, 23x2, 19x2, 15x2
    , 8x1 for LRI slower).

%magnetic field from a magnet to a point on the x axis= (u0*M
    )/(4*pi)(2*distance_along_z^2-distance_from_z)^2)/(
    distance_from_z^2+distance_along_z^2)^5/2)

con=(u0*M)/(4*pi);                        %just for ease of typing
    later

z=-0.15:0.01:0.25;                        %where along the z axis the
    field is measured, zeeman slower starts at z=0 and is
    0.156 m long


n_layer = [2,2,2,2,1].*n_row;                                  %
    calculates magnets in each layer of a fin, accounts for
    the rows in each layer
n_cs = [0 cumsum(2*n_row)];
n_cs(end) = n_cs(end)-n_row(end);                              %
    total number of magnets in a layer+ preceeding layers
for ii=1:5        %over all layers
     %layers
```

```
39      Magnets.layer((1:n_layer(ii))+n_cs(ii)) = ii;        %
            creates the struct 'Magnets' and adds the information
            on the number of magnets in each layer to that stuct
40
41
42      %xy positions
43      Magnets.ZdistXY((1:n_layer(ii))+n_cs(ii)) = 0.0184+ii
            *0.0052;            %Calculates the distance from the z
            axis in the xy plane and adds it the the 'Magnets'
            struct, 0.0052 is the distance between the magnet
            centres in triangular close packing
44      %z positions
45      z_dist = -d+(1:n_row(ii))*d +(ii-1)*ra;       %calculates
            the distance of each magnet along the z axis
46
47      if ii==5                                          %adds the
            distance along z of each magnet to the struct 'Magnets
            ', if ii=5 then we're on the top layer which only has
            one row of magnets contained within it.
48          Magnets.z((1:n_layer(ii))+n_cs(ii)) =  z_dist;
49      else
50          Magnets.z((1:n_layer(ii))+n_cs(ii)) = [z_dist; z_dist
                ];
51      end
52  end
53  nm = numel(Magnets.layer);                          %creates
        array of all magnets
```

```
54 mag_idx = 1:numel(Magnets.layer);                %index of the
       magnets in each layer
55
56 scatter(Magnets.z,Magnets.ZdistXY,30,'filled');      %plots
      position of each magnet in relation to each other and the
      z axis (creates picture of fin)
57 xlabel('z [m]'); ylabel('X-Y Combined Distance [m]');
58 legend('Magnets'); title('Side view of fin structure');
59 axis equal; grid on;
60
61 z_idx = 1:41;
62
63 [z_idx,mag_idx] = meshgrid(z_idx,mag_idx);
64
65 coord_z = linspace(-0.15,0.25,41);
66 B = -1.5*con.* ((2.*(Magnets.z(mag_idx) - coord_z(z_idx)).^2-
      Magnets.ZdistXY(mag_idx).^2)./ ...
67       (ZdistXY(Magnets.layer(mag_idx)).^2+(Magnets.z(mag_idx) -
            coord_z(z_idx)).^2).^(5/2));        %calculates the
          total magnetic field on each poin in z
          =-0.15:0.01:0.025 from one fin
68
69       B_tot = 4*sum(B);                                  %
          accounts for the (identical) contribution from each
          fin
70
71 figure; plot(coord_z,B_tot);                          %plots
      Zeeman slower magnetic field profile
```

```
72 xlabel('Z distance [m]'); ylabel('Total Field Strength [T]');
       title('4 finned longitudinal Zeeman slower simulated
      profile'); grid on;
```

.

This code is written specifically for the longitudinal self assembled design used in the iqClock and LRI systems at Birmingham, but should be relatively easily adapted to other permanent magnet longitudinal designs.

The codes for the presenting the potential atom percentage captured in the MOT were written previously by a masters student [154] in the group. The following code calculates the slowing of the atoms given the field profile calculated by .1 and provides the graphs seen in figure 4.8.

```
1 %{ A code to determine how much atoms of various velocities
     are affected when they are slowed within the permanent
     magnet zeeman slower. This code follows on from
     ZSFieldprofile
2 %}
3
4 %clear all; close all;
5 warning('off', 'MATLAB:table:ModifiedVarnames');
6 %
  ------------------------------------------------------------------------
7
8 run ZSFieldProfile.m
9
10 %z and B values come from ZSFieldProfile.m, alternatively
     data from a measured Zeeman slower can be loaded in.
```

```
11 %
   ------------------------------------------------------------------------

12 % Other input parameters
13
14 lambda = 4.6073e-7; % wavelength of laser in m
15 d0 = - 2*pi*300e6; % detuning of cooling laser in Hz
16 gamma = 2*pi*32e6; % transition width in Hz
17 Pz = 50e-3; % power of the Zeeman beam in W
18 Dz = 10e-3; % diameter of the Zeeman beam in m
19 Dmot = 8.3e-3; % diameter of MOT beams in m
20 T_room = 20; % room temperature in degrees Celsius
21 P_oven = 35; % power supplied to the oven in Watts
22
23 %
   ------------------------------------------------------------------------

24 % calculate saturation parameter
25 h = 6.62607004e-34; % Planck constant
26 c = 299792458; % speed of light in a vacuum
27 Isat = pi*h*c*gamma/(3*(lambda^3)); % saturation intensity
28 I = 2*Pz/(pi*(Dz/2)^2); % intensity of the Zeeman beam
29 s0 = I/Isat; % saturation parameter
30
31
32  %calculate s(z) (change this function depending on setup)
33 L = 2; % focal length of converging lens of Zeeman slower
       beam in m
```

```
34 d = 0.736; % distance in m from lens to start of z
35 df = L - d;
36 %s = (L./(z+df)).^2 .* s0; % s(z)
37
38 s = s0*ones(1,length(z)); % s(z) for collimated beam
39
40 %
   ------------------------------------------------------------------------
41
42 % calculate oven temperature
43 t = oven(P_oven,T_room);
44
45 % calculate atomic velocity distribution
46 v = vDist(z,B_tot,lambda,d0,gamma,s);
47
48 % calculate capture velocity of MOT and capture efficiency
49 [vc,eff] = CaptEff(lambda,gamma,Dmot,v,t);
50
51 % plot atomic velocity distribution
52 % for clarity, only plotting initial velocities in intervals
       of 25m/s
53 figure;
54 vmax = max(v(:,1)); vmin = min(v(:,1));
55 n = (max(v(:,1)) - min(v(:,1)))/25 + 1;
56 for k = 1:n
57     a = (k-1)*25 + 1;
58     plot(z, v(a,:),'LineWidth',1);
```

```
59      hold on;
60  end
61  xlabel('z-position (m)');
62  xlim([-0.15 0.40]);
63  ylabel('Velocity (ms^{-1})');
```

Bibliography

[1] "The International System of Units (SI) 9th Edition," Bureau international des poids et mesures, Tech. Rep., 2019.

[2] N. A. O. of the United Kingdom and U. S. of America, *Explanatory Supplement to the Astronomical Ephemeris and the American Ephemeris and Nautical Almanac*. H.M. Nautical Almanac Office, 1961, ch. 3, p. 66, ISBN: 0 11 880578 9.

[3] M. Schioppo, R. C. Brown, W. F. McGrew, *et al.*, "Ultrastable optical clock with two cold-atom ensembles," *Nature Photonics*, vol. 11, no. 1, pp. 48–52, Jan. 2017, ISSN: 17494893. DOI: 10.1038/nphoton.2016.231. eprint: 1607.06867.

[4] P. Gill, "When should we change the definition of the second," *Philosophical Transactions of the Royal Society A: Mathematical, Physical and Engineering Sciences*, vol. 369, no. 1953, pp. 4109–4130, 2011, ISSN: 1364503X. DOI: 10.1098/rsta.2011.0237.

[5] R. McEvoy and J. Betts, *Harrison Decoded: Towards a Perfect Pendulum Clock*. 2020, pp. 82–84, ISBN: 9780198816812. DOI: 10.1093/oso/9780198816812.001.0001.

[6] "Wells cathedral clock, england, 1392." (Oct. 2021), [Online]. Available: https://collection.sciencemuseumgroup.org.uk/objects/co1347/wells-cathedral-clock-clock.

[7] K. Barrett, "'explaining' themselves: The barrington papers, the board of longitude, and the fate of john harrison," *Notes Rec. R. Soc.*, no. 65, pp. 145–162, Jan. 2011. DOI: https://doi.org/10.1098/rsnr.2010.0089.

[8] F. L. Walls and A. E. Wainwright, "Measurement of the Short-Term Stability of Quartz Crystal Resonators and the Implications for Crystal Oscillator Design and Applications," *IEEE Transactions on Instrumentation and Measurement*, vol. 24, no. 1, pp. 15–20, 1975, ISSN: 15579662. DOI: 10.1109/TIM.1975.4314362.

[9] M. A. Lombardi, "The accuracy and stability of quartz watches," *Horological Journal*, pp. 57–59, Feb. 2008.

[10] F. Walls and J. Vig, "Fundamental limits on the frequency stabilities of crystal oscillators," *IEEE Transactions on Ultrasonics, Ferroelectrics, and Frequency Control*, vol. 42, no. 4, pp. 576–589, 1995. DOI: 10.1109/58.393101.

[11] L. Essen and J. V. L. Parry, "An atomic standard of frequency and time interval: A cæsium resonator," *Nature*, no. 176, pp. 280–282, Aug. 1955. DOI: 10.1038/176280a0.

[12] F. Droz, P. Mosset, G. Barmaverain, *et al.*, "The on-board galileo clocks: Rubidium standard and passive hydrogen maser - current status and performance," pp. 420–426, Jan. 2006.

[13] Microsemi, "Leading-edge technology enables a chip scale atomic clock," QUANTUM SA.45s White Paper Revision 1.1, Tech. Rep. [Online]. Available: https://www.microsemi.com/product-directory/clocks-frequency-references/3824-chip-scale-atomic-clock-csac#resources.

[14] J. L. Hall, M. Zhu, and P. Buch, "Prospects for using laser-prepared atomic fountains for optical frequency standards applications," *Journal of the Optical Society of America B*, vol. 6, no. 11, p. 2194, 1989, ISSN: 0740-3224. DOI: 10.1364/josab.6.002194.

[15] W. Moreno, M. Pellaton, C. Affolderbach, and G. Mileti, "Barometric effect in vapor-cell atomic clocks," *IEEE Transactions on Ultrasonics, Ferroelectrics, and Frequency Control*, vol. PP, pp. 1–1, Jun. 2018. DOI: 10.1109/TUFFC.2018.2844020.

[16] B. L. Schmittberger and D. R. Scherer, "A review of contemporary atomic frequency standards.," *arXiv: Atomic Physics*, 2020.

[17] by Sebastian Blatt Mag rer nat, "Ultracold Collisions and Fundamental Physics with Strontium," 2005. [Online]. Available: https://jila.colorado.edu/yelabs/sites/default/files/uploads/theses_2011_SebastianBlatt.pdf.

[18] C. Lisdat, G. Grosche, N. Quintin, *et al.*, "A clock network for geodesy and fundamental science," *Nature Communications*, vol. 7, 2016, ISSN: 20411723. DOI: 10.1038/ncomms12443. eprint: 1511.07735.

[19] A. D. Ludlow, "An optical clock to go," *Nature Physics*, vol. 14, no. 5, pp. 431–432, 2018, ISSN: 1745-2473. DOI: 10.1038/s41567-018-0047-6. [Online]. Available: http://dx.doi.org/10.1038/s41567-018-0047-6.

[20] T. E. Mehlstäubler, G. Grosche, C. Lisdat, P. O. Schmidt, and H. Denker, "Atomic clocks for geodesy," *Reports on Progress in Physics*, vol. 81, no. 6, 2018, ISSN: 00344885. DOI: 10.1088/1361-6633/aab409.

[21] W. F. McGrew, X. Zhang, R. J. Fasano, *et al.*, "Atomic clock performance enabling geodesy below the centimetre level," *Nature*, vol. 564, no. 7734, pp. 87–90, 2018, ISSN: 14764687. DOI: 10.1038/s41586-018-0738-2.

[22] J. Flury, "Relativistic geodesy," *Jounrnal of Physics: Conference Series 723*, 2016. DOI: 10.1088/1742-6596/723/1/012051.

[23] J. Grotti, S. Koller, S. Vogt, *et al.*, "Geodesy and metrology with a transportable optical clock," *Nature Physics*, vol. 14, no. 5, pp. 437–441, 2018, ISSN: 17452481. DOI: 10.1038/s41567-017-0042-3.

[24] M. Abgrall, B. Chupin, L. De Sarlo, *et al.*, "Atomic fountains and optical clocks at syrte: Status and perspectives," *Comptes Rendus Physique*, vol. 16, no. 5, pp. 461–470, 2015, The measurement of time / La mesure du temps, ISSN: 1631-0705. DOI: https://doi.org/10.1016/j.crhy.2015.03.010. [Online]. Available: https://www.sciencedirect.com/science/article/pii/S1631070515000614.

[25] "Iqclock project at university of birmingham." (Mar. 2022), [Online]. Available: https://www.strontium-birmingham.org/research.

[26] S. Nakamura, M. Senoh, N. Iwasa, and S.-i. Nagahama, "High-brightness InGaN blue, green and yellow light-emitting diodes with quantum well structures," vol. 34, no. Part 2, No. 7A, pp. L797–L799, Jul. 1995. DOI: 10.1143/jjap.34.l797. [Online]. Available: https://doi.org/10.1143/jjap.34.l797.

[27] S. Origlia, "A high-performance bosonic optical lattice clock," Ph.D. dissertation, 2018.

[28] T. Fortier and E. Baumann, "20 Years of Developments in Optical Frequency Comb Technology and Applications," *Communications Physics*, vol. 2, no. 1, pp. 1–16, 2019, ISSN: 23993650. DOI: 10.1038/s42005-019-0249-y. eprint: 1909.05384.

[29] C. Y. Wang, T. Herr, P. Del'Haye, *et al.*, "Mid-infrared optical frequency combs at 2.5 μm based on crystalline microresonators," *Nature Communications*, vol. 4, 2013, ISSN: 20411723. DOI: 10.1038/ncomms2335.

[30] M. Lezius, T. Wilken, C. Deutsch, *et al.*, "Space-borne frequency comb metrology," *Optical society of America*, vol. 3, no. 12, p. 1381, 2016, ISSN: 2334-2536. DOI: 10.1364/optica.3.001381.

[31] H. Bao, A. Cooper, M. Rowley, *et al.*, "Laser cavity-soliton microcombs," *Nature Photonics*, vol. 13, no. 6, pp. 384–389, 2019, ISSN: 17494893. DOI: 10.1038/s41566-019-0379-5. [Online]. Available: http://dx.doi.org/10.1038/s41566-019-0379-5.

[32] N. Huntemann, B. Lipphardt, C. Tamm, V. Gerginov, S. Weyers, and E. Peik, "Improved limit on a temporal variation of m_p/m_e from comparisons of Yb^+ and cs atomic clocks," *Phys. Rev. Lett.*, vol. 113, p. 210 802, 21 Nov. 2014. DOI: 10.1103/PhysRevLett.113.210802. [Online]. Available: https://link.aps.org/doi/10.1103/PhysRevLett.113.210802.

[33] M. A. S. O. A. Vela, *Borehole acoustic telemtry clock synchronisation system*, Mar. 1982.

[34] J. S. Hodges, N. Y. Yao, D. Maclaurin, C. Rastogi, M. D. Lukin, and D. Englund, "Timekeeping with electron spin states in diamond," *Physical Review A - Atomic, Molecular, and Optical Physics*, vol. 87, no. 3, pp. 1–11, 2013, ISSN: 10502947. DOI: 10.1103/PhysRevA.87.032118.

[35] E. Peik and M. Okhapkin, "Nuclear clocks based on resonant excitation of γ-transitions," *Comptes Rendus Physique*, vol. 16, no. 5, pp. 516–523, 2015, ISSN: 16310705. DOI: 10.1016/j.crhy.2015.02.007. [Online]. Available: http://dx.doi.org/10.1016/j.crhy.2015.02.007.

[36] M. A. Lombardi, "Legal and Technical Measurement Requirements for Time and Frequency," *NCSLI Measure*, vol. 1, no. 3, pp. 60–69, 2006, ISSN: 1931-5775. DOI: 10.1080/19315775.2006.11721335.

[37] F. Riehle, "Optical clock networks," vol. 11, no. 1, pp. 25–31, 2017, ISSN: 17494893. DOI: 10.1038/nphoton.2016.235.

[38] NIST, *Time measurement and analysis service (tmas)*, Feb. 2009. [Online]. Available: https://www.nist.gov/programs-projects/time-measurement-and-analysis-service-tmas.

[39] ——, *Nist enables precision time-stamping of financial transactions*, Dec. 2014. [Online]. Available: https://www.nist.gov/news-events/news/2014/12/nist-enables-precision-time-stamping-financial-transactions.

[40] P. Knight and I. Walmsley, "UK national quantum technology programme," *Quantum Science and Technology*, vol. 4, no. 4, 2019, ISSN: 20589565. DOI: 10.1088/2058-9565/ab4346.

[41] K. Bongs, Y. Singh, L. Smith, *et al.*, *Development of a strontium optical lattice clock for the SOC mission on the ISS*, 2015. DOI: 10.1016/j.crhy.2015.03.009.

[42] K. W. Holman, "Distribution of an Ultrastable Frequency Reference Using Optical Frequency Combs," *University of Colorado*, p. 165, 2005.

[43] R. Hartman, W. Hawkinson, and K. Sweeney, "Tactical underwater navigation system (tuns)," in *2008 IEEE/ION Position, Location and Navigation Symposium*, 2008, pp. 898–911. DOI: 10.1109/PLANS.2008.4570032.

[44] P.-M. Lee, B.-H. Jun, and Y.-K. Lim, "Review on underwater navigation system based on range measurements from one reference," in *OCEANS 2008 - MTS/IEEE Kobe Techno-Ocean*, 2008, pp. 1–5. DOI: 10.1109/OCEANSKOBE.2008.4531072.

[45] S. E. Webster, R. M. Eustice, H. Singh, and L. L. Whitcomb, "Advances in single-beacon one-way-travel-time acoustic navigation for underwater vehicles," *The International Journal of Robotics Research*, vol. 31, no. 8, pp. 935–950, 2012. DOI: 10.1177/0278364912446166.

[46] I. Consortium. [Online]. Available: https://www.iqclock.eu/.

[47] J. Vovrosh, L. Earl, H. Thomas, *et al.*, "Reduction of background scattered light in vacuum systems for cold atoms experiments," *AIP Advances*, vol. 10, no. 10, p. 105 125, 2020. DOI: 10.1063/5.0030041. eprint: https://doi.org/10.1063/5.0030041. [Online]. Available: https://doi.org/10.1063/5.0030041.

[48] D. W. Allan, "Atomic Ion Frequency Standards," *Proceedings of the IEEE*, vol. 54, no. 2, pp. 221–230, 1966, ISSN: 15582256. DOI: 10.1109/5.84970.

[49] W. M. Itano, J. C. Bergquist, J. J. Bollinger, *et al.*, "Quantum projection noise: Population fluctuations in two-level systems," *Physical Review A*, vol. 47, no. 5, pp. 3554–3570, 1993.

[50] e. a. Pierre Lemonde, *Cold-Atom Clocks on Earth and in Space*, ser. Frequency Measurement and Control. Springer, 2000, ISBN: 978-3-540-67694-2. DOI: https://doi.org/10.1007/3-540-44991-4_6.

[51] M. Riedel, P. Böhi, Y. Li, and et al., "Atom-chip-based generation of entanglement for quantum metrology," *Nature*, vol. 464, pp. 1170–1173, Mar. 2010.

[52] C. Gross, T. Zibold, E. Nicklas, J. Estève, and M. K. Oberthaler, "Nonlinear atom interferometer surpasses classical precision limit," *Nature*, vol. 464, no. 7292, pp. 1165–1169, 2010, ISSN: 00280836. DOI: 10.1038/nature08919.

[53] A. D. Ludlow, M. M. Boyd, and J. Ye, "Optical atomic clocks," vol. 87, no. 06, pp. 637–701, 2015. DOI: 10.1103/RevModPhys.87.637.

[54] P. G. Westergaard, J. Lodewyck, and P. Lemonde, "Minimizing the dick effect in an optical lattice clock," *IEEE Transactions on Ultrasonics, Ferroelectrics, and Frequency Control*, vol. 57, no. 3, pp. 623–628, 2010. DOI: 10.1109/TUFFC.2010.1457.

[55] J. Lodewyck, P. G. Westergaard, A. Lecallier, L. Lorini, and P. Lemonde, "Frequency stability of optical lattice clocks," *New Journal of Physics*, vol. 12, no. 6, p. 065 026, Jun. 2010. DOI: 10.1088/1367-2630/12/6/065026. [Online]. Available: https://doi.org/10.1088/1367-2630/12/6/065026.

[56] P. Lemonde and P. Wolf, "Optical lattice clock with atoms confined in a shallow trap," *Phys. Rev. A*, vol. 72, p. 033 409, 3 Sep. 2005. DOI: 10.1103/PhysRevA.72.033409. [Online]. Available: https://link.aps.org/doi/10.1103/PhysRevA.72.033409.

[57] D. W. Allan and J. Levine, "A Historical Perspective on the Development of the Allan Variances and Their Strengths and Weaknesses," *IEEE Transactions on Ultrasonics, Ferroelectrics, and Frequency Control*, vol. 63, no. 4, pp. 513–519, 2016, ISSN: 08853010. DOI: 10.1109/TUFFC.2016.2524687.

[58] M. A. Weiss and K. Shenoi, "The Time Deviation in Packet-Based Synchronization," *IEEE Transactions on Ultrasonics, Ferroelectrics, and Frequency Control*, vol. 63, no. 4, pp. 531–537, 2016, ISSN: 08853010. DOI: 10.1109/TUFFC.2015.2495011.

[59] N. Poli, C. W. Oates, P. Gill, and G. M. Tino, "Optical atomic clocks," *Rivista del Nuovo Cimento*, vol. 36, no. 12, pp. 555–624, 2013, ISSN: 0393697X. DOI: 10.1393/ncr/i2013-10095-x.

[60] A. D. Ludlow, "The Strontium Optical Lattice Clock: Optical Spectroscopy with Sub-Hertz Accuracy," Ph.D. dissertation, 2008, p. 251, ISBN: 0549558306.

[61] A. V. Taichenachev, V. I. Yudin, C. W. Oates, C. W. Hoyt, Z. W. Barber, and L. Hollberg, "Magnetic field-induced spectroscopy of forbidden optical transitions with application to lattice-based optical atomic clocks," *Phys. Rev. Lett.*, vol. 96, p. 083 001, 8 Mar. 2006. DOI: 10.1103/PhysRevLett.96.083001. [Online]. Available: https://link.aps.org/doi/10.1103/PhysRevLett.96.083001.

[62] S. Wolf, D. Gubser, and D. Cox, "Shielding of longitudinal magnetic fields with thin closely spaced concentric cylindrical shells, with applications to atomic clocks,"

[63] E. inc, "Guidelines For Installing Magnetic Shielding," Tech. Rep.

[64] J. Ye, H. J. Kimble, and H. Katori, "Quantum state engineering and precision metrology using state-insensitive light traps," *Science*, vol. 320, no. 5884, pp. 1734–1738, 2008. DOI: 10.1126/science.1148259. eprint: https://www.science.org/doi/pdf/10.1126/science.1148259. [Online]. Available: https://www.science.org/doi/abs/10.1126/science.1148259.

[65] H. Katori, M. Takamoto, V. G. Pal'chikov, and V. D. Ovsiannikov, "Ultrastable optical clock with neutral atoms in an engineered light shift trap," *Phys. Rev. Lett.*, vol. 91, p. 173 005, 17 Oct. 2003. DOI: 10.1103/PhysRevLett.91.173005. [Online]. Available: https://link.aps.org/doi/10.1103/PhysRevLett.91.173005.

[66] S. G. Porsev, A. Derevianko, and E. N. Fortson, "Possibility of an optical clock using the $6^1S_0 \rightarrow 6^3P_0^o$ transition in ^{171,173}Yb atoms held in an optical lattice," *Phys. Rev. A*, vol. 69, p. 021 403, 2 Feb. 2004. DOI: 10.1103/PhysRevA.69.021403.

[67] J. R. P. Angel and P. G. H. Sandars, "The hyperfine structure Stark effect I. Theory," *Proceedings of the Royal Society of London. Series A. Mathematical and Physical Sciences*, vol. 305, no. 1480, pp. 125–138, 1968, ISSN: 0080-4630. DOI: 10.1098/rspa.1968.0109.

[68] N. D. Lemke, A. D. Ludlow, Z. W. Barber, *et al.*, "Spin-1/2 optical lattice clock," *Phys. Rev. Lett.*, vol. 103, 6 Aug. 2009. DOI: 10.1103/PhysRevLett.103.063001.

[69] B. J. Bloom and et al, "An optical lattice clock with accuracy and stability at the 10^{18} level," *Nature*, vol. 506, pp. 71–75, Feb. 2014. DOI: https://doi.org/10.1038/nature12941.

[70] A. V. Taichenachev and et al, "Compensation of field-induced frequency shifts in ramsey spectroscopy of optical clock transitions," *JETP Letters*, vol. 90, pp. 713–717, 11 Feb. 2010. DOI: https://doi.org/10.1134/S0021364009230052.

[71] V. I. Yudin, A. V. Taichenachev, C. W. Oates, *et al.*, "Hyper-ramsey spectroscopy of optical clock transitions," *Phys. Rev. A*, vol. 82, p. 011 804, 1 Jul. 2010. DOI: 10.1103/PhysRevA.82.011804. [Online]. Available: https://link.aps.org/doi/10.1103/PhysRevA.82.011804.

[72] J. Lodewyck, M. Zawada, L. Lorini, M. Gurov, and P. Lemonde, "Observation and cancellation of a perturbing dc stark shift in strontium optical lattice clocks," *IEEE Transactions on Ultrasonics, Ferroelectrics, and Frequency Control*, vol. 59, no. 3, pp. 411–415, 2012. DOI: 10.1109/TUFFC.2012.2209.

[73] M. S. Safronova, M. G. Kozlov, and C. W. Clark, "Blackbody radiation shifts in optical atomic clocks," *IEEE Transactions on Ultrasonics, Ferroelectrics, and Frequency Control*, vol. 59, no. 3, pp. 439–447, 2012. DOI: 10.1109/TUFFC.2012.2213.

[74] F. Diedrich, J. C. Bergquist, W. M. Itano, and D. J. Wineland, "Laser cooling to the zero-point energy of motion," *Phys. Rev. Lett.*, vol. 62, pp. 403–406, 4 Jan. 1989. DOI: 10.1103/PhysRevLett.62.403. [Online]. Available: https://link.aps.org/doi/10.1103/PhysRevLett.62.403.

[75] W. H. Oskay, S. A. Diddams, E. A. Donley, *et al.*, "Single-atom optical clock with high accuracy," *Phys. Rev. Lett.*, vol. 97, p. 020 801, 2 Jul. 2006. DOI: 10.1103/PhysRevLett.97.020801. [Online]. Available: https://link.aps.org/doi/10.1103/PhysRevLett.97.020801.

[76] I. Bloch, "Ultracold quantum gases in optical lattices," *Nature Physics*, vol. 1, no. 1, pp. 23–30, Oct. 2005. DOI: 10.1038/nphys138.

[77] L.-S. Ma, P. Jungner, J. Ye, and J. L. Hall, "Delivering the same optical frequency at two places: Accurate cancellation of phase noise introduced by an optical fiber or other time-varying path," *Opt. Lett.*, vol. 19, no. 21, pp. 1777–1779, Nov. 1994. DOI: 10.1364/OL.19.001777. [Online]. Available: http://opg.optica.org/ol/abstract.cfm?URI=ol-19-21-1777.

[78] M. Menchetti, "Experimental set-up for realising long-range interaction using strontium atoms in an optical lattice," Ph.D. dissertation, University of Birmingham, 2019.

[79] M. D. Swallows, M. Bishof, Y. Lin, *et al.*, "Suppression of collisional shifts in a strongly interacting lattice clock," *Science*, vol. 331, no. 6020, pp. 1043–1046, 2011. DOI: 10.1126/science.1196442. [Online]. Available: https://www.science.org/doi/abs/10.1126/science.1196442.

[80] A. Rey, A. Gorshkov, C. Kraus, *et al.*, "Probing many-body interactions in an optical lattice clock," *Annals of Physics*, vol. 340, no. 1, pp. 311–351,

2014, ISSN: 0003-4916. DOI: https://doi.org/10.1016/j.aop.2013.11.002. [Online]. Available: https://www.sciencedirect.com/science/article/pii/S0003491613002546.

[81] R. Feynman, *Feynman Lectures*. 1964, vol. 1, ch. 15. [Online]. Available: https://www.feynmanlectures.caltech.edu/I_15.html (visited on 02/06/2022).

[82] R. F. C. Vessot, M. W. Levine, E. M. Mattison, *et al.*, "Test of relativistic gravitation with a space-borne hydrogen maser," *Phys. Rev. Lett.*, vol. 45, pp. 2081–2084, 26 Dec. 1980. DOI: 10.1103/PhysRevLett.45.2081. [Online]. Available: https://link.aps.org/doi/10.1103/PhysRevLett.45.2081.

[83] S. Schiller and et al, "Einstein gravity explorer–a medium-class fundamental physics mission," *Experimental Astronomy*, vol. 23, pp. 573–610, 2 Mar. 2009. DOI: https://doi.org/10.1007/s10686-008-9126-5.

[84] D. Kleppner, "Time too good to be true," *Physics Today*, vol. 59, no. 3, pp. 10–11, 2006, ISSN: 00319228. DOI: 10.1063/1.2195297.

[85] N. Poli, M. Schioppo, S. Vogt, *et al.*, "A transportable strontium optical lattice clock," *Applied Physics B: Lasers and Optics*, vol. 117, no. 4, pp. 1107–1116, 2014, ISSN: 09462171. DOI: 10.1007/s00340-014-5932-9. eprint: 1409.4572.

[86] W. Bowden, A. Vianello, I. R. Hill, M. Schioppo, and R. Hobson, "Improving the Q Factor of an Optical Atomic Clock Using Quantum Nondemolition Measurement," *Physical Review X*, vol. 10, no. 4, p. 41 052, 2020, ISSN: 21603308. DOI: 10.1103/PhysRevX.10.041052.

[87] R. Tyumenev, M. Favier, S. Bilicki, *et al.*, "Comparing a mercury optical lattice clock with microwave and optical frequency standards," *New Journal of Physics*, vol. 18, no. 11, pp. 1–16, 2016. DOI: 10.1088/1367-2630/18/11/113002.

[88] W. H. Oskay, S. A. Diddams, E. A. Donley, *et al.*, "Single-atom optical clock with high accuracy," *Physical Review Letters*, vol. 97, no. 2, pp. 1–4, 2006, ISSN: 00319007. DOI: 10.1103/PhysRevLett.97.020801.

[89] C. Degenhardt, H. Stoehr, C. Lisdat, *et al.*, "Calcium optical frequency standard with ultracold atoms: Approaching 10^{-15} relative uncertainty," *Phys. Rev. A*, vol. 72, p. 062 111, 6 Dec. 2005. DOI: 10.1103/PhysRevA.72.062111. [Online]. Available: https://link.aps.org/doi/10.1103/PhysRevA.72.062111.

[90] A. P. Kulosa, D. Fim, K. H. Zipfel, *et al.*, "Towards a mg lattice clock: Observation of the $^1S_0$–$^3P_0$ transition and determination of the magic wavelength," *Phys. Rev. Lett.*, vol. 115, p. 240 801, 24 Dec. 2015. DOI: 10.1103/PhysRevLett.115.240801. [Online]. Available: https://link.aps.org/doi/10.1103/PhysRevLett.115.240801.

[91] J. Mitroy, "Polarizabilities of the beryllium clock transition," *Phys. Rev. A*, vol. 82, p. 052 516, 5 Nov. 2010. DOI: 10.1103/PhysRevA.82.052516. [Online]. Available: https://link.aps.org/doi/10.1103/PhysRevA.82.052516.

[92] M. S. Safronova, S. G. Porsev, C. Sanner, and J. Ye, "Two Clock Transitions in Neutral Yb for the Highest Sensitivity to Variations of the Fine-Structure Constant," *Physical Review Letters*, vol. 120, no. 17, 2018, ISSN: 10797114. DOI: 10.1103/PhysRevLett.120.173001.

[93] S. Origlia, M. S. Pramod, S. Schiller, *et al.*, "A high-performance optical lattice clock based on bosonic atoms," *Arxiv*, 2018, ISSN: 1803.03157.

[94] M. Takamoto, F.-L. Hong, R. Higashi, Y. Fujii, M. Imae, and H. Katori, "Improved frequency measurement of a one-dimensional optical lattice clock with a spin-polarized fermionic 87sr isotope," *Journal of the Physical Society of Japan*, vol. 75, no. 10, p. 104 302, 2006. DOI: 10.1143/JPSJ.75.104302.

[95] X. Baillard, M. Fouché, R. Le Targat, *et al.*, "An optical lattice clock with fermionic and bosonic Sr atoms," *Optics InfoBase Conference Papers*, pp. 13–14, 2007, ISSN: 21622701.

[96] S. Knappe, V. Gerginov, P. D. Schwindt, *et al.*, "Atomic vapor cells for chip-scale atomic clocks with improved long-term frequency stability," *Optics Letters*, vol. 30, no. 18, p. 2351, 2005, ISSN: 0146-9592. DOI: 10.1364/ol.30.002351.

[97] R. Senaratne, S. V. Rajagopal, Z. A. Geiger, K. M. Fujiwara, V. Lebedev, and D. M. Weld, "Effusive atomic oven nozzle design using an aligned microcapillary array," *Review of Scientific Instruments*, vol. 86, no. 2, 2015, ISSN: 10897623. DOI: 10.1063/1.4907401. [Online]. Available: http://dx.doi.org/10.1063/1.4907401.

[98] S. C. Bell, M. Junker, M. Jasperse, *et al.*, "A slow atom source using a collimated effusive oven and a single-layer variable pitch coil Zeeman slower," *Review of Scientific Instruments*, vol. 81, no. 1, 2010, ISSN: 00346748. DOI: 10.1063/1.3276712.

[99] C. Vishwakarma, J. Mangaonkar, K. Patel, G. Verma, S. Sarkar, and U. D. Rapol, "A simple atomic beam oven with a metal thermal break," pp. 1–5, 2018. eprint: 1810.09090. [Online]. Available: http://arxiv.org/abs/1810.09090.

[100] M. Barbiero, M. G. Tarallo, D. Calonico, F. Levi, G. Lamporesi, and G. Ferrari, "A Sideband-Enhanced Cold Atomic Source For Optical Clocks," pp. 1–12, 2019. eprint: 1909.05810. [Online]. Available: http://arxiv.org/abs/1909.05810.

[101] O. Kock, W. He, D. Swierad, *et al.*, "Laser controlled atom source for optical clocks," *Scientific Reports*, vol. 6, pp. 1–6, 2016, ISSN: 20452322. DOI: 10.1038/srep37321. [Online]. Available: http://dx.doi.org/10.1038/srep37321.

[102] J. Bass, "Developments in quantum technology for portable strontium atomic systems," Ph.D. dissertation, University of Birmingham, 2021.

[103] W. D. Phillips and H. Metcalf, "Laser deceleration of an atomic beam," *Physical review letters*, vol. 48, no. 9, pp. 596–599, 1982.

[104] W. D. Phillips, "Laser cooling and trapping of neutral atoms," vol. 70, no. 3, pp. 721–741, 1998.

[105] M. Schioppo, N. Poli, M. Prevedelli, *et al.*, "A compact and efficient strontium oven for laser-cooling experiments," *Review of Scientific Instruments*, vol. 83, no. 10, 2012, ISSN: 00346748. DOI: 10.1063/1.4756936. [Online]. Available: https://doi.org/10.1063/1.4756936.

[106] H. J. Metcalf and P. van der Straten, "Laser cooling and trapping of atoms," *Journal of Optical society of America*, vol. 20, no. 5, 2003.

[107] C. Foot, *Atomic Physics (Oxford Master Series in Atomic, Optical and Laser Physics)*. Oxford University Press, 2005, ISBN: 100198506961.

[108] M. Bober, J. Zachorowski, and W. Gawlik, "Designing Zeeman slower for strontium atoms - Towards optical atomic clock," *Optica Applicata*, vol. 40, no. 3, pp. 547–555, 2010, ISSN: 00785466.

[109] M. L. Harris, "Design and construction of an improved zeeman slower," *Thesis*, 2003.

[110] Y. B. Ovchinnikov, "A Zeeman slower based on magnetic dipoles," *Optics Communications*, vol. 276, no. 2, pp. 261–267, 2007, ISSN: 00304018. DOI: 10.1016/j.optcom.2007.04.048. eprint: 0702074 (physics).

[111] I. R. Hill, Y. B. Ovchinnikov, E. M. Bridge, E. A. Curtis, and P. Gill, "Zeeman slowers for strontium based on permanent magnets," *Journal of Physics B: Atomic, Molecular and Optical Physics*, vol. 47, no. 7, 2014, ISSN: 13616455. DOI: 10.1088/0953-4075/47/7/075006.

[112] J. A. Rushton, M. Aldous, and M. D. Himsworth, "Contributed Review: The feasibility of a fully miniaturized magneto-optical trap for portable ultracold quantum technology," *Review of Scientific Instruments*, vol. 85, no. 12, 2014, ISSN: 10897623. DOI: 10.1063/1.4904066. arXiv: 1405.3148.

[113] K. Kowalski, V. Cao Long, K. Dinh Xuan, M. Głódź, B. Nguyen Huy, and J. Szonert, "Magneto-optical Trap: Fundamentals and Realization," *Computational Methods in Science and Technology*, vol. Special Is, no. 02, pp. 115–129, 2010. DOI: 10.12921/cmst.2010.si.02.115-129.

[114] W. Bowden, R. Hobson, I. R. Hill, *et al.*, "A pyramid MOT with integrated optical cavities as a cold atom platform for an optical lattice clock," *Scientific Reports*, vol. 9, no. 1, pp. 1–9, 2019, ISSN: 20452322. DOI: 10.1038/s41598-019-48168-3. eprint: 1907.13429.

[115] E. Imhof, B. K. Stuhl, B. Kasch, B. Kroese, S. E. Olson, and M. B. Squires, "Two-dimensional grating magneto-optical trap," *Physical Review A*, vol. 96, no. 3, 2017, ISSN: 24699934. DOI: 10.1103/PhysRevA.96.033636. eprint: 1703.07926.

[116] C. C. Nshii, M. Vangeleyn, J. P. Cotter, *et al.*, "A surface-patterned chip as a strong source of ultracold atoms for quantum technologies," *Nature Nanotechnology*, vol. 8, no. 5, pp. 321–324, 2013, ISSN: 17483395. DOI: 10.1038/nnano.2013.47.

[117] P. D. Lett, R. N. Watts, C. I. Westbrook, W. D. Phillips, P. L. Gould, and H. J. Metcalf, "Observation of atoms laser cooled below the doppler limit," *Physical Review Letters*, vol. 61, no. 2, pp. 169–172, 1988, ISSN: 00319007. DOI: 10.1103/PhysRevLett.61.169.

[118] A. Derevianko and H. Katori, "Colloquium: Physics of optical lattice clocks," *Reviews of Modern Physics*, vol. 83, no. 2, pp. 331–347, 2011, ISSN: 00346861. DOI: 10.1103/RevModPhys.83.331.

[119] R. Grimm, M. Weidemüller, and Y. B. Ovchinnikov, "Optical Dipole Traps for Neutral Atoms," *Advances in Atomic, Molecular and Optical Physics*, vol. 42, no. C, pp. 95–170, 2000, ISSN: 1049250X. DOI: 10.1016/S1049-250X(08)60186-X.

[120] R. H. Dicke, "The effect of collisions upon the doppler width of spectral lines," *Phys. Rev.*, vol. 89, pp. 472–473, 2 Jan. 1953. DOI: 10.1103/PhysRev.89.472. [Online]. Available: https://link.aps.org/doi/10.1103/PhysRev.89.472.

[121] H. G. Dehmelt, "Monoion oscillator as potential ultimate laser frequency standard," *IEEE Transactions on Instrumentation and Measurement*, vol. IM-31, no. 2, pp. 83–87, 1982. DOI: 10.1109/TIM.1982.6312526.

[122] J. Lodewyck, P. G. Westergaard, and P. Lemonde, "Nondestructive measurement of the transition probability in a sr optical lattice clock," *Phys. Rev. A*, vol. 79, p. 061 401, 6 Jun. 2009. DOI: 10.1103/PhysRevA.79.061401. [Online]. Available: https://link.aps.org/doi/10.1103/PhysRevA.79.061401.

[123] H. S. Margolis, "Spectroscopic applications of femtosecond optical frequency combs," *Chemical Society Reviews*, vol. 41, no. 15, pp. 5174–5184, 2012, ISSN: 14604744. DOI: 10.1039/c2cs35163c.

[124] Y. K. Chembo, D. V. Strekalov, and N. Yu, "Spectrum and dynamics of optical frequency combs generated with monolithic whispering gallery mode resonators," *Physical Review Letters*, vol. 104, no. 10, pp. 1–4, 2010, ISSN: 00319007. DOI: 10.1103/PhysRevLett.104.103902.

[125] V. Lebedev and D. M. Weld, "Self-assembled Zeeman slower based on spherical permanent magnets," *Journal of Physics B: Atomic, Molecular and Optical*

Physics, vol. 47, no. 15, 2014, ISSN: 13616455. DOI: 10.1088/0953-4075/47/15/155003.

[126] S. P. Krzyzewski, T. G. Akin, P. Dahal, and E. R. Abraham, "A clip-on Zeeman slower using toroidal permanent magnets," *Review of Scientific Instruments*, vol. 85, no. 10, 2014, ISSN: 10897623. DOI: 10.1063/1.4897151.

[127] Y. B. Ovchinnikov, "Longitudinal Zeeman slowers based on permanent magnetic dipoles," *Optics Communications*, vol. 285, no. 6, pp. 1175–1180, 2012, ISSN: 00304018. DOI: 10.1016/j.optcom.2011.10.027. eprint: arXiv:1104.5356v1.

[128] I. R. Hill, Y. B. Ovchinnikov, E. M. Bridge, E. A. Curtis, S. Donnellan, and P. Gill, "A simple, configurable, permanent magnet Zeeman slower for Sr," *EFTF 2012 - 2012 European Frequency and Time Forum, Proceedings*, pp. 545–549, 2012. DOI: 10.1109/EFTF.2012.6502439.

[129] G. Reinaudi, C. B. Osborn, K. Bega, and T. Zelevinsky, "Dynamically configurable and optimizable Zeeman slower using permanent magnets and servomotors," vol. 29, no. 4, pp. 729–733, 2011. DOI: 10.1364/JOSAB.29.000729. eprint: 1110.5351. [Online]. Available: http://arxiv.org/abs/1110.5351%0Ahttp://dx.doi.org/10.1364/JOSAB.29.000729.

[130] D. B. Ali, T. Badr, T. Brézillon, R. Dubessy, H. Perrin, and A. Perrin, "Detailed study of a transverse field Zeeman slower," *Journal of Physics B: Atomic, Molecular and Optical Physics*, 2017.

[131] Y. B. Ovchinnikov, "A permanent Zeeman slower for Sr atomic clock," *European Physical Journal: Special Topics*, vol. 163, no. 1, pp. 95–100, 2008, ISSN: 19516355. DOI: 10.1140/epjst/e2008-00812-x.

[132] K. Halbach, "Design of permanent multipole magnets with oriented rare earth cobalt material," *Nuclear instruments and methods*, no. 3, 1980.

[133] P. Cheiney, O. Carraz, D. Bartoszek-Bober, *et al.*, "A Zeeman slower design with permanent magnets in a Halbach configuration," *Review of Scientific Instruments*, vol. 82, no. 6, 2011, ISSN: 00346748. DOI: 10.1063/1.3600897.

[134] ——, "A Zeeman slower design with permanent magnets in a Halbach configuration," *Review of Scientific Instruments*, vol. 82, no. 6, 2011, ISSN: 00346748. DOI: 10.1063/1.3600897.

[135] D. B. Ali, T. Badr, T. Brézillon, R. Dubessy, H. Perrin, and A. Perrin, "Detailed study of a transverse field Zeeman slower," *Journal of Physics B: Atomic, Molecular and Optical Physics*, vol. 50, no. 5, 2017, ISSN: 13616455. DOI: 10.1088/1361-6455/aa5a6a. eprint: 1609.06525.

[136] S. K. Mayer, N. S. Minarik, M. H. Shroyer, and D. H. McIntyre, "Zeeman-tuned slowing of rubidium using $\sigma+$ and $\sigma-$ polarized light," *Optics Communications*, vol. 210, pp. 259–270, 3-6 2002.

[137] S. P. Krzyzewski, T. G. Akin, P. Dahal, and E. R. I. Abraham, "A clip-on Zeeman slower using toroidal permanent magnets," *Review of Scientific Instruments*, vol. 85, no. 10, pp. 1–6, 2014, ISSN: 10897623. DOI: 10.1063/1.4897151. [Online]. Available: http://dx.doi.org/10.1063/1.4897151.

[138] L. Zhao, J. Jiang, and Y. Liu, "Optimizing a spin-flip Zeeman slower," 2014. arXiv: 1401.7181. [Online]. Available: http://arxiv.org/abs/1401.7181.

[139] U. Qasim, "Towards a strontium based stationary optical clock," Ph.D. dissertation, University of Birmingham, Sep. 2018, ch. 4.

[140] L. C. Sinclair, F. R. Giorgetta, W. C. Swann, E. Baumann, I. Coddington, and N. R. Newbury, "The impact of turbulence on high accuracy time-frequency transfer across free space," *Optics InfoBase Conference Papers*, pp. 1–2, 2013, ISSN: 21622701. DOI: 10.1364/pcdvt.2013.ptu2f.2.

[141] C. Robert, J.-M. Conan, and P. Wolf, "Impact of turbulence on high-precision ground-satellite frequency transfer with two-way coherent optical links," *Phys. Rev. A*, vol. 93, p. 033 860, 3 Mar. 2016. DOI: 10.1103/PhysRevA.93.033860. [Online]. Available: https://link.aps.org/doi/10.1103/PhysRevA.93.033860.

[142] "Mynaric." (Mar. 2022), [Online]. Available: https://mynaric.com/.

[143] J. A. Shealy D. L.and Hoffnagle, "Laser beam shaping profiles and propagation," *Appl. Opt.*, vol. 45, no. 21, pp. 5118–5131, Jul. 2006. DOI: 10.1364/AO.45.005118.

[144] O. Wallner, P. J. Winzer, and W. R. Leeb, "Alignment tolerances for plane-wave to single-mode fiber coupling and their mitigation by use of pigtailed collimators," *Appl. Opt.*, vol. 41, no. 4, pp. 637–643, Feb. 2002. DOI: 10.1364/AO.41.000637.

[145] S. Thibault and J. Lacoursiere, "Advanced fiber coupling technologies for space and astronomical applications," International Society for Optics and Photonics, vol. 5578, SPIE, 2004, pp. 40–51. DOI: 10.1117/12.567347. [Online]. Available: https://doi.org/10.1117/12.567347.

[146] M. Lazzaroni and F. E. Zocchi, "Optical coupling from plane wave to step-index single-mode fiber," *Optics Communications*, vol. 237, no. 1, pp. 37–43, 2004, ISSN: 0030-4018. DOI: https://doi.org/10.1016/j.optcom.2004.03.092. [Online]. Available: https://www.sciencedirect.com/science/article/pii/S0030401804004201.

[147] A. Hati, C. W. Nelson, J. Taylor, N. Ashby, and D. A. Howe, "Cancellation of vibration-induced phase noise in optical fibers," *IEEE Photonics Technology Letters*, vol. 20, no. 22, pp. 1842–1844, 2008, ISSN: 10411135. DOI: 10.1109/LPT.2008.2004697.

[148] C. E. Calosso, E. K. Bertacco, D. Calonico, *et al.*, "Doppler-stabilized fiber link with 6 dB noise improvement below the classical limit," *Optics Letters*, vol. 40, no. 2, p. 131, 2015, ISSN: 0146-9592. DOI: 10.1364/ol.40.000131.

[149] C. E. Calosso, E. Bertacco, D. Calonico, *et al.*, "Frequency transfer via a two-way optical phase comparison on a multiplexed fiber network," *Optics Letters*, vol. 39, no. 5, p. 1177, 2014, ISSN: 0146-9592. DOI: 10.1364/ol.39.001177. eprint: 1308.2377.

[150] A. Tourigny-Plante, V. Michaud-Belleau, N. Bourbeau Hébert, H. Bergeron, J. Genest, and J. D. Deschênes, "An open and flexible digital phase-locked loop for optical metrology," *Review of Scientific Instruments*, vol. 89, no. 9, 2018, ISSN: 10897623. DOI: 10.1063/1.5039344. eprint: 1804.01028.

[151] T. Preuschoff, M. Schlosser, and G. Birkl, "Digital laser frequency and intensity stabilization based on the STEMlab platform (originally Red Pitaya)," *Review of Scientific Instruments*, vol. 91, no. 8, pp. 1–4, 2020, ISSN: 10897623. DOI: 10.1063/5.0009524. eprint: 2009.00343.

[152] M. Gellesch, R. Barron, J. M. Jones, *et al.*, "An optical lattice clock testbed system for the iqclock project demonstrator," in *2020 Joint Conference of the IEEE International Frequency Control Symposium and International Symposium on Applications of Ferroelectrics (IFCS-ISAF)*, 2020, pp. 1–2. DOI: 10.1109/IFCS-ISAF41089.2020.9234854.

[153] M. Gellesch, J. Jones, R. Barron, *et al.*, "Transportable optical atomic clocks for use in out-of-the-lab environments," *Advanced Optical Technologies*, vol. 9, no. 5, pp. 313–325, 2020, ISSN: 21928584. DOI: 10.1515/aot-2020-0023.

[154] C. Stirling, "Characterisation of a self assembled permanent magnet zeeman slower," Ph.D. dissertation, University of Birmingham, May 2017.